Technical Report

TR-12-11

TRUE-1 Completion

Final report

Johan Byegård, Eva Hakami, Calle Hjerne, Rune Nordqvist
Geosigma AB

Vladimir Cvetkovic, Royal Institute of Technology

Henrik Drake, Isochron Geoconsulting

Eva-Lena Tullborg, Terralogica AB

Anders Winberg, Conterra AB

February 2017

Svensk Kärnbränslehantering AB
Swedish Nuclear Fuel
and Waste Management Co

Box 250, SE-101 24 Stockholm
Phone +46 8 459 84 00

ISSN 1404-0344
SKB TR-12-11
ID 1447642
February 2017

TRUE-1 Completion

Final report

Johan Byegård, Eva Hakami, Calle Hjerne, Rune Nordqvist
Geosigma AB

Vladimir Cvetkovic, Royal Institute of Technology

Henrik Drake, Isochron Geoconsulting

Eva-Lena Tullborg, Terralogica AB

Anders Winberg, Conterra AB

Abstract

The Tracer Retention Understanding Experiments (TRUE) at the Äspö Hard Rock Laboratory embraces a number of projects performed over a 20 year period in order to increase the understanding of transport of dissolved solids in fractured crystalline rock. The various experiments within TRUE have been performed at laboratory scale (< 0.5 m), detailed scale (5–10 m) and in the block scale (10–50 m).

This report is a summary of the TRUE-1 Completion project which was performed, as a part of the TRUE-1 Continuation experimental programme, at the TRUE-1 site located at about 390 m depth in the Äspö Hard Rock Laboratory. The structure called Feature A was studied in all tests and analyses within the project. Six boreholes (KXTT1–KXTT5 and KA3005A) intercepting Feature A were used in the TRUE-1 Completion project, but most of the activities were focused on the intercepts of Feature A in borehole sections KXTT3:S3 and KXTT4:T3 and the associated flow path between the two. This flow path in Feature A was characterised in earlier investigations within the TRUE-1 project.

The primary overall objective of TRUE-1 Completion was to improve the knowledge of the internal structure and update the conceptual models of Feature A. This was carried out in three major parts consisting of:

- Tracer and hydraulic tests.
- Epoxy injection, overcoring and core logging.
- Analysis of core material.

Main findings and principal conclusions of the TRUE-1 Completion project, as presented in this report, do not contradict results and conclusion made in earlier parts of the TRUE projects. Instead, the results strengthen and provide added clarification to earlier findings.

One of the overall conclusions from the current work is that Feature A is heterogeneous in terms of transmissivity and/or connectivity within the borehole array and has an undulating and/or stepwise character.

The epoxy injection and associated image analysis of pore space pattern and structure resulted in a detailed description of the aperture distribution. In KXTT4, Feature A is dominated by one epoxy filled fracture whereas the area around Feature A in KXTT3 consists of five epoxy filled fractures. In Feature A' (in KXTT4), the amount of epoxy recovered is small and is limited to the area close to the borehole intercept. The detailed fracture geometry of Feature A varied and featured an equal distribution between a single open fracture plane, a slightly complex fracture and a complex fracture with several subparallel planes and embedded particles. The studied fractures of Feature A show an accumulated average physical aperture of 0.45 mm, with a variation in aperture in the span 0–1 mm and a spatial correlation distance (practical range) for the aperture of about 75 mm.

The microstructural model of Feature A was updated where the key components are a highly altered wall rock with several generations of fracture coatings with a coating of the main fracture surfaces dominated by chlorite and clay minerals together with some wall rock fragments, and calcite with related accessory minerals. Although clay minerals were found, the quantity does not seem to be large enough to provide explanation for the entire retention effect observed in earlier TRUE-1 tests. Instead, it is suggested that the rock matrix close to the fracture rim also plays a significant role in providing retention.

The tracer tests indicated, among other results, that caesium interactions with the rock material are subject to irreversible or slowly reversible sorption processes and that a simple cation exchange model is not sufficient for attaining satisfactory explanation and understanding.

Sammanfattning

TRUE-försöken (Tracer Retention Understanding Experiments) som genomförts i Äspölaboratoriet omfattar ett antal projekt som utförda under en 20-årsperiod för att öka förståelsen av transport av lösta ämnen i sprickigt kristallint berg. De olika experimenten inom TRUE har utförts i laboratorie-skala (< 0,5 m), detaljerad skala (5–10 m) och i block-skala (10–50 m).

Denna rapport är en sammanfattning av projektet TRUE-1 Completion som genomförts, som en del av TRUE-1 Continuation, vid experimentplatsen för TRUE-1 på ca 390 m djup i Äspölaboratoriet. Strukturen Feature A studerades i alla försök och analyser inom projektet. Sex borrhål (KXTT1–KXTT5 och KA3005A) som skär Feature A användes i projektet, men fokus för de flesta aktiviteterna var skärningen med borrhålsektionerna KXTT3:S3 och KXTT4:T3 med Feature A samt flödesvägen däremellan. Denna flödesväg är tidigare karakteriserad inom ramen för TRUE-1 projektet.

Det primära övergripande målet för TRUE-1 Completion var att förbättra kunskapen om den inre strukturen och uppdatera de konceptuella modellerna av Feature A. Detta utfördes i tre huvudsakliga delar bestående av:

- Spårämnesförsök och hydrauliska tester.
- Epoxi-injektion, överborrning och kärnkartering.
- Analys av kärnmaterial.

Resultat och huvudsakliga slutsatser av TRUE-1 Completion, presenterade i denna rapport, motsäger inte tidigare resultat och slutsatser från andra delar av TRUE. Istället förtydligas och förstärks tidigare resultat.

En av de övergripande slutsatserna från det aktuella arbetet är att Feature A är heterogen i fråga om transmissivitet och/eller konnektivitet inom den del som täcks upp av borrhålen och är undulerande och/eller trappstegsformad.

Epoxi-injektionen och den efterföljande bildanalysen av porgeometrin resulterade i en detaljerad beskrivning av aperturfördelningen. I KXTT4 är Feature A dominerad av en epoxi-fylld spricka medan det i området vid Feature A i KXTT3 finns fem epoxi-fyllda sprickor. I Feature A' (i KXTT4) är mängden epoxi liten och begränsad till området närmast borrhålet. Den detaljerade sprickgeometrin i Feature A varierar och uppvisar en lika fördelning mellan ett enkelt öppet sprickplan, en något komplex spricka och en komplex spricka med flera subparallella plan och med inbäddade partiklar. Den ackumulerade fysiska aperturen i de analyserade sprickorna i Feature A uppvisar ett medelvärde på 0,45 mm med en variation mellan 0 och 1 mm. Det rumsliga korrelationsavståndet för apertur bestämdes till c. 75 mm.

Den mikrostrukturella modellen av Feature A uppdaterades där de viktigare komponenterna är ett mycket omvandlat berg med flera generationer av sprickfyllnad vilka huvudsakligen består av klorit och lermineral tillsammans med bergfragment och kalcit med associerade mineral. Även om före-komst av lermineral konstaterats är mängden troligen för liten för att helt förklara den retention som observerats i tidigare TRUE-1 försök. Därför är det troligt att bergmatrisen också spelar en viktig roll för den observerade retentionen.

Spårförsöken indikerade (bland annat) att interaktionen mellan cesium och berget påverkas av icke eller långsamt reversibel sorption och att en enkel katjonutbytesmodell inte är tillräcklig för att ge en tillfredställande förståelse och beskrivning.

Contents

1 Introduction

1.1 Background

The Swedish concept for geological disposal of spent nuclear fuel at depth in the crystalline bedrock relies on a multi-barrier system for isolation of nuclear waste from the biosphere. The barriers consist of the spent fuel encapsulated in a copper-steel canister, the bentonite buffer surrounding the canister, and the natural bedrock barrier beyond the underground openings hosting the above mentioned engineered barriers (SKB 2011). The natural geological barrier should provide a stable mechanical and chemical environment for the engineered barriers, and should also prevent entry of corrodants and reduce and retard transport of radionuclides released from the engineered barriers, in case these barriers are breached.

In planning the experiments to be performed during the Operating Phase of the Äspö Hard Rock Laboratory, the Swedish Nuclear Fuel and Waste Management Company (SKB) identified the need for improving the understanding of radionuclide transport and retention processes in fractured crystalline rock. It was also considered important, from the performance assessment perspective, to be able to show that adequate transport data and parameters (distribution coefficients, diffusivity, flow-related transport parameters, etc) could be obtained or deduced from site characterisation (field experiments and associated modelling), and furthermore that laboratory results could be related to retention parameters obtained in situ. To answer these needs, SKB in 1994 initiated the Tracer Retention Understanding Experiments (TRUE).

1.2 Previous investigations within TRUE

1.2.1 TRUE-1

The First Stage of TRUE (Winberg et al. 2000) was performed in the detailed scale (0–10 m) and was focused on characterisation, experimentation and modelling of an interpreted single feature, cf. Figure 1-1. The First TRUE Stage (TRUE-1) was aimed at understanding tracer transport in a single fracture, which could e.g. be considered to represent a fracture intersecting a canister deposition hole. TRUE-1 was initially aimed at testing of equipment, adaptation of tracer test methodology to Äspö conditions, and the understanding of conservative tracer transport. The programme was later expanded to also include field tests with sorbing tracers. In addition, a technology for obtaining the internal structure of pore space in the fracture from injection of epoxy resin was developed.

Work performed included staged drilling of six boreholes, site characterisation, and installation of multi-packer systems to isolate interpreted hydraulic structures. Subsequent cross-hole hydraulic tests and a comprehensive series of tracer tests were used to plan a series of three tracer tests with radioactive sorbing tracers. The in situ tests were supported by a comprehensive laboratory programme performed on generic as well as on site-specific material from the studied feature. In addition, techniques for characterisation of the pore space of the investigated flow paths using epoxy resin have been developed and successfully tested in situ.

The various phases of tracer testing performed as part of TRUE-1 were subject to blind model predictions and subsequent evaluation (Elert 1999, Elert and Svensson 2001, Marshall and Elert 2003). The results of the TRUE-1 experiments showed clear evidence of diffusion, attributed by some researchers as diffusion into the rock matrix with associated sorption on inner pore surfaces (Widestrand et al. 2007, Cvetkovic et al. 2007, Cvetkovic and Cheng 2008). Other researchers claimed that the observed retention could be attributed to diffusion/sorption in fine-grained fault gouge material (Mazurek et al. 2003, Jakob et al. 2003) or be due effects of a 3D connected network of flow channels (Neretnieks 2002, Neretnieks and Moreno 2003). Distinction between alternative interpretations could only be further elucidated by applying the methodology developed within the project whereby epoxy resin injection, followed by overcoring is used to investigate the internal pore structure of Feature A, as described by the work presented in this report. Interim steps which include the successful investigation of fault rock zones at Äspö Hard Rock laboratory (HRL) are described by Mærsk Hansen and Staub (2004), Hakami and Wang (2005) and Winberg (2010).

1.2.2 TRUE Block Scale

The TRUE Programme identified early that the understanding of radionuclide transport and retention in the Block Scale (10–100 m), cf. Figure 1-1, required a separate experiment. Consequently the TRUE Block Scale project was devised (cf. Winberg 1997). The experiment was hosted in the south western parts of the laboratory centred on the 450 m level. The investigated rock block (approximately 200×250×100 m) was investigated in a first step during the period 1996 through 1999, reported early 2002.

The TRUE Block Scale project was executed by a partnership of six international funding organisations. The specific objectives were to; 1) increase understanding of tracer transport in a fracture network and improve predictive capabilities, 2) assess the importance of tracer retention mechanisms (diffusion and sorption) in a fracture network, and 3) assess the link between flow and transport data as a means for predicting transport phenomena. Experimentation was conducted in an array of six cored boreholes. Drilling and characterisation of each new borehole was followed by analysis and decision regarding the need and proposed geometry of a subsequent borehole. Details on the characterisation process and construction of hydrostructural and microstructural models are provided by Andersson et al. (2002a).

Hypotheses formulated in relation to defined basic questions were addressed in the in situ tracer tests and in the subsequent evaluation using numerical models. The in situ tracer test programme was crowned by four injections of cocktails of radioactive sorbing tracers in three different source-sink pairs over distances ranging between 15 and 100 m, as integrated along the deterministic structures of the hydrostructural model, defining flow paths of variable complexity, see Andersson et al. (2002b, 2004) for further details. The fractured crystalline rock volume was here conceptualised as a dual porosity medium (mobile-immobile). Model predictions of the sorbing tracer tests were followed by evaluation modelling where the various modelling results were used to elevate the understanding of block scale transport and retention and the relative role of processes. Diffusion to the immobile pore space, sorption in the immobile pore space and surface sorption on the fracture surfaces along the transport paths were interpreted as the main retention processes. This interpretation was supported both by the characteristics of in situ breakthrough curves and modelling, where in the latter case the measured residence time distributions were reproduced more accurately with diffusional mass transfer invoked. Geological information from the site also provided support for the assumption of multiple immobile zones along the investigated flow paths. Details on implementation of the common conceptual basis, model predictions and evaluation are provided by Poteri et al. (2002).

One important contribution of the TRUE Block Scale experiment was the establishment of a common framework for transport and retention. This enabled a unified comparison of relative contributions to modelled retention, despite apparent differences in the type (site characterisation/performance assessment-related) and complexity (dimensionality, representation of conductive elements, analytical/numerical) of the model representations, see Poteri et al. (2002). An important basis for the analysis was the further developed conceptual microstructural models. The latter developed significantly through the combined use of detailed mineralogy/geochemistry, porosity determinations and polymer impregnation (PMMA) of core samples. Furthermore, the sorption characteristics of altered wall rock and fine-grained (clayey) fault gouge were estimated based on ambient water chemistry, cation exchange capacity (CEC) and mineralogy of the geological materials and the selectivity coefficients of the tracers. These models and parameterisations were generalised further for usage in performance assessment context by Dershowitz et al. (2003). These example parameterisations were used as role models for the site-specific parameterisations of the "retardation model" for Forsmark, see Byegård et al. (2008). Furthermore, the basic methodology for site descriptive transport modelling, including applicable conceptual models, which paved the way for the subsequent safety analysis in SR-Site, were in part derived from the TRUE experiments (Crawford 2008).

At the termination of the TRUE Block Scale project it was recognised that a number of questions remained incompletely analysed and/or understood (Winberg et al. 2003), and hence a continuation project was set up whereby the integrated knowledge base from TRUE was applied on a yet untested part of the TRUE Block Scale rock volume. In this context, special emphasis was put on the geological understanding and the distinction between retention experienced in a fault structure (featured by fault

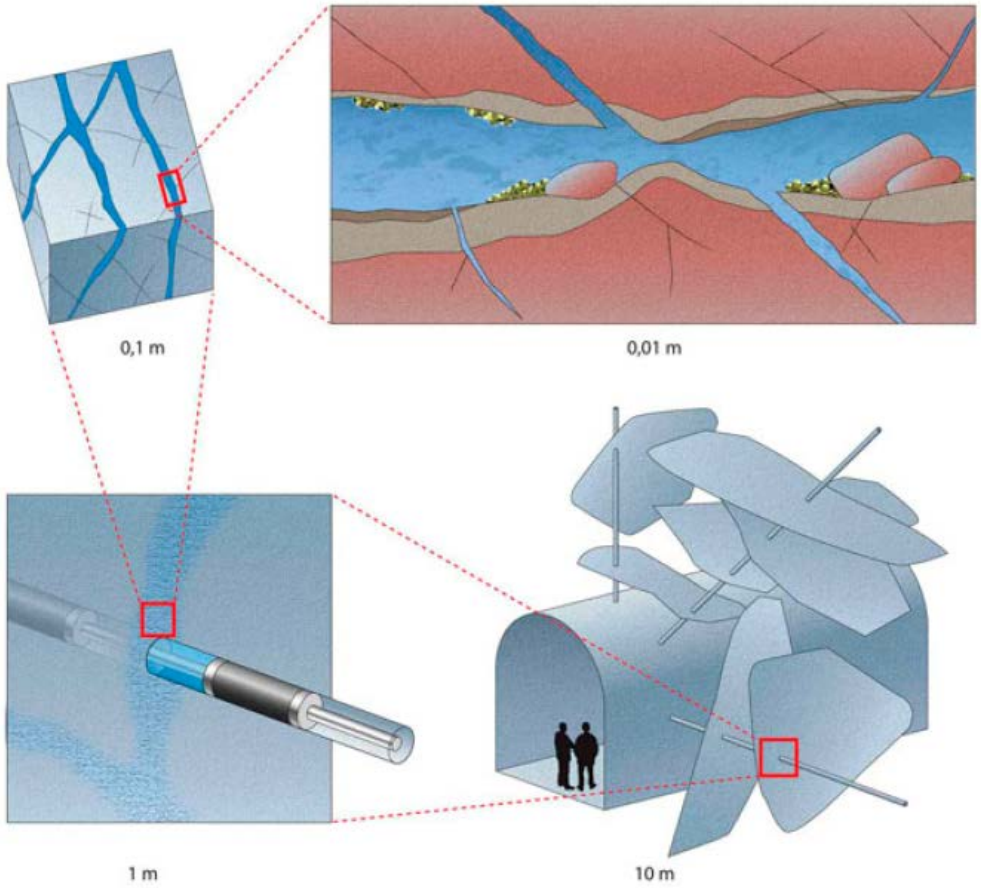

Figure 1-1. *Schematic representation of transport scales addressed in the TRUE programme.*

rock, fault gouge, fracture mineral coating and wall rock alteration) as opposed to the retention seen in a background fracture (featured by wall rock alteration and fracture mineral coating), see Dershowitz et al. (2003) and Andersson et al. (2007) for further details. The in situ breakthrough data and the integrated evaluations presented by Cvetkovic et al. (2010), Cvetkovic and Frampton (2010) and Cvetkovic (2010a) further strengthened the viewpoint of diffusion-controlled retention as the primary explanation of the observed retention. Furthermore, Cvetkovic (2010a) analysed and emphasised the role of the enhanced porosity (and associated heterogeneity) in the wall rock immediately adjacent to a conductive fracture for the retention, as noted both in the detailed and block scale experiments.

1.3 Overview of the TRUE-1 site

The field activities of TRUE-1 Completion were performed at the TRUE-1 site located at about 390 m depth in the Äspö Hard Rock Laboratory (Figure 1-2). The structure called Feature A was used for all tests and analyses within the TRUE-1 Completion project. All six boreholes intercepting Feature A as shown in Figure 1-3 were used in the TRUE-1 Completion project but most of the activities were focused on the intercepts of Feature A contained in borehole sections KXTT3:S3 and KXTT4:T3 and the flow path in between as illustrated in Figure 1-4. The hydrostructural model established based on previous hydraulic and transport tests indicates that Feature A consists of a single plane (Feature A) at the intersection of KXTT3:S3 and that this feature has a splay (Feature A') such that two fracture planes intersects KXTT4:T3 (Figure 1-3). These flow paths, in Feature A and Feature A', are characterised from earlier investigations at the TRUE-1 site (Andersson et al. 2002c, Winberg et al. 2000).

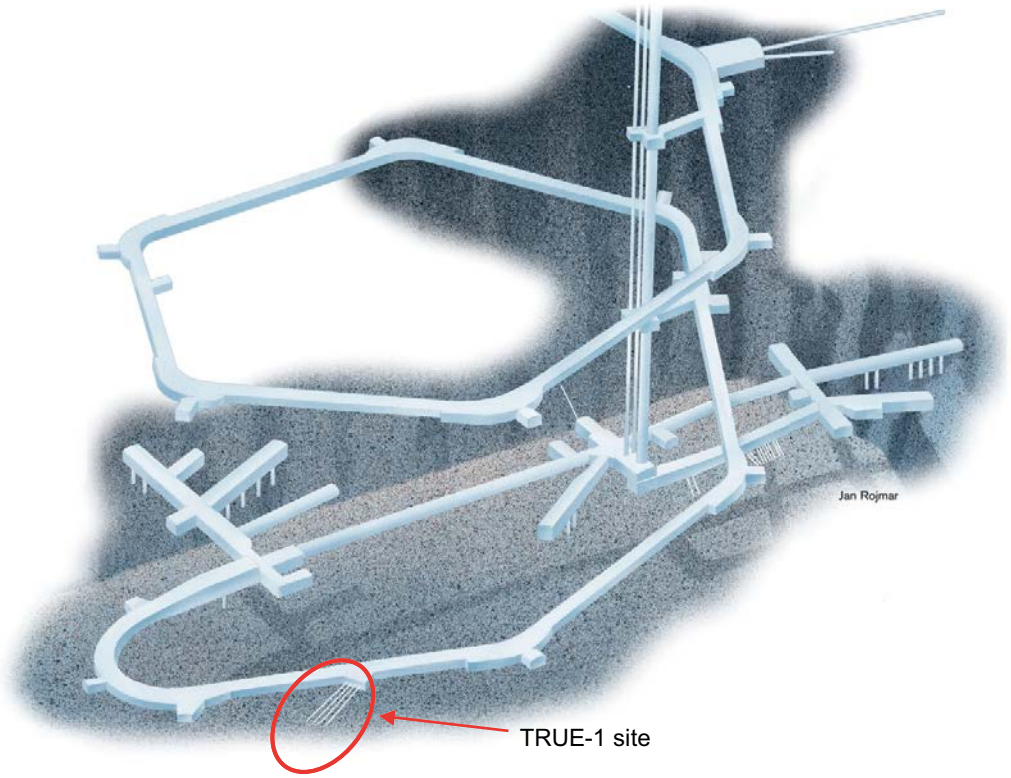

Figure 1-2. *View of Äspö HRL showing location of the TRUE -1 experiment site.*

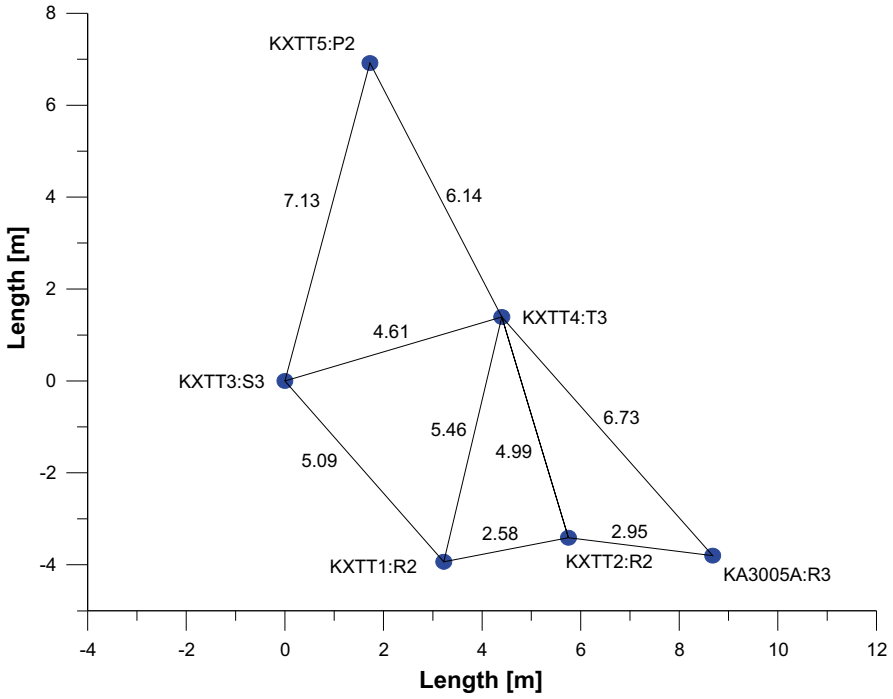

Figure 1-3. *Borehole intersection pattern with Feature A (as seen in the plane of the feature from the tunnel and inwards). Numbers indicated between boreholes give the Euclidian distances between borehole intersections (from Nordqvist et al. 2014).*

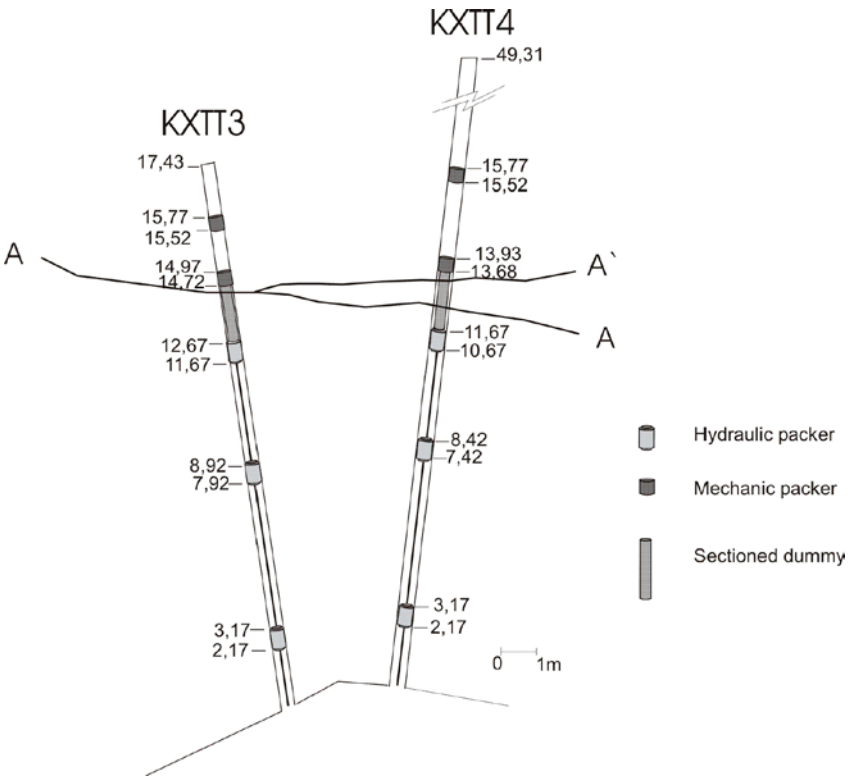

Figure 1-4. *Schematic drawing (plan view) of the boreholes KXTT3, KXTT4 and Feature A. Indicated numbers provide length coordinates along the borehole (from Nordqvist et al. 2014).*

2 Objectives and scope of TRUE-1 Completion

2.1 General objectives

TRUE-1 Completion is a sub project of TRUE-1 Continuation project which in turn is a follow up of the TRUE-1 project. It was decided that TRUE-1 Completion should be performed at the TRUE-1 site to complement already performed experiments. The main activity within TRUE-1 Completion is the injection of epoxy in the fracture with subsequent over-coring of relevant parts of Feature A and analysis of pore structure and identification of sorption sites. Furthermore, a number of complementary in situ experiments were performed in order to collect important information from Feature A and the TRUE-1 site before the epoxy injection and subsequent destruction of the site.

The general objectives of the TRUE-1 Completion are to:

1. Improve the knowledge of the internal structure of Feature A through epoxy injection and subsequent analyses, including improvement of the identification and description of the immobile zone(s) that are involved in observed retention effects.
2. Perform complementary tests useful to the SKB Site Investigations, including in situ K_d and SWIW (Single Well Injection Withdrawal) tests.
3. Improve the description of zones of immobile water that contribute to observed retention effects. The approach was identification and mineralogical-chemical characterisation of the sorption sites where Cs was found.
4. Update the conceptual microstructure and sorption models of Feature A.

2.2 Overview of experimental programme

The primary reporting of TRUE-1 Completion is divided in three parts; tracer and hydraulic tests (Nordqvist et al. 2014), epoxy injection and overcoring (Sigurdsson and Hjerne 2014) and analysis of core material (Hakami et al. 2014). Besides a summary of these primary reports, the present report also includes an update of conceptual models and conclusions in general of the TRUE-1 Completion project. For details about tests, methods, analysis, results etc refer to the three primary reports listed above.

Major activities in the project are listed in Table 2-1 together with the associated time period for the actual work and primary reference. The time periods listed below do not include the time for analysis and reporting of the tests. As seen in Table 2-1, the project extended over a rather long time period, mainly because heavy involvement of most project members in other highly prioritised SKB projects such as site investigations, site modelling and LTDE-SD.

Table 2-1. Major events in TRUE-1 Completion.

Event	Time period	Primary reference
Re-installation of borehole equipment	Oct 2005	Sigurdsson and Hjerne 2014
SWIW tests	Nov 2005 – Feb 2006	Nordqvist et al. 2014
Crosshole interference tests	April 2006 – May 2006	Nordqvist et al. 2014
Cation exchange capacity test	May 2006 – Dec 2006	Nordqvist et al. 2014
Epoxy injection	March 2007	Sigurdsson and Hjerne 2014
Overcoring	May 2007 – Aug 2007	Sigurdsson and Hjerne 2014
Core logging	May 2007 – Dec 2007	Sigurdsson and Hjerne 2014
Analysis of core material	April 2009 – April 2010	Hakami et al. 2014

3 Tracer and hydraulic tests

Tracer and hydraulic tests were performed in the TRUE-1 Feature A as complementary tests useful to the SKB Site Investigations, including in situ K_d and SWIW tests for providing new results useful for updating conceptual models.

The specific objectives of the tracer and hydraulic tests were to:

- Verify the distribution of tracer around a SWIW-test borehole by employing passive sampling in the surrounding multi-borehole array intersecting Feature A.
- Evaluate the SWIW test and to compare the results with previously performed tracer tests at the TRUE-1 site.
- Study the cation exchange capacity (CEC) in situ and study the de-sorption of the previously injected ^{134}Cs and ^{137}Cs in the flow path, possibly making the (overcore) drill cores more manageable for image analysis and microscopy (radiation safety aspects).
- Enhance the presence of Cs in the Feature A flow path from KXTT4 to KXTT3, to enable study of adsorbed non-radioactive Cs+ instead of the radioactive ^{134}Cs and ^{137}Cs, which are presumed to be present in rather low amounts.
- Examine and evaluate effects of possible channelling in a single fracture (Feature A) using cross-hole interference tests.

Prior to the TRUE-1 Completion tracer and hydraulic tests, the borehole instrumentation of KXTT3 and KXTT4 was modified so that the borehole section around Feature A was identical to that employed during the earlier performed STT-tests (Andersson et al. 1997, 1999a, b) and to facilitate the epoxy injection and overcoring in the mentioned boreholes.

If nothing else is stated, all results, figures, interpretations etc. in this chapter are from Nordqvist et al. (2014) where the tracer and hydraulic tests carried out within TRUE-1 Completion are presented in full.

3.1 SWIW tests in KXTT4

In a SWIW test, water with one or several tracers is injected into a rock formation in a borehole section and subsequently pumped back. The tracer breakthrough during the pump-back phase (recovery phase) may then provide information about solute transport properties of the rock formation.

A SWIW tracer test may consist of some or all of the following phases:

1. Injection of fluid to establish steady state hydraulic conditions.
2. Injection of one or more tracers.
3. Injection of chaser fluid after tracer injection is stopped, possibly the chaser fluid is labelled with a different tracer.
4. Waiting phase.
5. Recovery phase with pumping back of the previously injected tracer.

The injection of chaser fluid has the effect of pushing the tracer out in the formation surrounding the tested section. One advantage of employing a chaser fluid is that when the tracer is pumped back, a complete recovery breakthrough curve with a rising part, a peak and a decreasing part is obtained. During the waiting phase there is no injection or withdrawal of fluid. The purpose of this phase is to increase the time available for time-dependent transport-processes to act so that these may be more easily identified and evaluated from the resulting breakthrough curve. The TRUE-1 SWIW tests were carried out with tracer injection, chaser injection and recovery, i.e. phases 2, 3 and 5 above. An idealised schematic illustration of a recovery breakthrough curve during a SWIW test is shown in Figure 3-1.

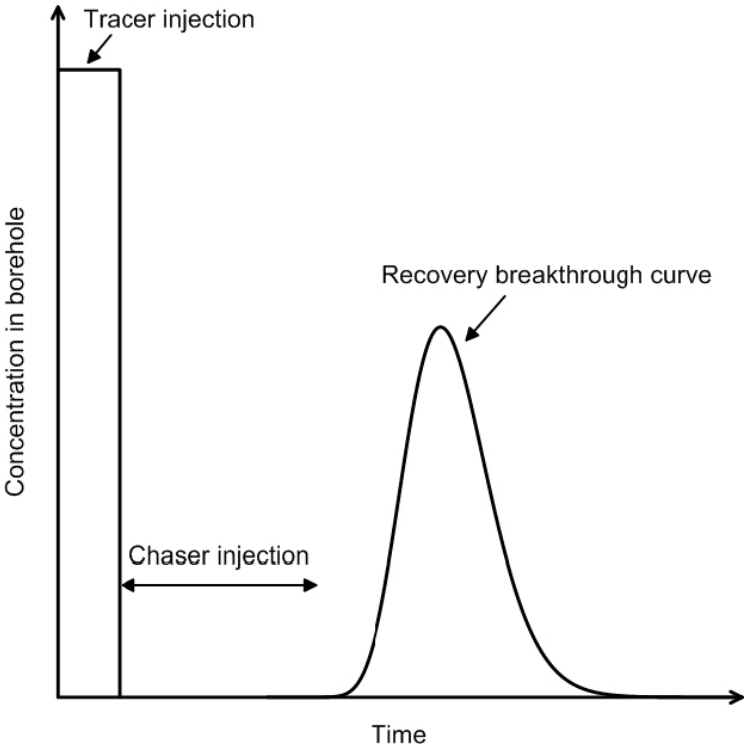

Figure 3-1. *Idealised schematic tracer concentration sequence during a SWIW test.*

SWIW tests differ significantly in several ways from cross-hole tracer tests. The experimental scale in each method represents a major conceptual difference. In SWIW tests, only the rock volume adjacent to the borehole section is involved. The extent of the tested volume is given by how far the injection water has travelled along conductive features out into the formation before beginning of recovery pumping phase. However, this cannot be determined without additional borehole sections sufficiently close to the SWIW section. In cross-hole tests, it is reasonable to expect that the tested domain is comprised of connected transport paths between injection and pumping sections.

The perhaps most significant attribute of a SWIW experiment compared to a cross-hole test, is the reversal of the flow field. Thus, under ideal conditions, an injected tracer moves away from the borehole section and then back again along the same flow path(s). The flow reversal that occurs in a SWIW test affects the interpretation of transport processes. For example, unlike for cross-hole tests, advective attributes such as fracture aperture (or porosity) and longitudinal dispersivity (or Peclet number) may not be determined independently from a SWIW test because of the unknown tracer travel distance (Becker and Shapiro 2003). Even if the porosity (or e.g. aperture) is independently known, dispersivity values evaluated from SWIW tests should be expected to be different from values evaluated from other types of tracer tests because the reversal of the flow field obscures the dispersion resulting from flow paths with different velocities (Gelhar et al. 1992).

The principal objectives for the SWIW tests in Feature A were initially formulated as follows:

- to verify the distribution of tracer around the SWIW test borehole by passive sampling in the surrounding multi-borehole array intersecting Feature A
- to evaluate the SWIW test and to compare the results to previously performed cross-hole tracer test at the TRUE site

The first of the above objectives was considered especially valuable for the SWIW tests performed within the SKB site investigations (Nordqvist 2008). In these SWIW tests, no other surrounding borehole sections were available where it was possible to observe the propagation of the tracer into the rock formation. At the TRUE-1 test site, several boreholes are available of which one may be used as a SWIW test borehole (injection and pumping hole) while the others may be used as observation holes.

A number of scoping calculations were carried out prior to the SWIW test in order to obtain an understanding of tracer (sorbing and non-sorbing) behaviour in peripheral boreholes and to provide support for experimental design. The specific purpose of the scoping calculations was to indicate suitable experimental flow rates and duration of various phases. These scoping calculations are presented in more detail by Nordqvist et al. (2014), but it may be of interest here to illustrate the theoretical tracer breakthrough in observation boreholes at varying distance from the central SWIW borehole. Figure 3-2 shows tracer breakthrough curves for non-sorbing tracers at radial distances of 3, 6 and 8 m, respectively. The appearance of the breakthrough curves is very sensitive to the radial distance from the SWIW section. The closest observation section at 3 m shows two peaks, well separated in time, of which the second peak occurs when the tracer travels back during the recovery phase. At a distance of 6 m, the peaks are not fully separated, but the start of the recovery pumping phase is clearly seen just after the peak in the breakthrough curve. At a radial distance of 8 m, tracer breakthrough is barely visible because in this case only the leading front edge of the tracer "cloud" enters the borehole section before the recovery pumping starts.

The original experimental plan for the TRUE-1 Completion SWIW tests included the use of sorbing and radioactive tracers. First, a pre-test was to be carried out with only a fluorescent dye tracer in order to optimize experimental conditions, such as injection flow rates, pressures, etc. The pre-test was to be followed by a main SWIW tests with injection of a relatively large number of conservative, sorbing (weakly and strongly) and radioactive tracers.

However, the planned main test with sorbing and radioactive tracers was never carried out due to a very low tracer (Uranine) recovery (about two percent) during the pre-test. The pre-test was repeated with a modified (shorter) chaser injection period in order to increase tracer recovery. The repeated test resulted in improved tracer recovery, but still with a very low recovery (about 11 percent). Due to the low recovery and associated radioprotection issues, it was decided not to proceed with radioactive/sorbing tracers.

Despite the reduced experimental scope, an interesting set of data from the two tracer injections (herein called SWIW 1 and SWIW 2, only differing in the amounts of chaser fluid volume) was obtained. Tracer breakthrough curves were established in all of the four peripheral boreholes sections as well as in the central SWIW section (although with low tracer recovery, as already mentioned).

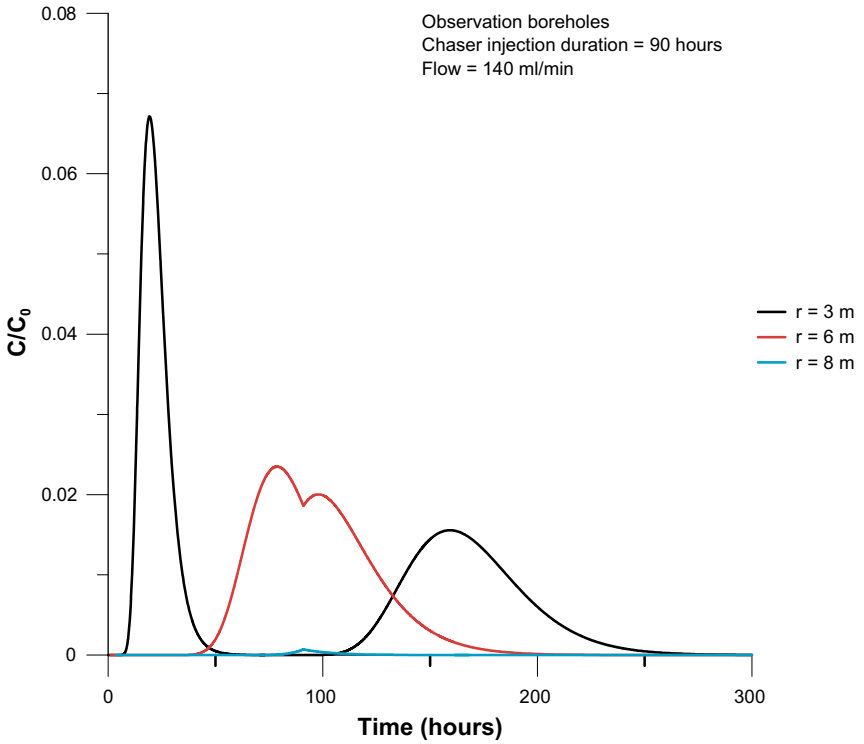

Figure 3-2. *Simulated tracer breakthrough curves for non-sorbing tracers at various radial distances.*

Details of equipment and experimental performance used are given by Nordqvist et al. (2014). In both of the SWIW tests, tracer solution was injected for approximately one hour with total injected tracer solution volumes of approximately 9 and 8 L for SWIW 1 and SWIW 2, respectively. The main difference between the two tests is that 618 L chaser fluid was used in SWIW 1 while this volume was reduced to 162 L in SWIW 2. The flow rates for the various experimental phases did not differ significantly between the tests.

The resulting tracer breakthrough curves from the two SWIW tests are shown in Figure 3-3. Tracer breakthrough is clearly visible for the central SWIW section and all of the observation sections. Figure 3-3 also indicates a significant amount of variability in tracer arrival times and peak values of the breakthrough curves. Although the radial distances vary somewhat among the observation sections (see Figure 1-3), this variability presumably is, at least partially, a result of flow heterogeneity.

A more detailed plot of the tracer breakthrough curves from both tests in the central injection/withdrawal borehole KXTT4, section T3, is shown in Figure 3-4. The tracer breakthrough curves during the pump-back phase look approximately as what is expected from a SWIW experiment. However, the tracer recovery is remarkably low in both of the SWIW tests.

The low recoveries from the SWIW tests means that most of the tracer mass did not return to the SWIW section during the pump-back phase. One possible explanation for this may be the influence of the ambient hydraulic background gradient, which might act to carry tracer sufficiently far away to prevent it from being re-captured by the change in gradient imposed by recovery pumping. Such a strong gradient is not indicated from available measurements of hydraulic head in the experimental boreholes but may nonetheless be a possibility, considering the close proximity to the tunnel.

Supporting evidence for a strong background gradient may be found in the breakthrough curves themselves. The tracer peak during the pump-back phase appears very soon after flow reversal and there appears not to be any significant visible difference between the two SWIW tests, despite the fact that the total injection time (and thereby injected water volume) is about four times longer in SWIW test 1. Such an early peak is characteristic for a SWIW test influenced by a hydraulic gradient, as the “upstream” part of the tracer plume returns faster to the SWIW section.

Because of the low tracer recoveries, no quantitative modelling of the SWIW section results was made. For the observation sections, on the other hand, most of the breakthrough curves were evaluated with a standard one-dimensional advection-dispersion model. The modelling of the observation hole breakthrough curves is described by Nordqvist et al. (2014).

In summary, it may be more appropriate to regard the SWIW experiment as a combination of a SWIW test and a radially diverging tracer test because the observations of tracer response in the four surrounding borehole sections are at least as interesting as the recovery in the SWIW section itself. Observations in other borehole sections have not been possible for the SWIW tests carried out within the site investigation programs, and the TRUE SWIW test results are therefore somewhat unique in this respect and provide in-situ experimental observations of tracer spreading during a SWIW test.

An unexpected result is the low tracer recovery in the SWIW section. However, tracer breakthrough was observed in all of the four observation boreholes and one interpretation is that most of the tracer may have been lost to fractures or zones with high hydraulic gradients due to the vicinity of the tunnel. Irrespective of the low recovery in the SWIW section, the results from the observation sections clearly demonstrate the heterogeneous nature of the radial solute spreading during the water injection phase. Although the distances between the SWIW section and the different observation sections are fairly similar, tracer residence times as well as peak tracer concentrations vary within an order of magnitude. Tracer breakthrough was faster and with higher peak concentrations in KXTT3 and KXTT5 than in KXTT1 and KXTT2.

One-dimensional transport modelling indicated that only one of the observation sections gave consistent results for both of the SWIW experiments. In other sections, interpretation is more ambiguous when considering the combined results from both tests. This may be taken as a further indication of the complexity of tracer transport during a SWIW test and that tracer transport paths may vary depending on the flow direction.

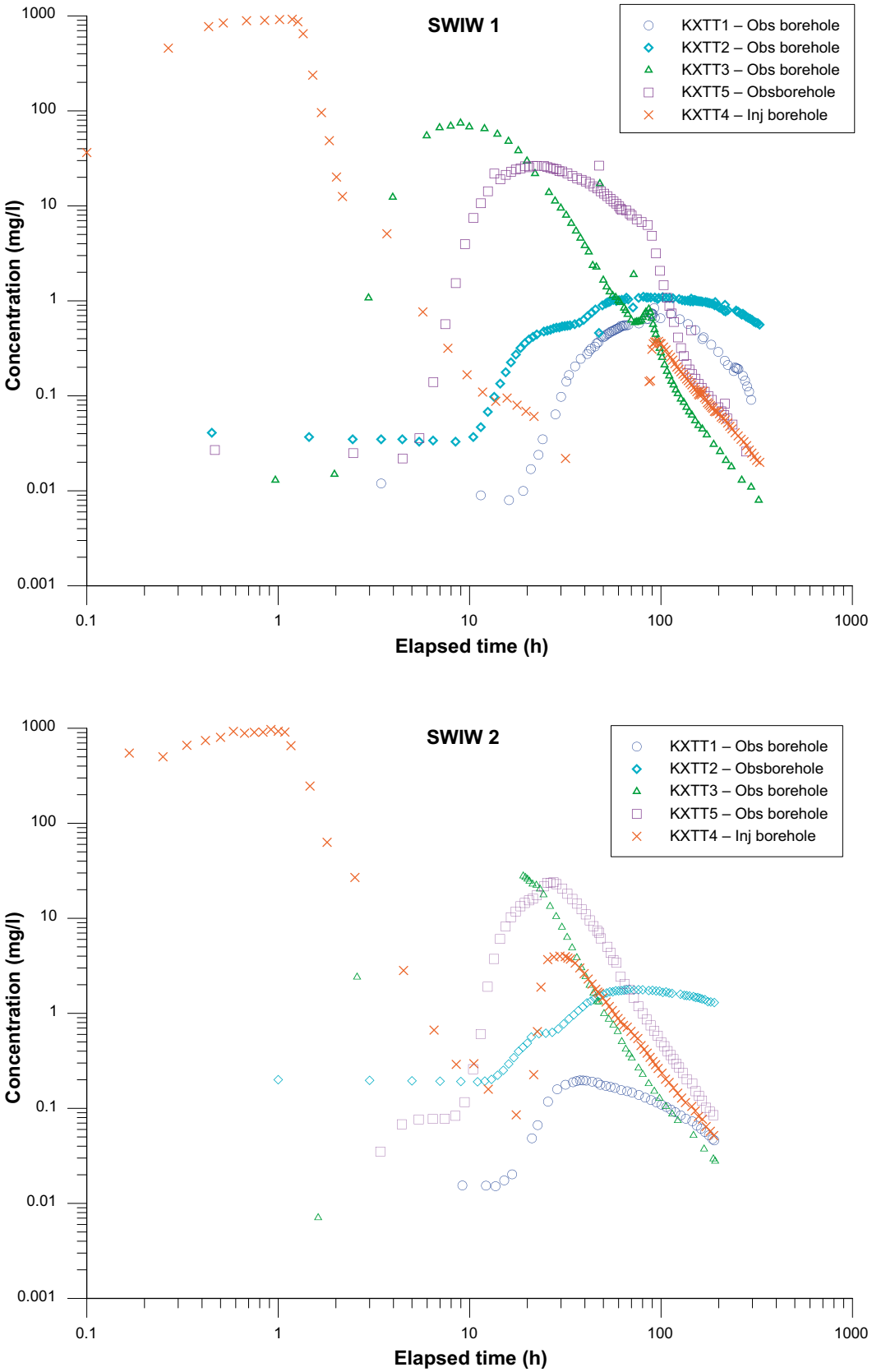

Figure 3-3. *Tracer breakthrough for test SWIW test 1 and 2 with injection in KXTT4 and observation in KXTT1, KXTT2, KXTT3 and KXTT5. Logarithmic concentration and time scales.*

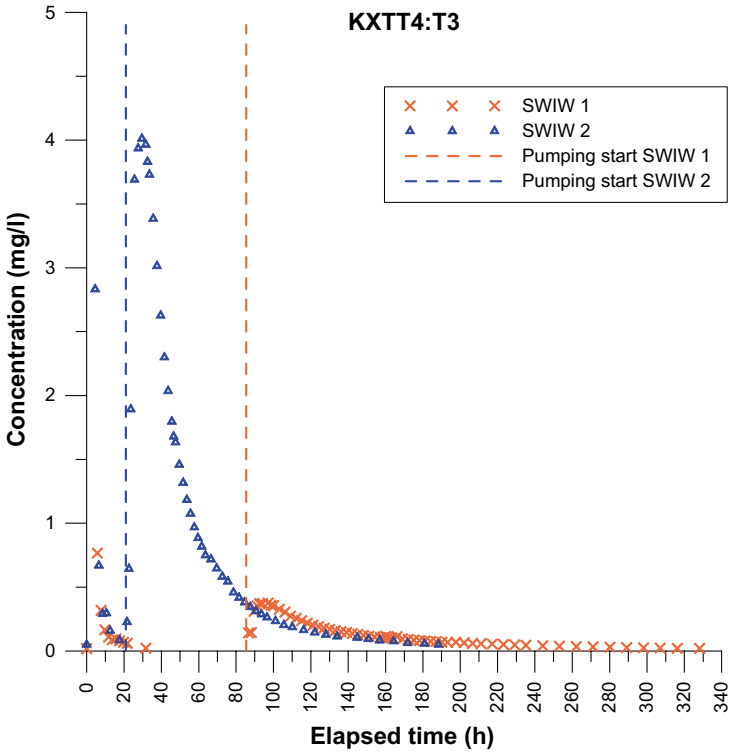

Figure 3-4. *Tracer breakthrough in the SWIW section (KXTT4, section T3). Dashed vertical line shows the start of the pump-back phase for each SWIW experiment.*

3.2 Crosshole interference tests

Crosshole interference tests (COM) were performed with the purpose of examining and evaluating effects of channelling in Feature A. The COM tests were carried out as a series of tests, where each test consisted of pumping in one borehole section while pressure and flow responses were observed in surrounding borehole sections. All borehole sections used for pumping and observations included Feature A, based on earlier investigations at the TRUE-1 site. The pumping sections were alternated in order to evaluate hydraulic interference in several directions and to investigate whether responses were reciprocal when flow directions were reversed. A total of eight tests were carried out with six different pumping sections.

Several previous hydraulic interference tests, some also in combination with flow response estimates, have been performed at the TRUE-1 site (Winberg 1996, Winberg et al. 2000, Andersson et al. 2002c). These tests focused on distinguishing between different features, such as Feature A and Feature B, while the COM tests focused only on internal responses within Feature A.

Pressure responses were assessed with respect to transient behaviour and magnitude. Flow responses were measured by means of the tracer dilution method under ambient as well as pumped conditions. In order to compare responses between different tests and observation sections, the following ratios were calculated for each observation section and test:

$$\frac{s_p}{Q_{pump}} = \frac{\text{Final drawdown}}{\text{Pumping flow rate}} \qquad \text{Equation 3-1}$$

$$\frac{t_R}{r^2} = \frac{\text{Pressure response time}}{\text{Euclidian distance}^2} \qquad \text{Equation 3-2}$$

$$\frac{T_{Th}}{T_M} = \frac{\text{Transmissivity according to Thiem's well equation}}{\text{Transmissivity according to Moye's equation}} \qquad \text{Equation 3-3}$$

$$\frac{Q_{flow}}{Q_{theory}} = \frac{\text{Observed groundwater flow rate}}{\text{Theoretical groundwater flow rate}} \qquad \text{Equation 3-4}$$

For t_R/r^2, T_{Th}/T_M and Q_{flow}/Q_{theory} the results were expected to be similar within each ratio for the various flow paths if the tests were performed in a two-dimensional homogenous feature. A higher value than expected for these ratios would indicate that the specific combination of observation and pumping section are affected by an area of high transmissivity and/or connectivity. Likewise would a low value indicate effects of an area of low transmissivity and/or connectivity. The ratio s_p/Q_{pump} will also increase with higher transmissivity and/or connectivity, although distance is not taken into account in this ratio. Thus, a high value may also be a result of a short distance between the pumping and observation section.

For each ratio above, responses were classified into different groups in order to facilitate comparison, visualisation and interpretation of the results. Figure 3-5 shows an example of a diagnostic plot of the flow rate responses during the tests. In this case it obvious that the flow rate responses between borehole section KXTT1:R2, KXTT2:R2, KXTT4:T3 and KA30005A:R3 are weak, suggesting a relatively low transmissivity or poor connectivity between these sections. Another observation is that the flow rates in KXTT3:S3 and to some degree in KXTT5:P2 were relatively high when pumping the other sections, while the flow rates in the other sections in most cases were relatively low during pumping in KXTT3:S3 or KXTT5:P2. For more examples of diagnostic plots and tables refer to Nordqvist et al. (2014).

The interpretation of the COM tests in Nordqvist et al. (2014) were made assuming a dominant two-dimensional flow character of the tested region. This is consistent with the earlier conceptualisation describing Feature A as a single fracture plane with a few subparallel fractures, or possibly splay fractures (Winberg et al. 2000). The interpretation in Nordqvist et al. (2014) is presented graphically in Figure 3-6, where red indicates areas with higher transmissivity, white medium transmissivity and blue lower transmissivity. This interpretation was mainly based on the following observations from the COM-tests:

- Higher transmissivity at KXTT3 and lower at KXTT2 (indicated by T_M).
- Lower transmissivity between KXTT1, KXTT2, KXTT4 and KA3005A (indicated by t_R/r^2 and Q_{flow}/Q_{theory}).
- Medium transmissivity between KXTT3 and KXTT2 (indicated by T_{Th}/T_M).
- Higher transmissivity to the left of KXTT3 and KXTT5 (indicated by high Q_{flow}/Q_{theory} in KXTT3 and to some degree in KXTT5 while pumping the other boreholes).

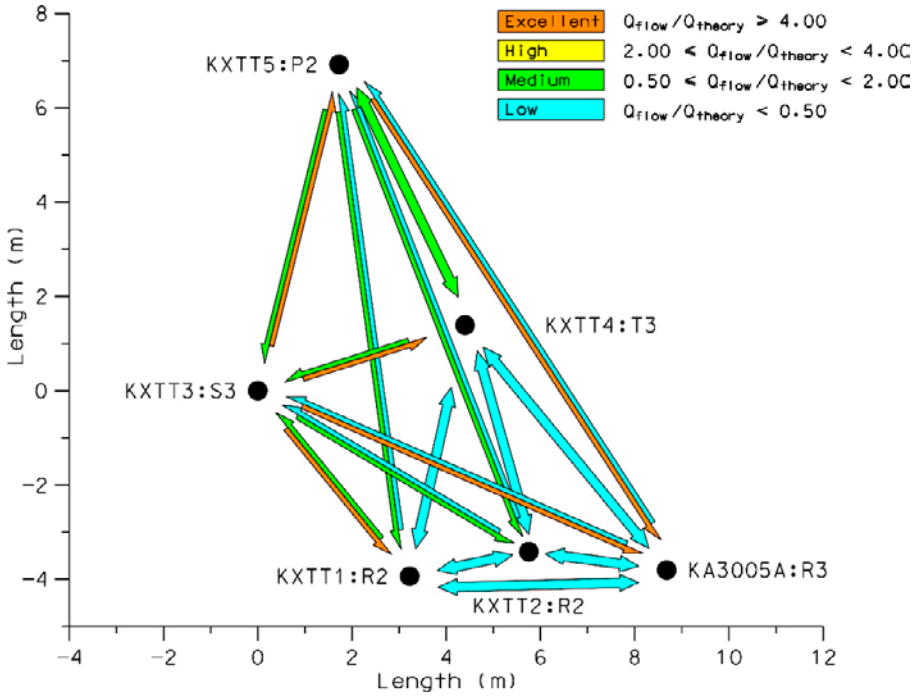

Figure 3-5. *Example of figure used for interpretation of results from crosshole interference tests. The figure shows the flow rate response during pumping where the arrows origins at the observation hole and points to the pumping hole (i.e. indicates the flow direction) (from Nordqvist et al. 2014).*

It is noted that the conductivities in this interpretation are only relative to Feature A, i.e. red, white and blue colours are not given absolute limits. However, guidance may be obtained from evaluated values of T_M where KXTT3:S3 was in the order of 10^{-7} m^2s^{-1}, KXTT2:R2 in the order of 10^{-9} m^2s^{-1} and the other sections in the order of 10^{-8} m^2s^{-1}, compatible with findings in Winberg et al. (2000).

Other interpretations are possible, especially if a network of interconnecting flowing fractures is assumed to play a dominant role in the tested rock. Previous analyses of flow dimension from hydraulic tests generally indicated flow dimensions higher than two (Winberg et al. 2000). This could be interpreted as a system influenced by interconnecting fractures in a three-dimensional network, as proposed by Neretnieks and Moreno (2003), which would contradict the concept of a planar two-dimensional flow region. A hydraulic test made in a feature with increasing transmissivity with distance from the borehole is expected to display a flow dimension higher than two. The interpretation of a high transmissivity area to the left of KXTT3 and KXTT5 may therefore be considered consistent with the earlier interpretation of flow dimensions from hydraulic tests in Feature A (Winberg et al. 2000). Contact with another fracture with higher transmissivity, i.e. a positive hydraulic boundary, would also contribute to a flow dimensions higher than two.

Despite the uncertainties related to the interpretation discussed above, it is clear that the COM tests reveal variations in the transmissivity field in the studied part of Feature A where channelling effects may play a role. For example, the low transmissivity area indicated between KXTT1, KXTT2, KXTT4 and KA3005A is intercepted by a higher transmissivity field between KXTT3 and KXTT2, which may be interpreted as a channel in Feature A. However, it is not possible to firmly establish whether physical channels exist or not in this part of Feature A based solely on the results from the COM tests.

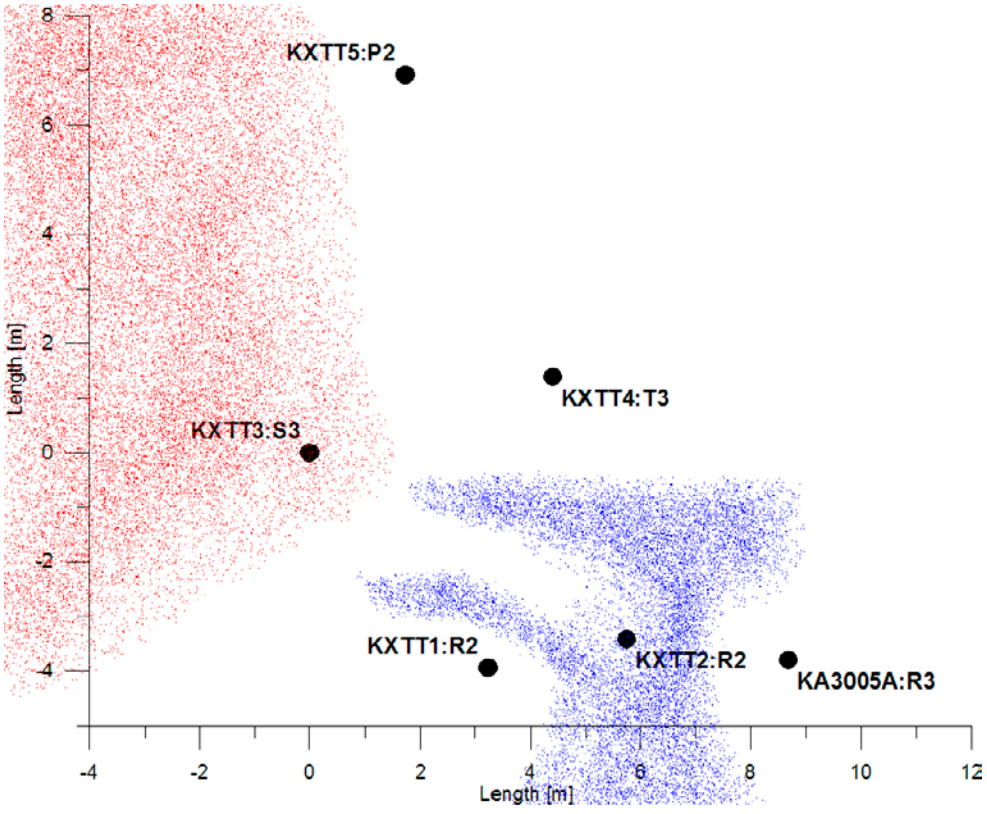

Figure 3-6. *Interpretation of the relative transmissivity distribution in Feature A based on the COM-test results. Red colour indicates higher transmissivity, white medium and blue lower transmissivity (from Nordqvist et al. 2014).*

In the SWIW experiments, KXTT4 was the injection/pumping section and the other boreholes were used as passive sampling sections. There were clear differences in tracer breakthrough among the observation sections. The fastest transport occurred from KXTT4 to KXTT3 and KXTT5, while travel times to the other two observations wells were about one order of magnitude higher. The same pattern was observed for the peak values of the breakthrough curves, i.e. much less dilution was observed for the two fastest transport paths. These general observations regarding tracer transport along the various transport paths agree qualitatively quite well with the connectivity analysis of the COM test results. Of the applied indices in the COM test analysis, the flow rate ratio (Q_{flow}/Q_{theory}) may be argued to most directly indicate groundwater flow (and thus tracer residence time) between injection and pumping. As shown in Figure 3-5, the flow rate ratio is low for the slowest and most diluted transport paths (T4 to T1 and T2, respectively) and higher for the faster and less diluted paths (T4 to T3 and T5, respectively).

3.3 Cation exchange capacity tests

In the attempts of increasing the knowledge of the flow pathways involved in the different tracer experiments performed in the Feature A, an experiment addressing the Cation Exchange Capacity (CEC) was performed. The basic idea of the experiment was to saturate the rock in the vicinity of the transport path with a sorbing tracer presumably undergoing cation exchange and thereby obtain a measure of the total cation exchange sorption capacity of the flow path involved in the earlier performed transport experiments. The aim was to perform the experiment with relatively high flow rates and thereby obtain a saturation of the sorption sites in close vicinity to the transport path, i.e. obtaining only a negligible interaction caused by the diffusion and the sorption in the rock matrix. By relating the sorption capacity of the flow path to CEC determined in laboratory experiment for well-defined rock surfaces, it would be possible to quantify the amount of surface area "seen" by the flow path. Accordingly, in the modelling and the scoping calculation of the experiment only a surface sorption model was used for quantifying a distinct sorption loss caused by the surface sorption sites only. Caesium (Cs^+) was selected as a tracer due to its high selectivity in adsorption, i.e. the sorption is stronger than any of the naturally competing cations, e.g. Na^+ and Ca^{2+}. Concerning the Cs^+interaction with site specific relevant geologic material, data was available from laboratory batch sorption experiments performed within the TRUE programme (e.g. Byegård et al. 1998), and had also been demonstrated by the strong retardation obtained in the TRUE-1 in situ experiments (e.g. Winberg et al. 2000). The CEC experiment is described in detail by Nordqvist et al. (2014) with only a short summary provided in this report.

The CEC experiment was performed employing a continuous injection of Cs^+ combined with injection of a non-sorbing tracer (Uranine) with the intention of reaching a steady-state plateau for the non-sorbing tracer concentration. The injection was performed in three steps, each step employing increased injection concentration of Cs^+ and Uranine. If effects of site saturation affect the sorption behaviour of Cs^+, this should be more readily visible as injection concentration increases.

Figure 3-7 illustrates the effects of site-limitation on sorption and shows simulations of one-dimensional advective-dispersive transport with an equilibrium non-linear sorption isotherm (Langmuir) for Cs. Two cases are simulated: one with moderate and one with relatively strong Cs^+ retardation. At low injection concentrations (step 1), no significant site limitation occurs in the simulated results of Cs^+ transport. The breakthrough curves of Cs^+ in step 1 would look the same regardless of injection concentration, as long as the injection concentration is not high enough to induce site limitation.

During injection step 2, seen in Figure 3-7, the retardation of Cs^+ is significantly decreased due to site limitation effects; the more moderate sorption case is here not possible to distinguish from the non-sorbing tracer. For the highest injection concentration (step 3), even the case with the stronger sorption shows very little retardation. It is also possible to discern the front-sharpening effect by comparing the steepness of the breakthrough curves for the case with stronger sorption. Thus, the absence of retardation after a concentration increase would suggest that the concentration in the preceding injection step was high enough to obtain a more or less full occupation of all available sorption sites. By integration of the difference between the breakthrough curves for the non-sorbing and sorbing tracers, an estimate of the total mass of adsorbed Cs can be obtained.

In order to obtain saturation of cation exchange sites, it is necessary that (given the present example) the adsorption of Cs^+ is strong enough to outcompete adsorption of other cations present in the system. This makes it necessary to apply a significantly higher injection concentration than the natural concentration. This is somewhat of an optimisation process as too high concentration would result in only a negligible part of the sorbing tracer lost in the experiment; i.e. more or less identical breakthrough curves for the non-sorbing and sorbing tracers during the entire experiment (see Figure 3-7). Scoping calculation based on selectivity coefficients and CEC determined in laboratory experiments (Byegård et al. 1998) indicated (Figure 3-7) that concentrations in the range of 1 mM would be appropriate to obtain a reasonable saturation but still having a clearly observable retardation of Cs^+ compared to Uranine. This concentration can be compared with the natural concentration of Cs^+ in the groundwater which has been measured at $2.4 \cdot 10^{-5}$ mM, i.e. any contribution from the natural concentration will be negligible compared with that of the injected Cs^+. However, the strong retardation observed in the in situ experiments (STT1 and STT2 e.g. Winberg et al. 2000) could be interpreted as a higher CEC of the transport path compared with the results of the laboratory experiments. The planning therefore included successive increase of the injection concentration to 3 mM and 10 mM, respectively.

The field experiment was carried out according to the injection sequence described above. However, equipment failure at two separate occasions affected the shape of the breakthrough curves, but the calculation of the integrated difference between breakthrough curves of Cs^+ and Uranine was not considered to be severely affected by the disturbances caused by the failures.

In Figure 3-8, relative concentrations of Uranine and Cs^+ are shown for both the injection section (KXTT4:T3) and the pumping section (KXTT3:S3). As can be seen, the breakthrough curves of Cs^+ did not reach steady-state in either of the injection steps. Furthermore, there are no visually obvious front-sharpening effects, indicative of site-limitation with increasing injection concentration.

The Uranine concentration in the pumping section was constant towards the end of the last step despite that the concentration of Uranine in the injection section was increasing. This is unexpected but could possibly be explained if the flow rate from KXTT4 to KXTT3 was decreasing at the time. However, no such continuous measurements of the flow rate in KXTT4 were made during the experiment.

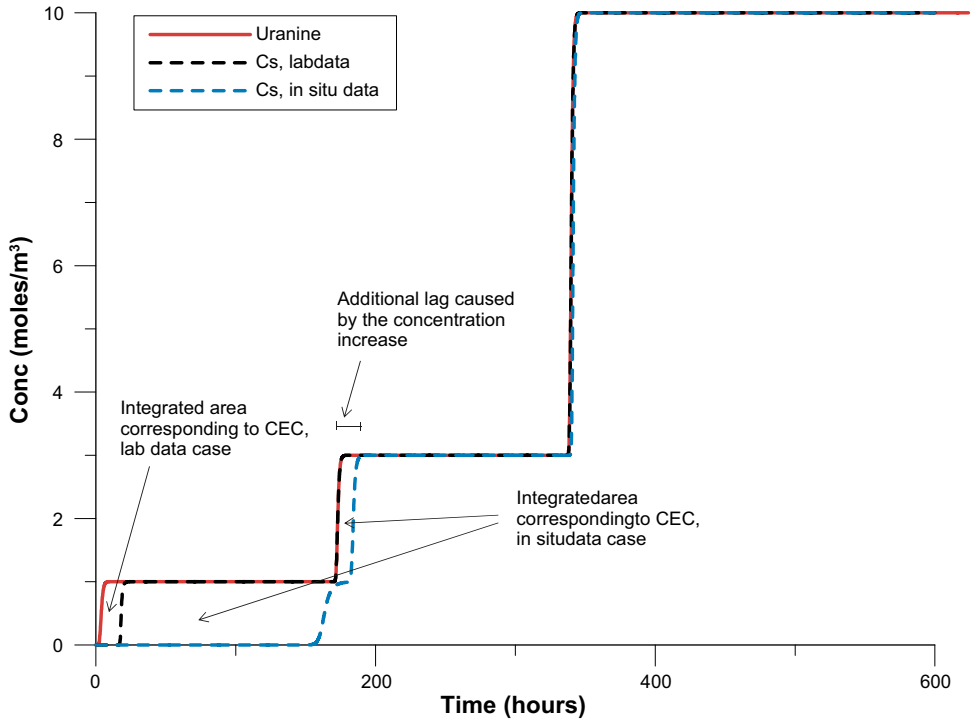

Figure 3-7. *Scoping simulations for the CEC experiment, assuming one week of continuous injection of 1, 3 and 10 mM, respectively, of Cs^+ and Uranine. The black dashed line shows breakthrough of Cs^+ provided that the retardation is determined from the cation exchange characteristics of the batch laboratory experiments performed on mylonite. The blue dashed line corresponds to a case of stronger retardation based on data from previous in situ tracer experiments (STT1).*

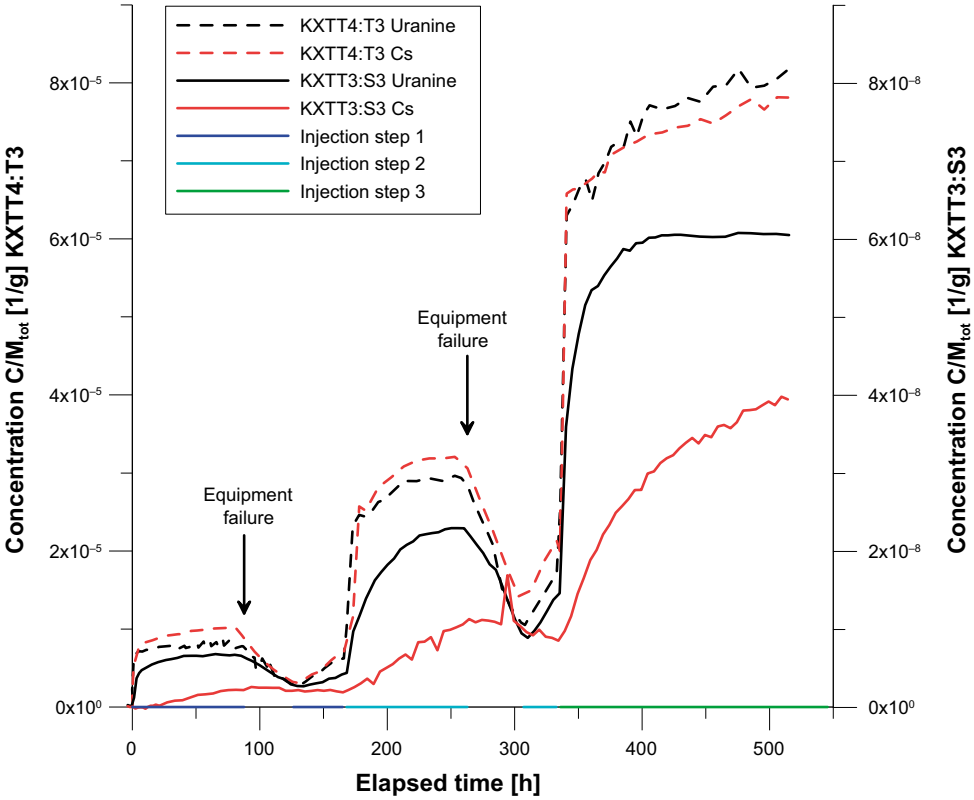

Figure 3-8. *Experimental tracer injection curves (continuous injection in borehole section KXTT4:T3, shown as dashed lines and projected on the left axis) and breakthrough data collected in KXTT3:S3 (solid lines). Injection was performed in three steps with different concentrations 1, 3 and 10 mM. The steps are indicated using lines of different colour along the X-axis. The values on the y-axis refer to the normalized concentration, i.e. concentration divided by the total injected mass during the entire experiment.*

An integration of the breakthrough in the pumping section over time revealed that 0.047 moles of Cs^+ had been lost during the experiment, which thus can be interpreted as the minimum amount of cation exchange sites available in association with the flow path. However, since there is no obvious observation of any site-limiting effect, it is likely that the total sorption capacity of Cs^+ in the tested flow path is considerably higher.

Several models were used to try to make a better estimation of the Cs^+ lost in the flow path if the third and final injection step had been longer. Figure 3-9 shows the result of one such estimation from Nordqvist et al. (2014) using an one-dimensional advection-dispersion model combined with a Langmuir sorption isotherm. In this case the estimation resulted in a loss of 0.06 moles of Cs^+ if the experiment had been prolonged.

A number of possible explanations are provided for the noted indication of higher number of sorption sites obtained from the results of the CEC experiment compared with the results of the scoping calculation based (cf. Figure 3-8) on the laboratory experiments (Byegård et al. 1998). One possibility would be that gouge material with a high content of clay minerals would be present in the transport path which would increase the cation exchange capacity of the transport path. The presence of such material was not addressed in the scoping calculation since no observation of such material was made in the core sampling during the original drilling of the borehole. However, since this drilling was performed without applying the triple tube technique, one can speculate that such material may have been flushed away during the drilling, i.e. the core sampling would not be representative to the real conditions in the transport path, or at least not of conditions at the points of borehole intercept. Based on experimental results from gouge materials sampled at other locations in the Äspö HRL (Byegård and Tullborg 2012) a CEC of 0.14 mole/kg could be anticipated if a clay rich gouge material would be present in the flow path. To reach this magnitude of the number of cation exchange sites estimated from the modelling, a total amount of at least 0.6 kg of gouge material has to be present in the flow path. However, the results from the excavation of parts of the flow path (Section 5.3 in this report) still show very minor traces of gouge material present in fracture and therefore do not support this hypothesis.

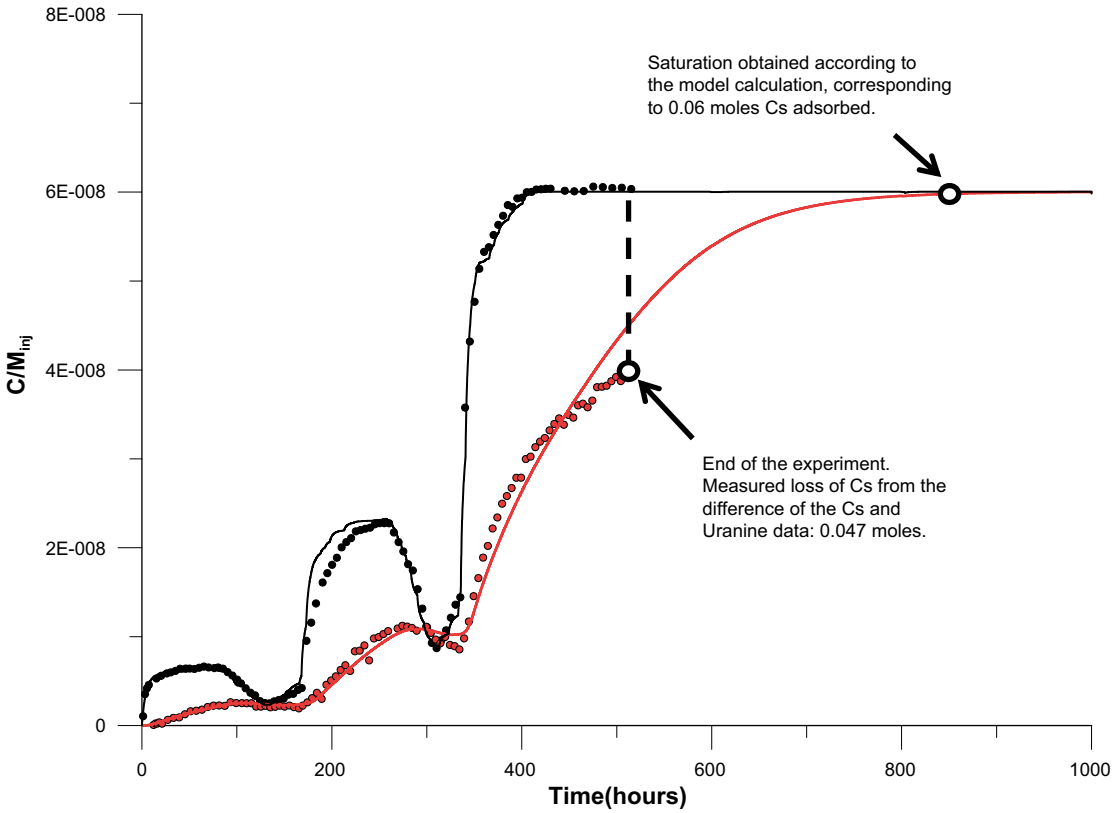

Figure 3-9. *Extension of the calculated breakthrough curve to a steady-state concentration of Cs.*

Another possible explanation of the high amount of CEC necessary to explain the results of the experiment is that diffusion of Cs^+ into the inner surfaces of the rock would take place during the experiment. However, penetration depths for a strongly sorbing tracer like Cs^+ can both from experimental experience (e.g. Byegård et al. 1998) and diffusion calculations, presented by Nordqvist et al. (2014), be assumed to be extremely small in the case of the relatively short experimental time frames. Nevertheless, one can assume that the use of an elevated Cs^+ concentration in this experiment causes a successive saturation of the surfaces of the pores along where the diffusion is taking place. Thereby an increased effective diffusion rate of the tracer would occur and a larger amount of cation exchange sorption sites would be made accessible. Matrix diffusion may thus provide a plausible explanation for the results of the experiment. In the work of Nordqvist et al. (2014), a rough estimation was performed of the maximum additional CEC which could be obtained by this matrix diffusion process. In this calculation, it was assumed that a saturation of the sorption sites was obtained already at the diffusion front and that this front therefore was spread at a rate corresponding to a non sorbing tracer, i.e. no retardation in the diffusion due to sorption. By applying an obvious overestimation of the diffusion penetration depth, it was found that a maximum of 10 times higher CEC (compared with the surface sorption model) should be possible to obtain within the time frames of the experiment. However, since the lost amount of Cs was far more than 10 times of the Cs loss predicted using the sorption model, it is obvious that the matrix diffusion concept in itself is not sufficient to explain the results obtained.

Another possible explanation for the higher observed sorption capacity in the in situ experiment compared with the scoping calculation could be that that the transport path has far more available fracture surface area than what was estimated with the simple single fracture model used in the scoping calculation. Several concepts of estimating the surface area of the transport path, based on various geometrical assumptions are described in Nordqvist et al. (2014). By dividing the minimum amount of Cs^+ proven lost in the in situ experiment (i.e. 0.047 moles) by the estimated surface area, a surface-based minimum CEC can be obtained which can be compared with the laboratory determined value. However, irrespective of which surface concept that is used, a minimum CEC is in any case obtained that is significantly higher than the corresponding value estimated from the laboratory experiments.

On the other hand, the selectivity coefficient for the presumed dominant cation exchange reaction between Cs^+ and Ca^{2+} (i.e. the parameter determining the sorption strength of the tracer) has been found to be significantly lower for the in situ CEC test compared with the values determined in the laboratory experiments (30 and 700 $M^{½}$, respectively). This observation could be indicative of a concentration-dependent sorption pattern in which the interaction, in the case of low Cs^+ concentration (i.e. the laboratory experiment together with the STT1 and STT2 experiment), mainly takes place with a low number of highly selective sorption sites. Increased Cs^+ concentration (as in the present CEC experiment) would, according to this explanation, imply that an increased part of the sorption occurs by interaction with sorption sites that are less selective for Cs^+.

It should also be acknowledged that there is a general lack of fit in the modelling of the Cs^+ breakthrough curve; the experimental data seem to level out in a way that cannot be explained by the model assuming equilibrium sorption (i.e. a sorption model implying that all sorption sites are directly accessible for sorption, independent of the contact time applied). From a qualitative perspective, matrix diffusion would cause increased sorption of Cs^+ with increased contact time.

The CEC experiment also included a desorption part in which the behaviour of the radioactive Cs^+ tracer previously used in STT1 and STT2 experiment was studied. It was demonstrated that less than 1 % of the "old" Cs^+ was desorbed and recovered in the pumping section during the experiment while the corresponding calculation for the Cs^+ injected during the CEC experiment suggests that more than 70 % of the tracer injected in to the fracture reached the pumping borehole. This discrepancy may be associated with one or several of the following possible explanations:

- An irreversible (or at least kinetically restricted) sorption process: This would imply that the use of Cs^+ in low concentration (as in the previously performed tracer experiment) to a high degree would be characterized by interaction with irreversible sorption sites and the use Cs^+ in high concentrations (as in the CEC experiment) would be less characterized by irreversible sorption; i.e. some kind of saturation of the irreversible sorption sites should be anticipated. The existence of such irreversible (or at least kinetically restricted) processes is known from the literature (e.g. Cornell 1993) and has also been motivated from the results of different laboratory experiment using site specific rock material (e.g. Byegård et al. 1998). This explanation is also supported by the modelling of the CEC experiment where adding a component of irreversible sorption gives a better explanation of the shape of the breakthrough curve. However, if irreversible sorption should have an impact on the breakthrough curve of the high concentration experiment, the number of available sites for irreversible sorption must be comparatively high; certainly high enough, from a mass balance perspective to have caused a complete irreversible sorption of the radiotracer concentration of Cs^+ in the STT1 and STT2 experiment. Since this did not occur (i.e. breakthrough of Cs^+ was obtained in both these experiments) a simplified sorption model involving irreversible sorption sites cannot provide a consistent explanation for the Cs^+ behaviour in the different experiments. However, one can address a kinetic transport model where the entrapment of Cs in irreversible (or slowly reversible) sorption sites requiring long contact time, i.e. the part of the Cs arriving to the observation borehole should not have had time to reach the irreversible sorption sites and have only interacted with reversible sorption sites. This hypothesis is nevertheless contradicted by the results in Byegård et al. (1998) where no strong evidence of increased irreversibility with increasing sorption time was found in the results; a large part of irreversibility could be found already using a sorption time of two days.
- It is possible that different flow paths were activated in the different experiments, i.e. the high concentration Cs^+ was transported in different flow paths compared with the STT1 and STT2 experiments and was therefore not able to cause desorption of Cs^+. This explanation is to some extent supported by the variation in flow responses between the pump borehole and the injection borehole over time, illustrated by Nordqvist et al. (2014, Table 4-12) .
- It is approximately 10 years between the CEC and the STT tests. During this time it is possible that some of the Cs^+ desorbed and transported with the natural flow to a location in the fracture not affected by the elevated Cs^+ concentration during the CEC test and therefore not desorbed. This explanation is to some extent contradicted by the results of the excavation part of this project (Section 5.4) where the highest amount of radioactive Cs^+ actually is found in the closest vicinity of the injection borehole. No proof of an ongoing desorption combined with transport in natural background flow could thus be found.

- During sorption of Cs^+, diffusion further in to the rock will occur and it is therefore possible that one can have a higher sorption capacity compared with the case when only addressing surface sorption. An attempt to address matrix diffusion performed in Nordqvist et al. (2014) shows that as a maximum a factor of 10 higher sorption capacity would be obtained by diffusion into the pores of the rock, which however cannot explain the difference in sorption capacity between the laboratory experiments and the CEC observed in the in situ Cs+ sorption experiment.

4 Epoxy injection, overcoring and core logging

Epoxy injection and overcoring of KXTT3 and KXTT4 were necessary in order to fulfil the project's general objective of improving the knowledge of the internal structure of Feature A, including identification and description of the immobile zones that are involved in the noted retention.

The specific objectives of the epoxy injection, overcoring and core logging of the target sections including Feature A in sections KXTT4:T3 and KXTT3:S3 were to:

- Stabilise features in the vicinity of the borehole.
- Provide protection against flushing out of adsorbed tracers during the overcoring.
- Recover large diameter cores of resin injected sections.
- Provide material and overview characterisation as a basis for subsequent sample preparation, analysis and mapping of Feature A.

The techniques used for epoxy injection and overcoring of KXTT3 and KXTT4 have earlier been used successfully in the TRUE-1 Pilot Resin Experiment as reported by Birgersson et al. (2000a, b) and the TRUE-1 Continuation Fault Rock Zones Characterisation project (Mærsk Hansen and Staub 2004, Winberg 2010) at Äspö HRL.

The epoxy injection, overcoring and core logging of KXTT3 and KXTT4 are described in Sigurdsson and Hjerne (2014).

4.1 Epoxy injection

The epoxy injection in sections KXTT3:S3 and KXTT4:T3 was performed using the epoxy EpoTek 301 with Uranine added (essential for the subsequent analysis). Prior to the epoxy injection, isopropanol was injected in order to facilitate the injection and adhesion to the structures of the epoxy by replacing the water.

It was important to not use a higher pressure than necessary during the isopropanol and epoxy injections in order to reduce the risk for displacement of filling material in the fracture. On the other hand, the epoxy injection had to be performed within a reasonable time, otherwise the epoxy would harden before a sufficient amount had been injected. Hence, the injections were carried out according to a prepared strategy based on injection pressure and estimated required flow rate. It was foreseen based on injection of water in KXTT4:T3 during a SWIW-test (Nordqvist et al. 2014), that an injection pressure of 2 to 3 bars above the natural pressure (approximately 32 bar) would be sufficient, despite the slightly higher viscosity of the epoxy. Feature A has a higher hydraulic transmissivity in KXTT3 than in KXTT4 (Winberg et al. 2000), implying that 2–3 bars also would be sufficient in the case of KXTT3:S3.

In KXTT3, 4.2 litres of epoxy was injected over 5 hours following the exchange from isopropanol to epoxy with a final pressure in the target section of 2.5 bars above the original section hydraulic pressure. In KXTT4, a final pressure of up to 10 bars above the original section hydraulic pressure had to be applied in order to achieve a reasonable epoxy flow rate. In total, 0.4 litres epoxy was injected over 12 hours in this case.

4.2 Overcoring

In between the epoxy injection and the overcoring, the hydraulic packers outside the target sections were removed. Furthermore, in order to enable good guidance for the subsequent overcoring the original 56 mm boreholes were reamed to 76 mm down to the target sections.

The overcoring of KXTT3 and KXTT4 was performed with a drill bit diameter of 300 mm, resulting in a core with a diameter of 278 mm. A pilot was used in the existing 76 mm borehole to provide guidance for the overcoring. The overcoring was an iterative process of drilling and successively retrieving core pieces. If the core did not break naturally within a certain distance, breaking tools were inserted and a break of the core was induced. After a few metres the overcoring in KXTT4 was deviating from the desired direction towards KXTT3, so the overcoring had to continue without the steering in the pilot hole. Fortunately, the deviation was limited such that the original 56 mm borehole was included in the retrieved core covering the target section.

The goal with the overcoring was to retrieve core pieces from the target sections including Feature A and A' were the epoxy injected kept the fractures intact. However, the stabilisation effect of the epoxy was not sufficient to withstand the forces acting on the core during drilling and retrieval, such that the fractures containing epoxy were not recovered intact from the boreholes. At the subsequent inspection of the cores it turned out that the penetration of epoxy into Feature A was good in both KXTT3 and KXTT4. The epoxy itself did not break, instead it seemed like the points of breakage for the most part occurred between the fracture wall rock boundary and the fracture surface mineral. The fracture filling in the open fractures was mainly, chlorite, resulting in a core relatively easily broken during drilling.

4.3 Core logging

The cores from the target sections of KXTT3 and KXTT4 turned out more broken than anticipated before the overcoring. Accordingly, the orientation and length position of the cores had to be reconstructed using BIPS images from the original 56 mm boreholes. All core pieces in the target sections that could be re-combined were given a number for easy identification. Four orientation lines were drawn along the core in four colours with length markings every 10 cm. The target sections of both boreholes were mapped in detail including borehole length, fracture position, fracture orientation, fracture wall alteration, fracture mineral fill and locations of identified epoxy filling. Fracture position and orientation were determined by measuring the borehole length to the intercepts between the fracture and the four orientation lines.

The main rock type in the target sections of KXTT3 and KXTT4 is medium to coarse grained, mainly massive Äspö diorite (porphyritic quartz monzonite to granodiorite) with minor amounts of fine-grained granite. The rock types are usually massive, with some deformation occurring in conjunction with Feature A. The main fracture filling mineral is chlorite, with lesser amounts of epidote and calcite. Chlorite and epidote occur in both open and closed fractures, while calcite only appears in open fractures within the target section of KXTT3. The observed features in the retrieved core from the overcoring coincide with the lithological description presented by Bossart et al. (2001) for both KXTT3 and KXTT4.

Figure 4-1 shows an overview of the mapped large diameter core from the target sections of KXTT3 and KXTT4 including core piece numbers. Yellow dashed lines indicate fracture surfaces where epoxy was found. The maps show the structures as they appear in the borehole wall of the large diameter borehole, i.e. this map is comparable with the BIPS images from the original 56 mm pilot boreholes. The notation at the right and left side of core refers to the directions when looking from the tunnel and inwards and top of cores refers to the upward side of the drill core as oriented in the borehole. Figure 4-2 shows a detail of Figure 4-1a showing the core close to Feature A in KXTT3. The fractures in this part were also given the number 1–5 to enable further reference.

According to the original logging of the 56 mm borehole and core, fractures characterised as open within the target section of KXTT3 were found at 13.075, 13.39, 13.41 with Feature A at 14.10 m borehole length (Bossart et al. 2001). These fractures were also found to contain epoxy during the overcoring, see Figure 4-1a, but that the fracture between core pieces 3, 5, 7, 8 and 12 (corresponds to 13.39 and 13.41 m) only contained trace amounts of epoxy. Fractures 1 to 3 and 5 in Figure 4-2 display a strike and dip similar to earlier reports for Feature A (Winberg 1996). Fracture 4, on the other hand, display a distinctly different dip than the rest of the fractures associated with Feature A. In fact, Fracture 4 has a dip and strike similar to the fracture at 13.1 m (between core pieces 2 and 3). These observations in KXTT3 support the conclusion in Winberg et al. (2000) that Feature A is a structure made up of several interconnected fractures.

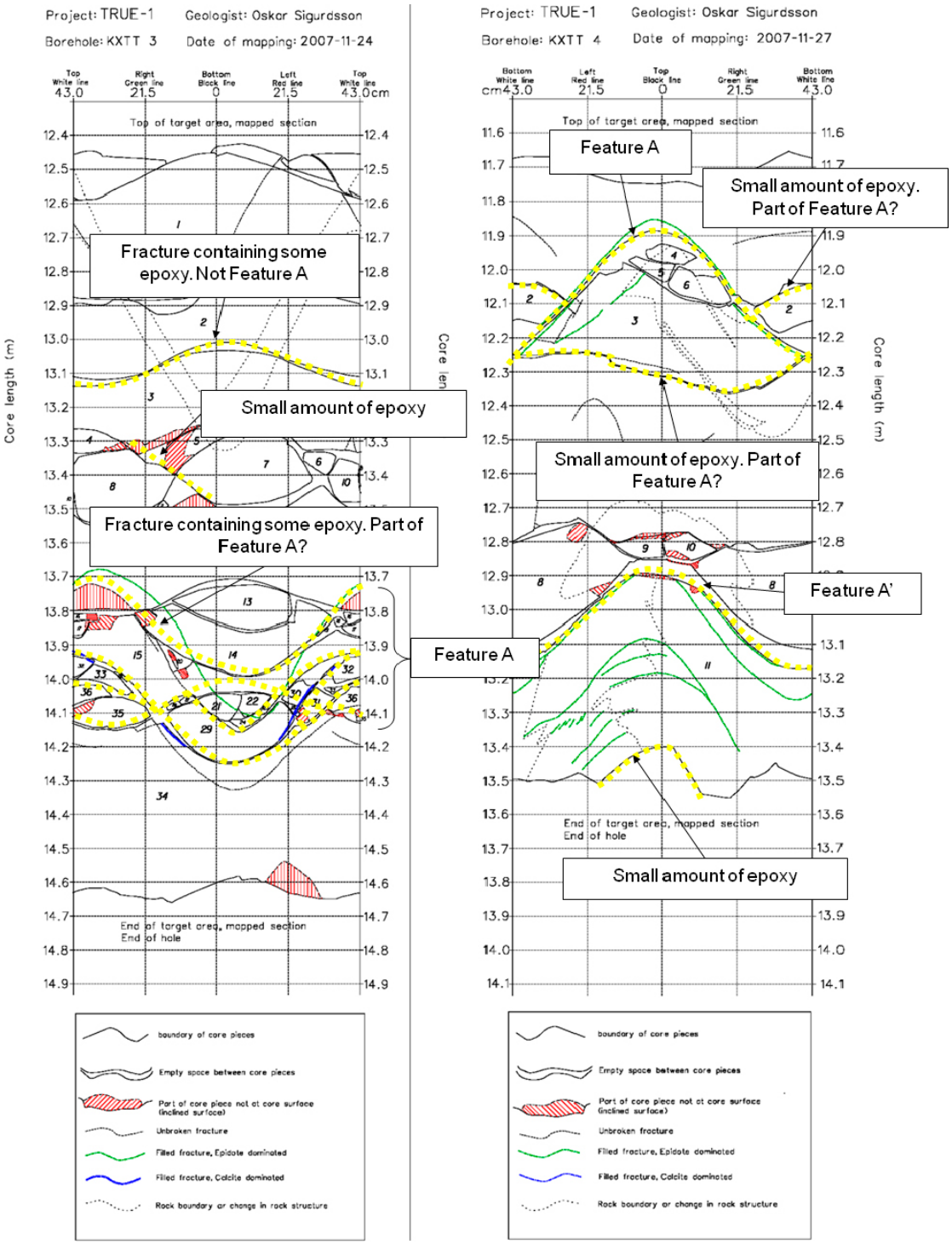

Figure 4-1. *a) KXTT3 b) KXTT4. These maps shows the structures as they appear on the borehole wall. Dashed yellow lines indicate fractures containing epoxy.*

Fractures within the target section characterised as open in the original core logging of the 56 mm KXTT4 borehole were found at 12.11 (Feature A), 13.02 (Feature A') and at 13.49 m borehole length (Bossart et al. 2001). This is in agreement with epoxy observed from the overcoring. However, small amounts of epoxy were also found in the fractures between core pieces 1 and 2 as well as between core pieces 3 and 7, see Figure 4-1b. These fractures deviate from Feature A in both strike and dip and lack natural fracture filling. These two fractures have very small apertures and may be interpreted as not being significantly flowing compared with Feature A, at natural conditions. The same interpretation may also be applicable to the fracture at the bottom of core piece 11.

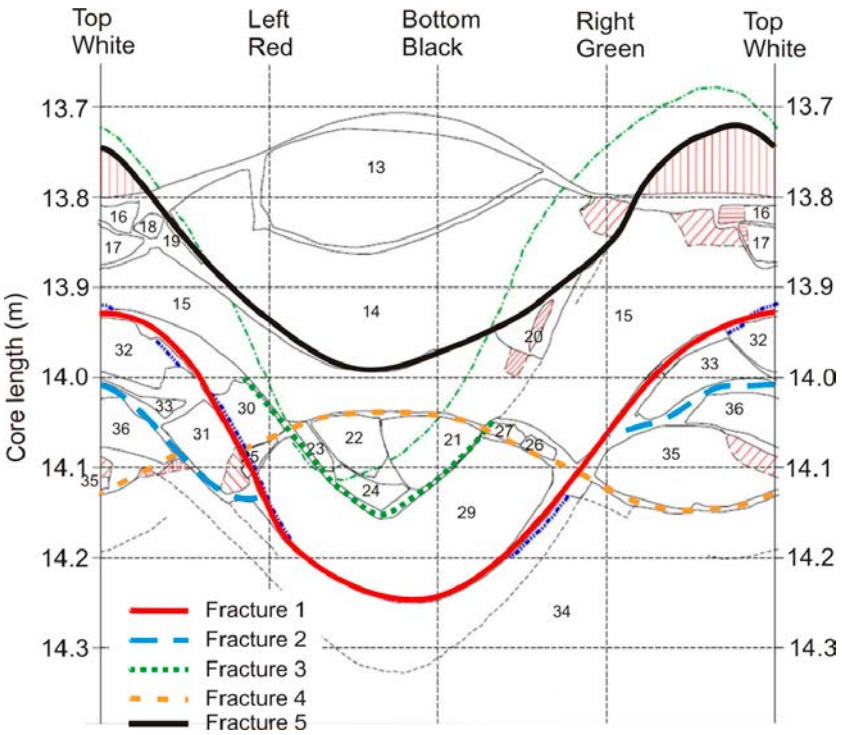

Figure 4-2. *Detail of the target section of Feature A in KXTT3. The picture is a mirror image of Figure 4-1a, thus showing how the drill core looked.*

Epoxy was found to cover, at least partially, the entire overcored part of Feature A in both KXTT3 and KXTT4, implying that a sufficient amount of epoxy had been injected. Figure 4-3 through Figure 4-8 show some major fractures in both KXTT3 and KXTT4 containing epoxy, clearly visible due to the added Uranine and the UV-lighting used in the photography. The darker areas in the overview photographs should not be regarded as not being covered by epoxy because the epoxy is in some areas covered by a thin layer of clay materials that make the epoxy surface appear dark in UV-light. Also, the epoxy most often was attached to only one, but varying, side of the fracture. Furthermore, the epoxy layer was slightly loose at some points and some minor pieces have fallen off, but the selected surfaces for study seemed to be largely intact.

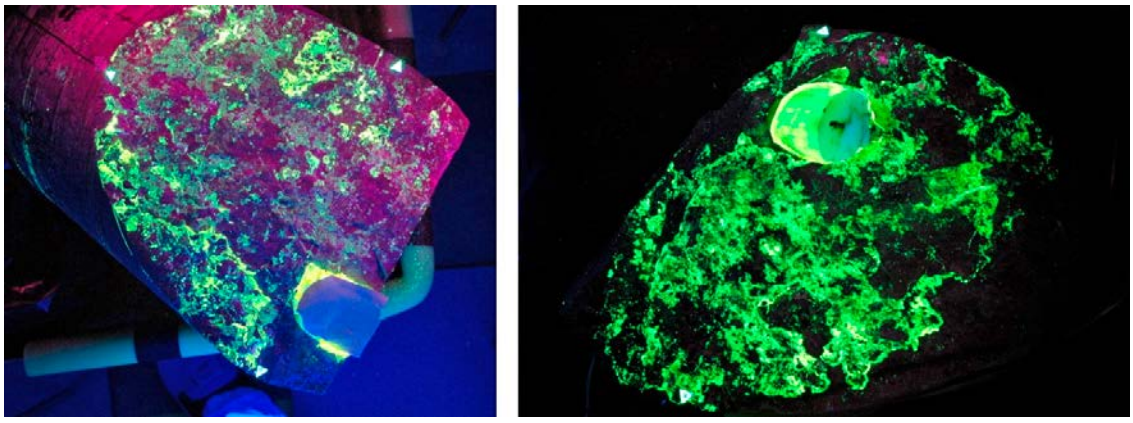

Figure 4-3. *KXTT4, Feature A, core piece 1 (to the left) and 3 (to the right) in UV-lighting.*

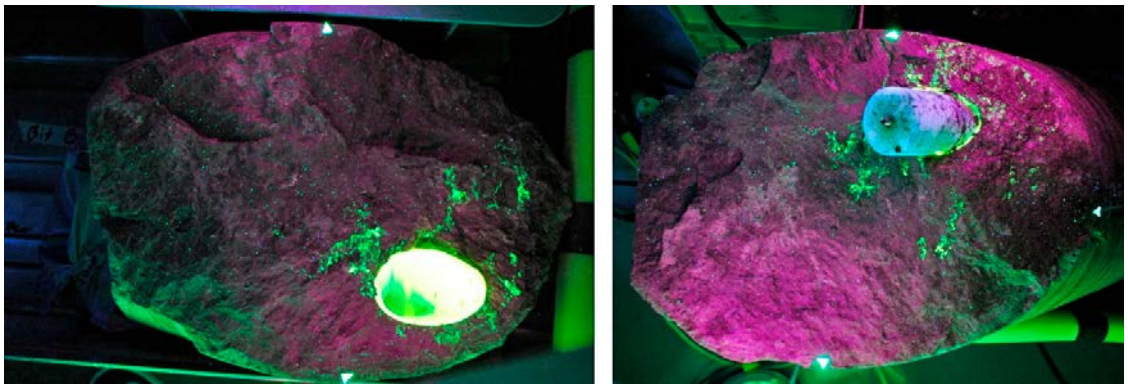

Figure 4-4. *KXTT4, Feature A', core piece 8 (to the left) and 11 (to the right) in UV-lighting.*

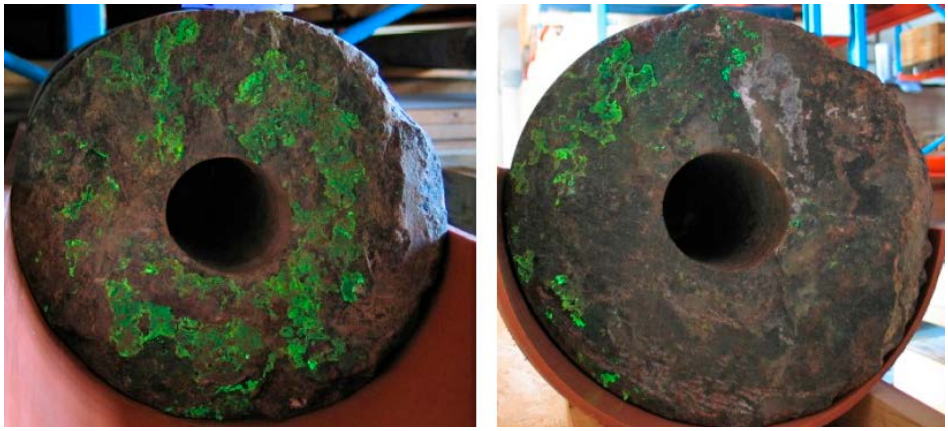

Figure 4-5. *KXTT3, fracture at c. 13.1 m, core piece 2 (to the left) and 3 (to the right) in UV-lighting.*

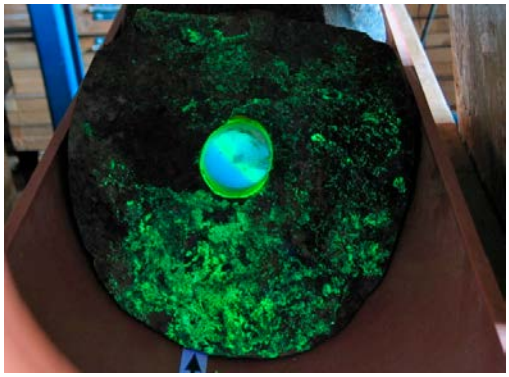

Figure 4-6. *KXTT3, core piece 14 in UV-lighting (Fracture 5 according to Figure 4-2).*

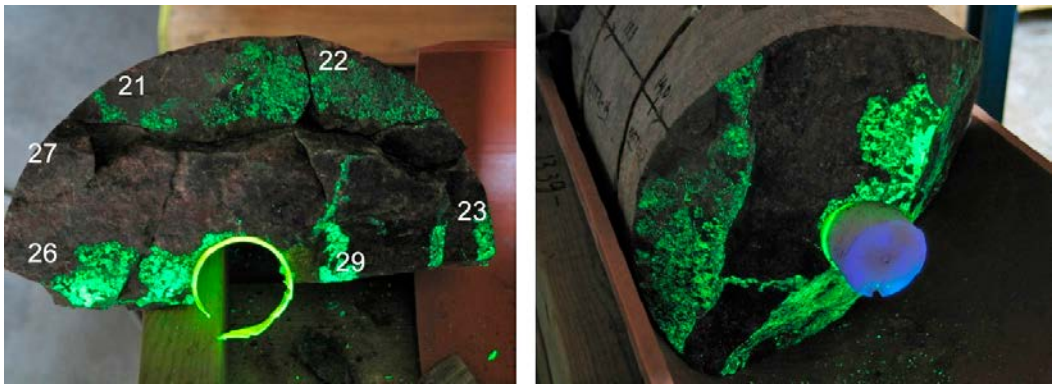

Figure 4-7. *KXTT3, core pieces 21–23, 26, 27, 29 (to the left) and 15 (to the right) in UV-lighting (Fracture 4 according to Figure 4-2).*

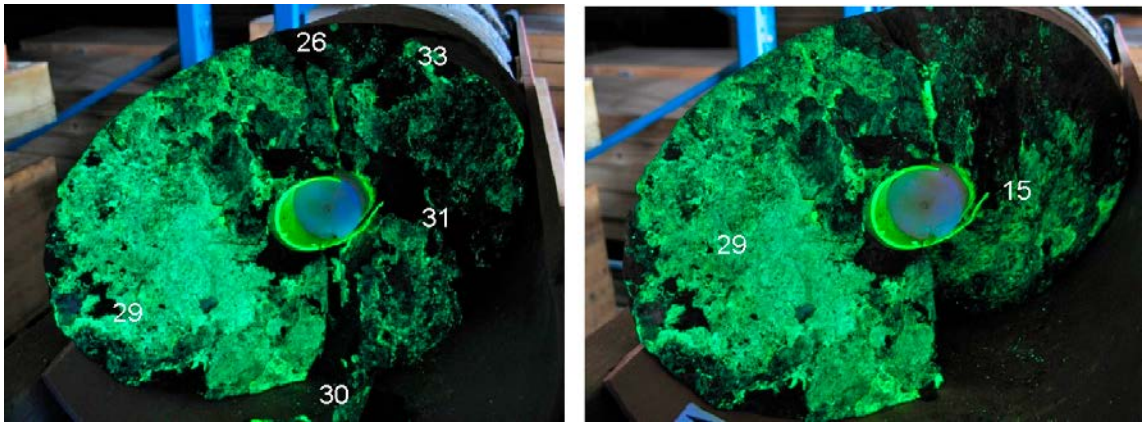

Figure 4-8. *KXTT3, core pieces 26, 29, 30, 31, 33 (to the left) and 15 (to the right) in UV-lighting (Fracture 1 and 2 according to Figure 4-2).*

4.4 Geometrical modelling of open fractures

Open fractures found to contain a significant amount of epoxy in the large diameter cores, as described above, were included in a 3D model made in MicroStation. The four length marks (top, bottom, left and right) of each fracture were used to decide the position and direction of each structure in the model. Since only three length marks are necessary to determine the position and direction, there are four alternative extrapolations for each fracture. Figure 4-9 and Figure 4-10, show examples were the differences between the extrapolations of the four alternatives are small and large, respectively. In the subsequent figures, the alternative regarded as closest to the average in terms of strike and dip is shown.

The extrapolated structures considered as the major fracture planes, Feature A and A' in KXTT4 and Fracture 1 of Feature A in KXTT3, are shown in Figure 4-11. The corresponding extrapolations based on BIPS images of Feature A and A' are shown in Figure 4-12. When comparing the two figures, it is obvious that the extrapolations from the large diameter core and BIPS images, respectively, are different. It is difficult to firmly establish if the extrapolation from the large cores or the BIPS images is the most reliable. Both are associated with possible sources of error, but they are not quantified further here. However, they both indicate a similar deviation from Figure 1-4. The extrapolation of Feature A from KXTT4 intercepts borehole KXTT3 closer to the tunnel (at shorter borehole length) than Feature A in KXTT3. Vice versa, the extrapolation of Fracture 1 from KXTT3 is intercepting KXTT4 further into the borehole than Feature A in KXTT4. Based on these extrapolations it seems unlikely that Feature A is a simple single fracture with the splay Feature A' as illustrated in Figure 1-4.

Figure 4-13 shows extrapolations of all fractures, except Fracture 3 in KXTT3, found to contain a significant amount of epoxy in the large diameter cores. This gives a more complex view of the fracture system than previous figures.

The intercepts of Feature A in boreholes KXTT1 through KXTT4 and KA3005A as reported by Winberg et al. (2000) and KXTT5 (taken from BIPS logging) were interpolated with a single plane by using a least squares method to have a strike and dip of 341/79. The largest deviation from the interpolated fracture plane to any of the borehole intercepts is 10 cm, indicating that the six intercepts interpreted as Feature A are all rather close to a planar feature.

It was found during this work that earlier reports of strike and dip of Feature A intercepts in Winberg (1996) and Winberg et al. (2000) were not reported in the Äspö local coordinate system (Äspö-96). Strike and dip of Feature A intercepts were therefore reinterpreted from available BIPS files in Äspö-96 which are shown in Table 4-1. It is evident from Table 4-1 that there is a spread in strike and dip between the different intercepts of Feature A, but that the average strike and dip are similar to the interpolation of the six borehole intercepts.

The intercepts, interpolation and extrapolations presented above and in the figures below may be interpreted in at least two ways. The first interpretation is that the extrapolations presented in Figure 4-11 and Figure 4-12 are realistic. These separated fractures must in this case be interconnected via some other fracture since it has been firmly established in this project as well as in previous investigations (e.g. Winberg et al. 2000) that there is a clear hydraulic connection between the intercepts of Feature A. The fractures could be connected via the fracture at 13.12 m borehole length in KXTT3 as shown in Figure 4-13. There are however a number of observations suggesting that this interpretation is not valid. First of all, no intercepts of open fractures with a suitable strike and dip are found in the other boreholes where, according to the extrapolation, it should be. Besides, it is regarded as unlikely that the intercepts of Feature A in all six boreholes should be so very close to a plane if they in fact were not belonging to the same feature. Also the fact that the intercepts have a good hydraulic connection suggests that it is not a system of interconnected individual fractures. Instead, the persisting interpretation is that Feature A is a continuous feature. The different values of strike and dip presented in Table 4-1 may indicate that Feature A is undulating. The distance between the extrapolation of fractures from the large core diameters as well as from the BIPS images may suggest that a stepwise character of Feature A between KXTT3 and KXTT4 may also very well be the case. Such a stepwise character has previously been shown by e.g. Mazurek et al. (1996). The conclusion is that Feature A is undulating and/or has a stepwise character. This supports earlier conclusions in Winberg et al. (2000) of Feature A as undulating structure or a structure of interconnected fractures.

Table 4-1. Strike and dip of Feature A intercepts and interpolated integrated geometry in the Äspö local coordinate system (Äspö96).

Borehole	Feature	Borehole length [m]	Strike	Dip
KXTT1	A	15.77	343	79
KXTT2	A	15.02	353	77
KXTT3	A	14.10	338	78
KXTT4	A	12.10	338	75
KXTT4	A'	13.05	327	78
KXTT5	A	9.64	325	89
KA3005A	A	44.97	351	85
Average of Feature A intercepts			341	80
Interpolation of KXTT1 through KXTT5 and KA3005A	A	–	341	76

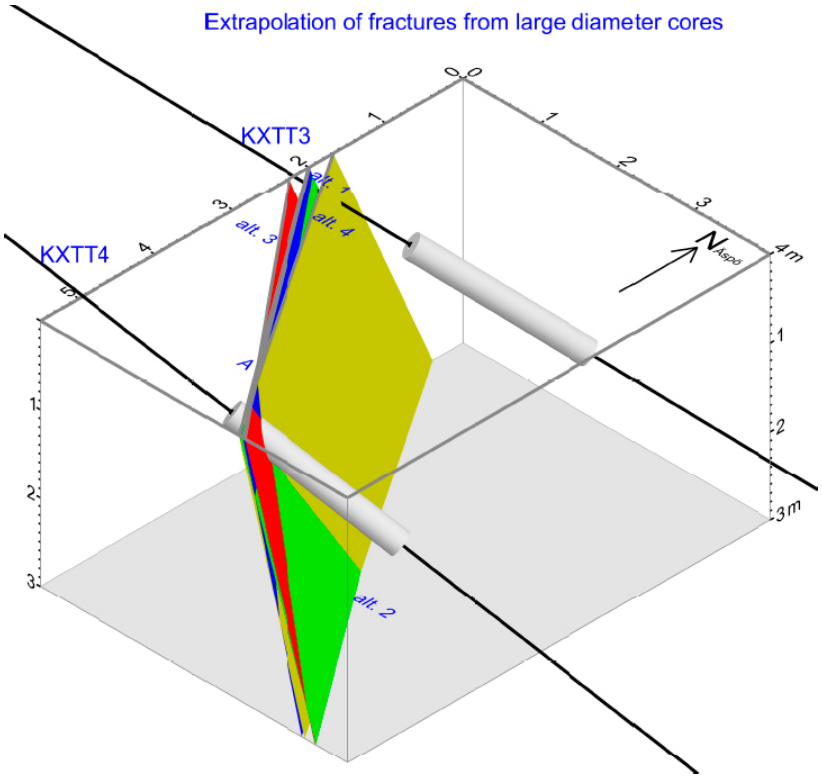

Figure 4-9. *Example of small differences in extrapolation of a fracture from a large diameter core intercept (Feature A, KXTT4).*

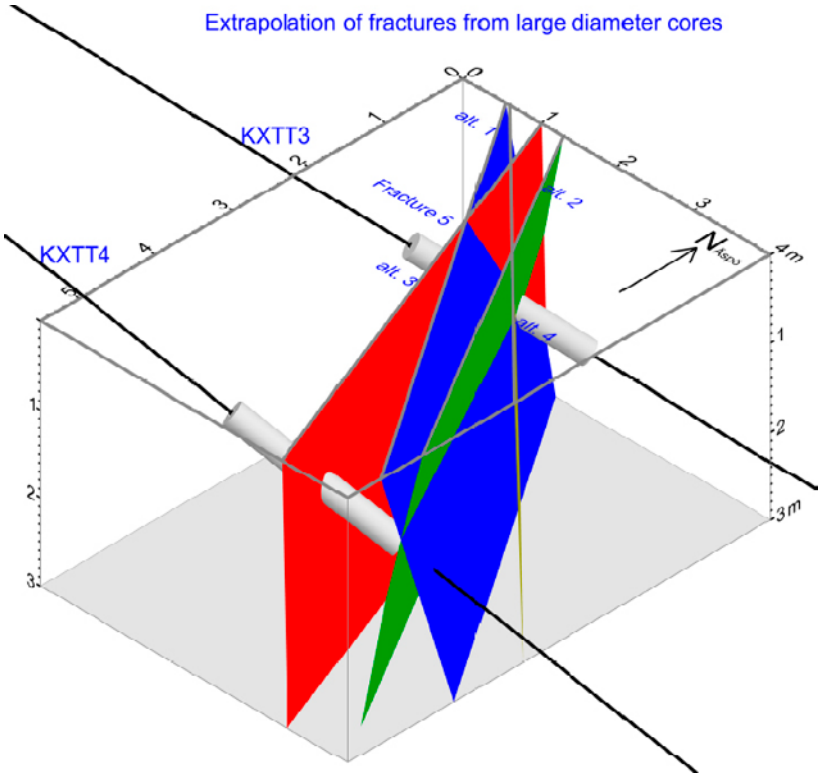

Figure 4-10. *Example of large differences in extrapolation of a fracture from a large diameter core intercept (Fracture 5, KXTT3).*

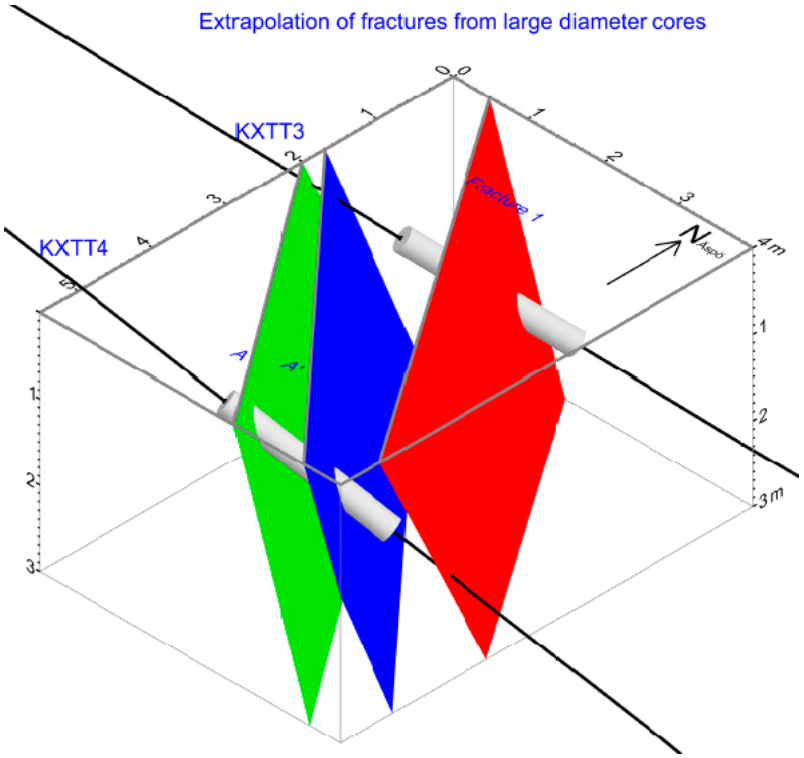

Figure 4-11. *Extrapolation from large diameter core intercepts of Feature A, KXTT4 (green), Feature A', KXTT4 (blue), Fracture 1, KXTT3 (red).*

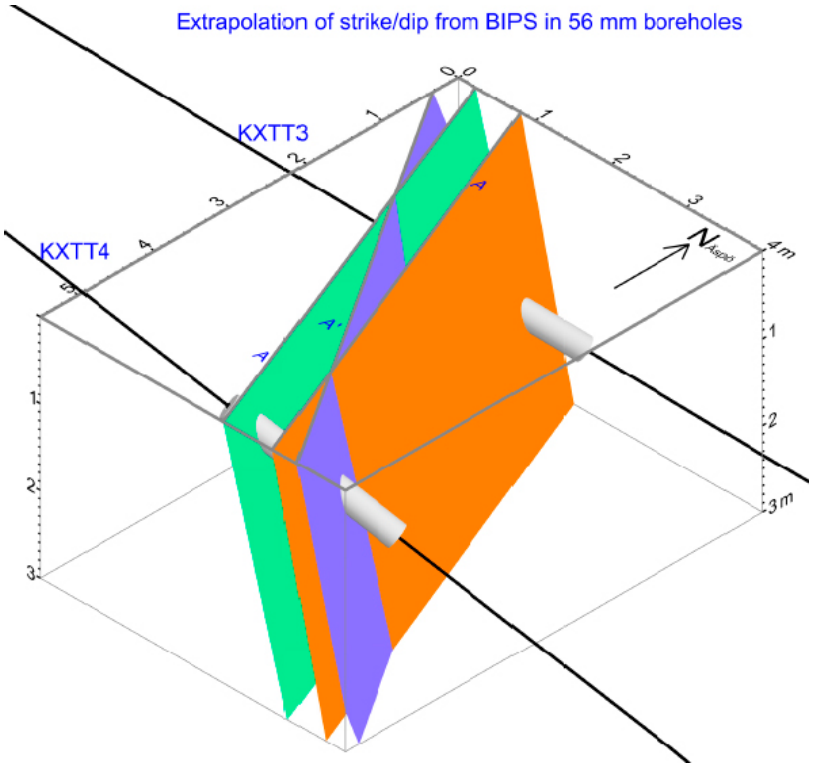

Figure 4-12. *Extrapolation from BIPS of fractures Feature A, KXTT4 (green), Feature A', KXTT4 (purple) and Feature A, KXTT3 (orange).*

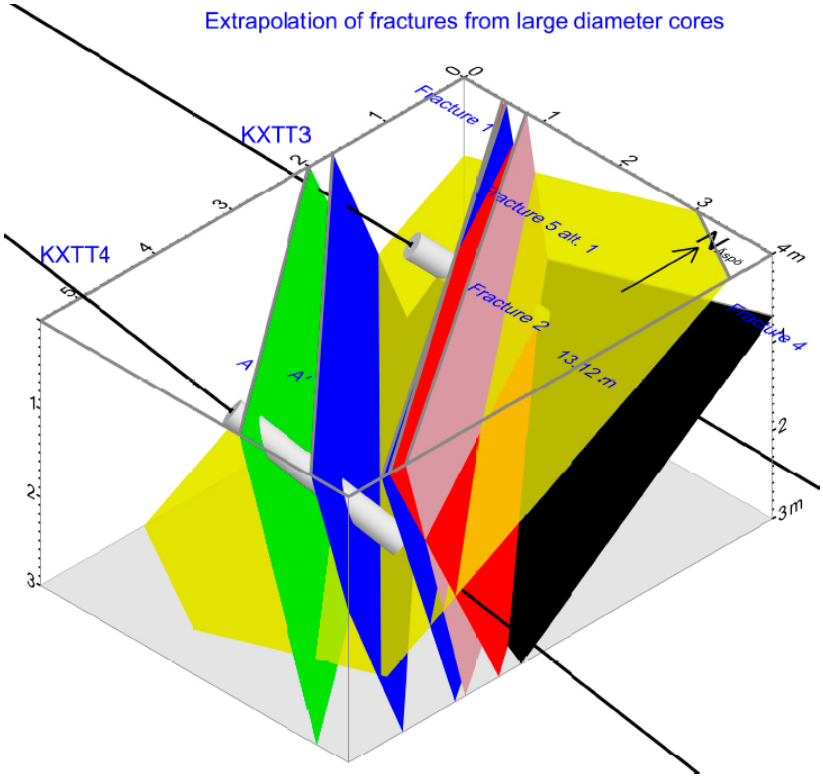

Figure 4-13. *Extrapolation from large diameter core intercepts of Feature A, KXTT4 (green), Feature A', KXTT4 (blue), Fracture 1, KXTT3 (red), Fracture 2, KXTT3 (purple), Fracture 4, KXTT3 (black), Fracture 5, KXTT3 (blue), fracture at 13.12 m in KXTT3 (yellow).*

5 Analysis of core material

Analysis of the material from the overcoring was carried out in order to provide results useful for updating of conceptual models, foremost improving the knowledge and description of the inner structure of Feature A, including identification of zones involved in retention processes.

The following questions were identified as important:

- How much, and what type of fault gouge material, is present in the feature?
- What does the aperture distributions look like?
- How much accessible surface for sorption exists in Feature A?
- Is it possible to show firm evidence of channelized flow?
- Do the intercepts of Feature A in KXTT3 and KXTT4 differ, and if so how?

If not stated otherwise in this chapter the results, figures, interpretations etc. are from Hakami et al. (2014) where the analysis of core material carried out within TRUE-1 Completion are presented.

5.1 Sample preparation

In order to carry out the analyses planned for the core material, it had to be cut into slices and rods. The surfaces were first reinforced with a thin layer of strong dark blue epoxy. Reference tapes were added on top of this surface to keep track of the relative coordinates of the slices (Figure 5-1). The result of the cutting of pieces from Feature A, and labelling of the slices are presented in Figure 5-2. Fracture A' pieces were cut in a corresponding way.

Figure 5-1. *a) KXTT3, core piece 15 with reinforced surface and measurement tapes added as reference lines before cutting. b) First cut of core pieces moulded in boxes using a larger cutter. c) Second cut into slices and rods using a smaller cutter. d) Slices and rods of core piece 15 from KXTT3.*

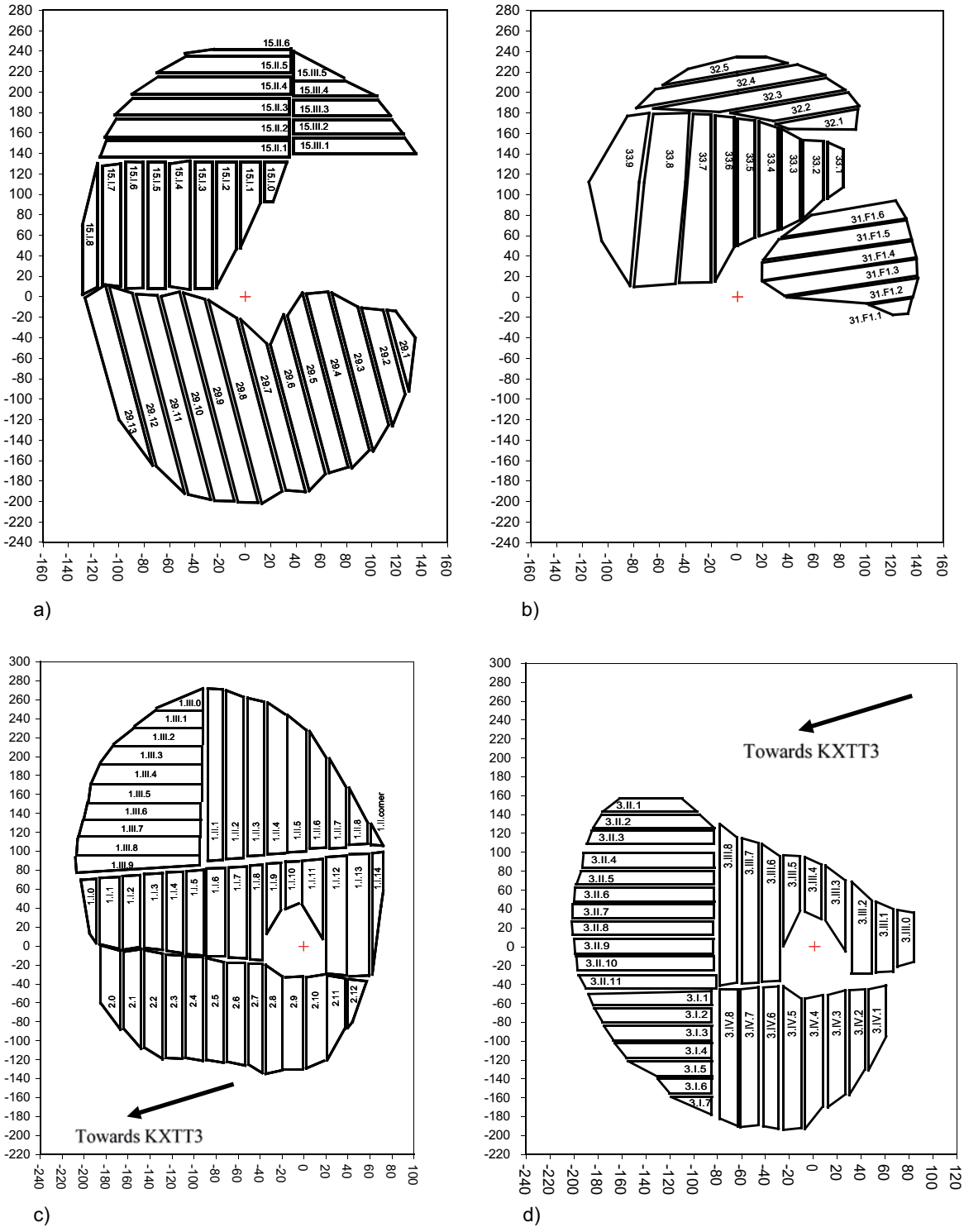

Figure 5-2. *Slices and fracture specific coordinate system of Feature A, Fracture 1, KXTT3, a) upper surface b) lower surface. The y-axis is positive towards the top of the core. The x-axis is positive towards the left side of the core looking into the borehole from the tunnel. c) Slices and fracture specific coordinate system of Feature A, KXTT4, upper surface d) lower surface. The x-axis is in this case positive towards the right side of the core looking into the borehole from the tunnel. The arrow shows the approximate direction from source borehole KXTT4 to sink borehole KXTT3 along Feature A.*

As expected, it was established during the overcoring that the core from the target section of KXTT4 was showing levels of radioactivity above the natural background due to the previously performed tracer tests (Sigurdsson and Hjerne 2014). Hence, cutting and analysis of the drill core sample from borehole KXTT4 was made at the interim storage facility for spent nuclear waste (CLAB), due to radiation protection measures and regulations. Apart from this, exactly the same procedures and equipment for cutting and photography was otherwise used for these samples as for the samples from KXTT3.

5.2 Analysis of geometry of fracture pore volume geometry

A digital camera was used to take overview photographs of the slices from the side showing the cut section through the fracture surface and the epoxy layer. For close-up photography, a microscope equipped with an eyepiece camera was employed. Two spotlights were used for ordinary lighting and two separate UV-lamps for UV-lighting photographs. Examples of overview photographs in UV-light of slices from the side as a stack from Feature A in KXTT4 and KXTT3 as well as Feature A' in KXTT4 are shown in Figure 5-3 to Figure 5-5. These images illustrate how easily and clear the epoxy occurrence may be studied when all other materials become dark except the fluorescent dye in UV-light. In Figure 5-3 and Figure 5-4 (Feature A) it is noted that there is a clear fairly continuous, although complex, epoxy layer covering most of the surface. At some points, it may be observed that a piece of epoxy has fallen off (or is attached on the opposite side of the fracture). In Figure 5-5 (Feature A') it is clear that the epoxy only occurs spot wise and in a single thin layer. Many slices of A' pieces are fully dark, but this is not believed to be explained by loosening or missing pieces to any significant extent, but rather represents a true lack of resin invasion. This conclusion was drawn from close visual examination of the surfaces before cutting and of the sides of the cut slices.

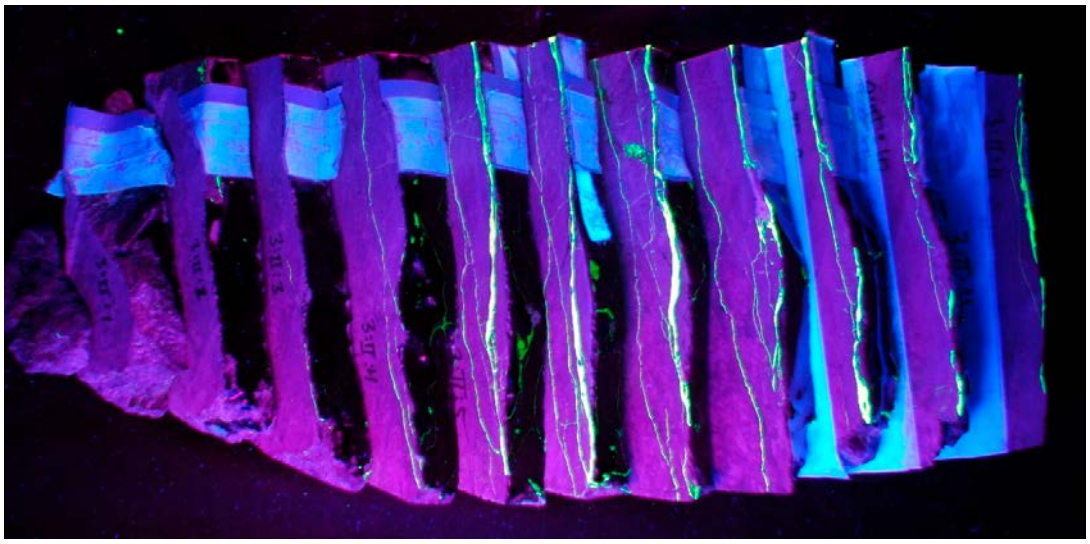

Figure 5-3. *Example of overview photograph of slices from KXTT4, Feature A, core piece 3, slices 3.II.0 to 3.II.11 (see Figure 5.2). The violet in this image is rock, the bright green is the epoxy injected into the fracture. The surface was reinforced with a dark-blue epoxy which is shown here on the top of each slide as almost black areas. Tapes for length reference of different kinds show up in white, e.g in the upper part of the image.*

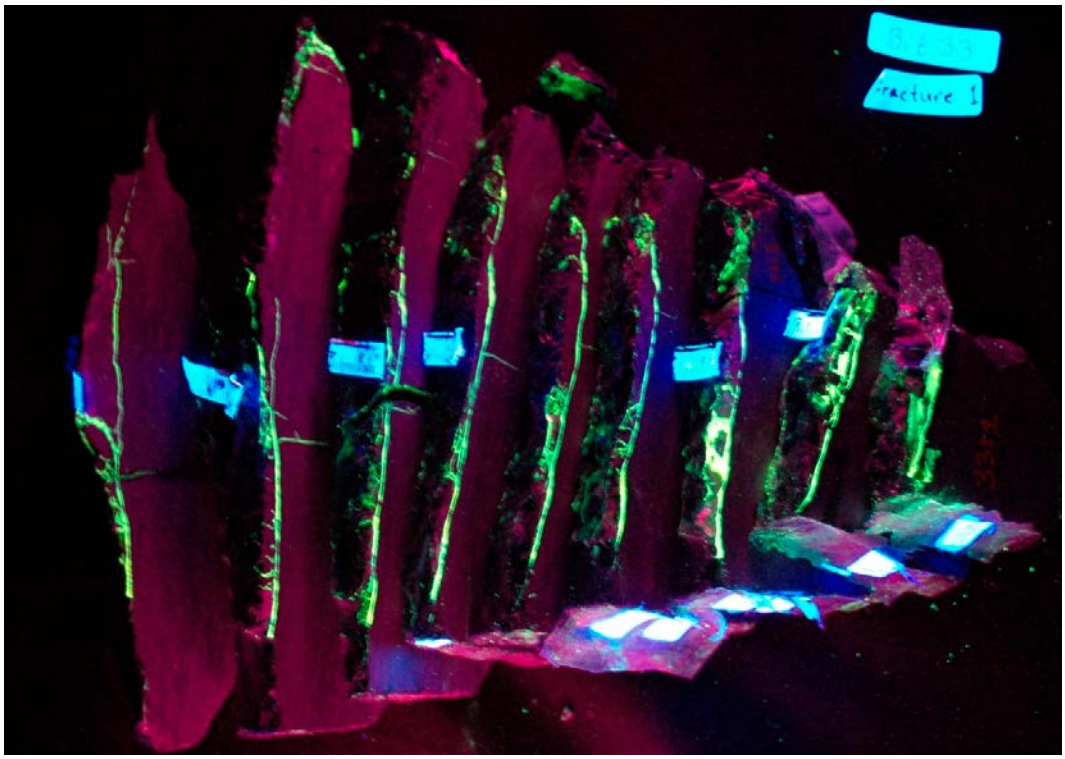

Figure 5-4. *Example of overview photograph of slices from KXTT3, Feature A, Fracture 1, core piece 33, slices 33.1 to 33.9. The bright green pattern shows the cut sections through the fluorescent epoxy. Note that all slices show a clear and fairly similar amount of epoxy. The white pieces are pieces of tape used for length reference used to indicate the spatial coordinates of the slices.*

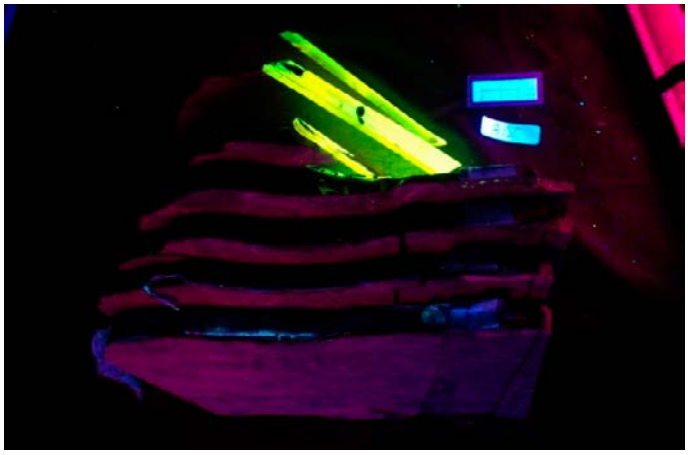

Figure 5-5. *Example of overview photograph of slices from KXTT4, Feature A', core bit and piece 8.V. Slices 8.V.0 to 8.V.7. On the first slice some trace of bright green fluorescent epoxy is visible, but most of the profiles along the slice cuts are dark. For the uppermost three slices intersecting the injection borehole, the slice side is bright green, since the borehole walls are covered with a layer of fluorescent epoxy. The top of the slices are dark because the fracture surface was covered with a dark blue resin as reinforcement.*

A total of 691 close-up photographs were taken and analysed. The majority of these were from Fracture 1 in KXTT3 (512) and Feature A in KXTT4 (149). The remaining close-up photographs were from Fracture 2 in KXTT3 and Feature A' in KXTT4. Different examples of how the fracture profiles looked like in the close-up images are given, and commented upon, in Figure 5-6 through Figure 5-8.

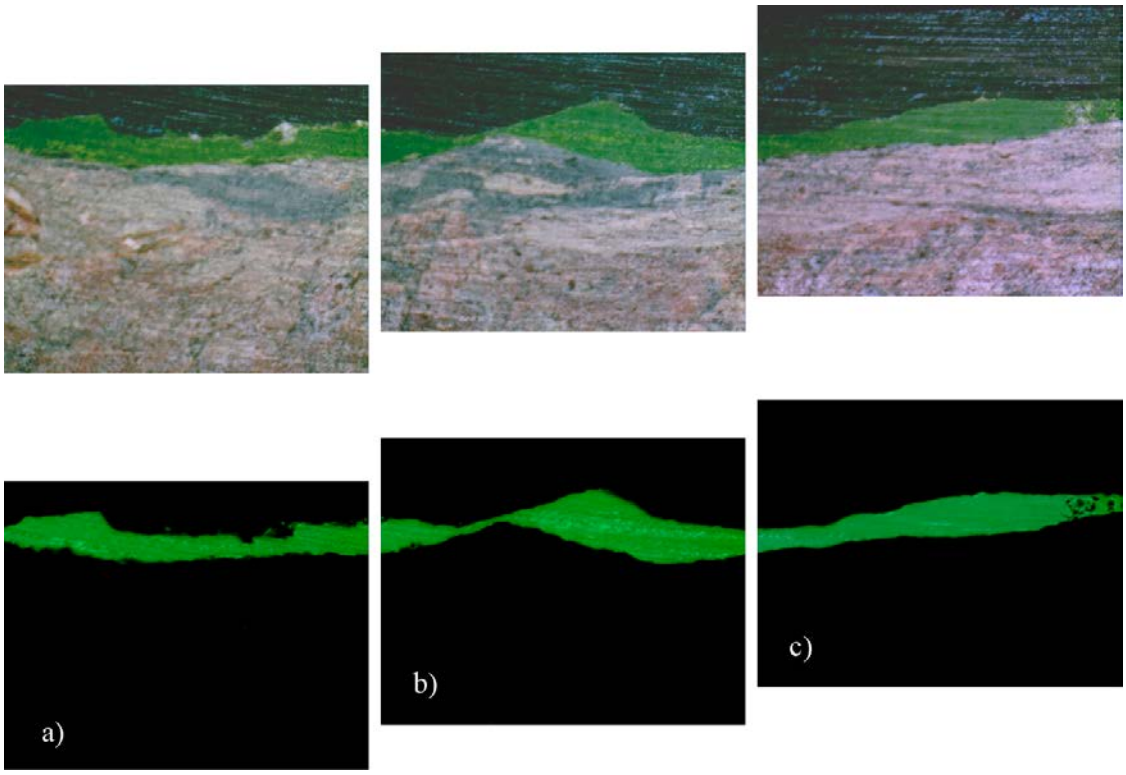

Figure 5-6. *Three close-up images (at ordinary and UV light) for slice 9 of core piece 29 (photographs 29.9.14–29.9.16). The frame size is 12.8×10.3 mm (width × height).*

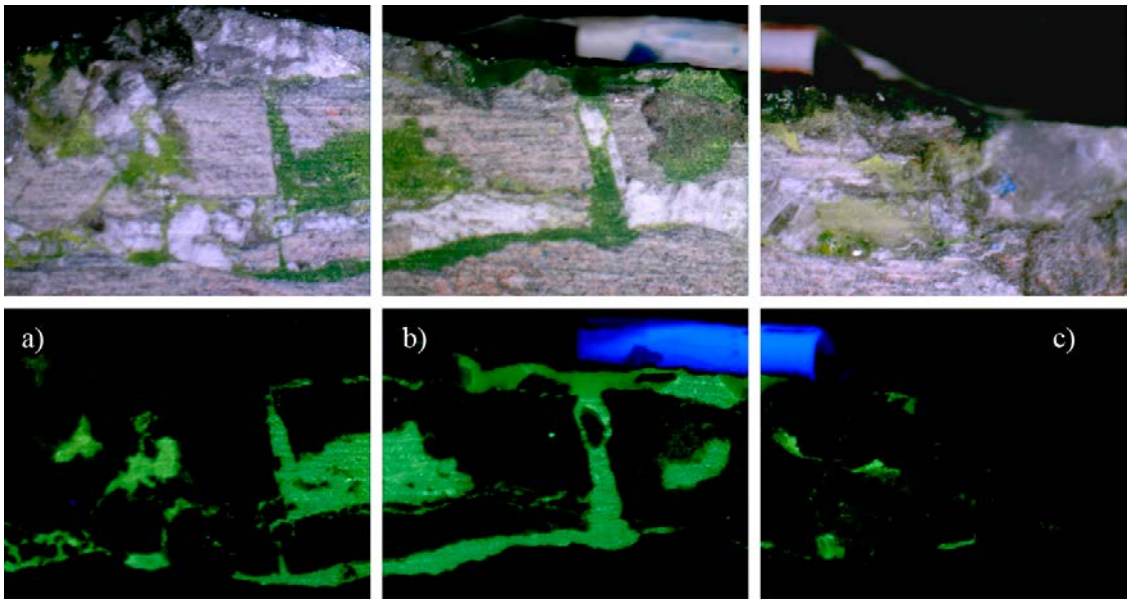

Figure 5-7. *Three close-up images (at ordinary and UV light) for slice 2 of core piece 33 (photographs 33.2.3–33.2.5). The frame size is 12.1×9.6 mm (width × height). The white areas in the photographs (blue in UV light) are parts of a measuring tape glued on top of the reinforced fracture surface.*

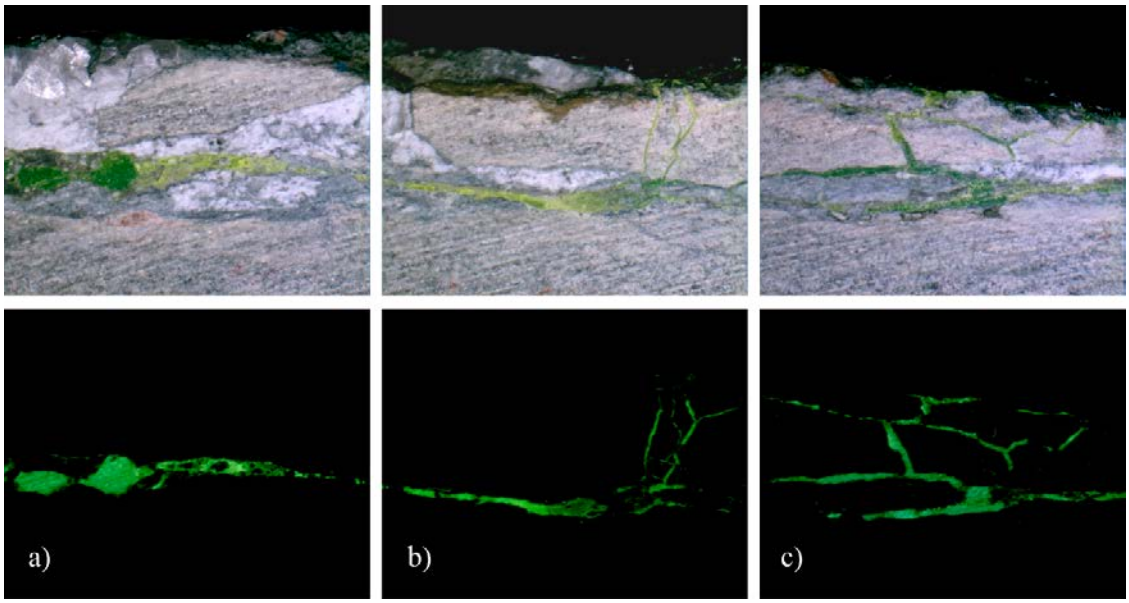

Figure 5-8. *Three close-up images (at ordinary and UV light) for slice 6 of core piece 33 (photographs 33.6.3–33.6.5). The frame size is 9.6×7.7 mm (width × height).*

To enable quantitative characterisation of the variation of character over the fracture surface, the images were classified depending on the pattern of the epoxy in each image according to:

- Class A: Single plane fracture (example Figure 5-6b).
- Class B: Single slightly complex fracture (example Figure 5-8a).
- Class C: Two fractures without connection.
- Class D: Thin fault with plenty of fragments and particles (example Figure 5-8c).
- Class E: Fault zone; complex geometry.
- Class F: Lack of epoxy.

Apart from the classification (classes A–F) described above related to the geometrical character of the actual fracture pore space, the quality of the fracture samples was also classified according to a number of groups related to the judged intactness of the epoxy.

Out of all close-up images (691) 246 were classified as F, i.e. no epoxy was found in the photographs. Very few (< 6 % in total of the remaining 445 images) were classified as C or E. Classes A (single plane fracture), B (single slightly complex fracture) and D (thin fault with plenty of fragments and particles) were almost equally frequent in the case of Feature A. Noteworthy is that this distribution is quite similar for Feature A in both boreholes.

The spatial distribution of the various classes was investigated by plotting the sample position on the fracture plane, see Figure 5-9. No clear correlation and/or trend in the spatial distribution was found by visual inspection.

The average thickness of the epoxy in each close-up image was determined by using a binary transformation and dividing the area of white pixels (epoxy) with the length of the fracture in the image. This average epoxy "thickness" for each close-up image is here used as the definition of the *mean cumulative aperture* parameter value, b_m, even in the case when the pore geometry is complex and actually consists of several stacked epoxy layers (c.f. Figure 5-8c). It is noteworthy here that the mean cumulative aperture, b_m, is thus not the same as the commonly used point aperture. However, in a single fracture plane case the true mean of the point wise aperture in an image will be equal to the mean cumulative aperture b_m as defined here for the whole image.

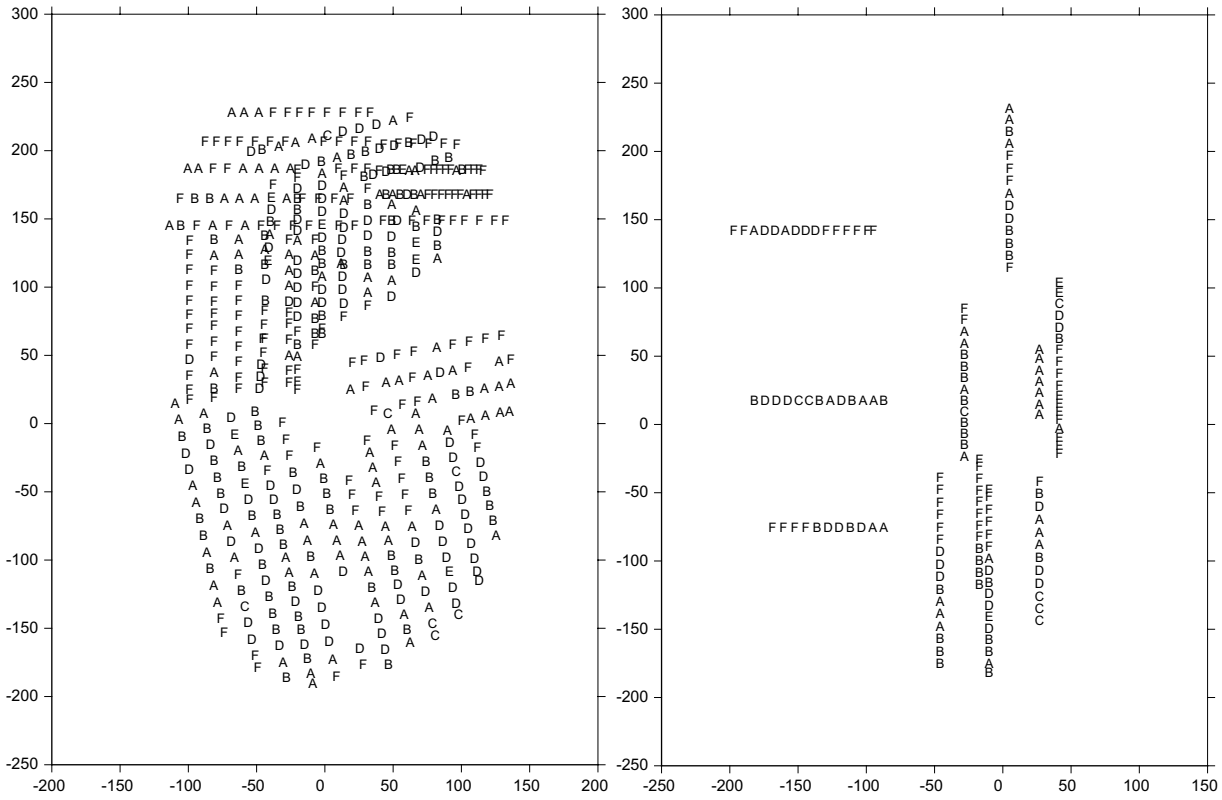

Figure 5-9. *Spatial distribution of fracture classification for a) KXTT3, Fracture 1, b) KXTT4, Feature A. Results from both sides of the fracture are shown in the same plane. All axes are in mm.*

The aperture measurement showed that the average of the mean cumulative aperture, b_m, was quite similar for Fracture 1 and 2 in KXTT3 and Feature A in KXTT4 (0.4–0.5 mm) while the aperture in Feature A' in KXTT4 was significantly smaller (0.04 mm). It also showed that the average values are of the same order of magnitude for all classes of images (A–E), in the span 0.25–0.80 mm. It should be remembered that since there is a complexity in the geometry of the aperture entity, is not possible to simply translate into the aperture of a single conductive plane. However, it is reasonable to find that the sum of apertures is in the same order if it is considered that the repeated opening and shearing of the feature must have resulted in almost the same overall separation of the two stiff rock blocks on either side of the fracture. Also, the feature is at some locations fractured into several parallel planes (or fragments) and at other locations only constitute a single plane. The fracture mineral infilling, which builds up with time, will on the other hand be a factor that increases the heterogeneity and aperture variability.

The spatial distribution of the mean cumulative aperture in the fracture planes is shown in Figure 5-10. Each dot represents the mean value corresponding to a full image of about 10 mm size. In order to detect an aperture variation and spatial correlation at a smaller scale than this full image size, a few short profiles were selected for measuring the aperture as point values at short distances along the profiles. Figure 5-11 shows variograms from two short profiles with detailed point measured aperture values. The sample underlying these curves is too small to enable any firm conclusion regarding the actual spatial correlation. However, both variograms show increasing values for at least 30 mm lag distances, which supports the use of the mean cumulative aperture data from the 10 mm full images for further analysis of the spatial correlation. Figure 5-12 shows two variograms of mean cumulative aperture of Fracture 1 in KXTT3 and Feature A in KXTT4, respectively. It can be concluded from these two variograms that the practical range is in the same order, around 75 mm for both samples.

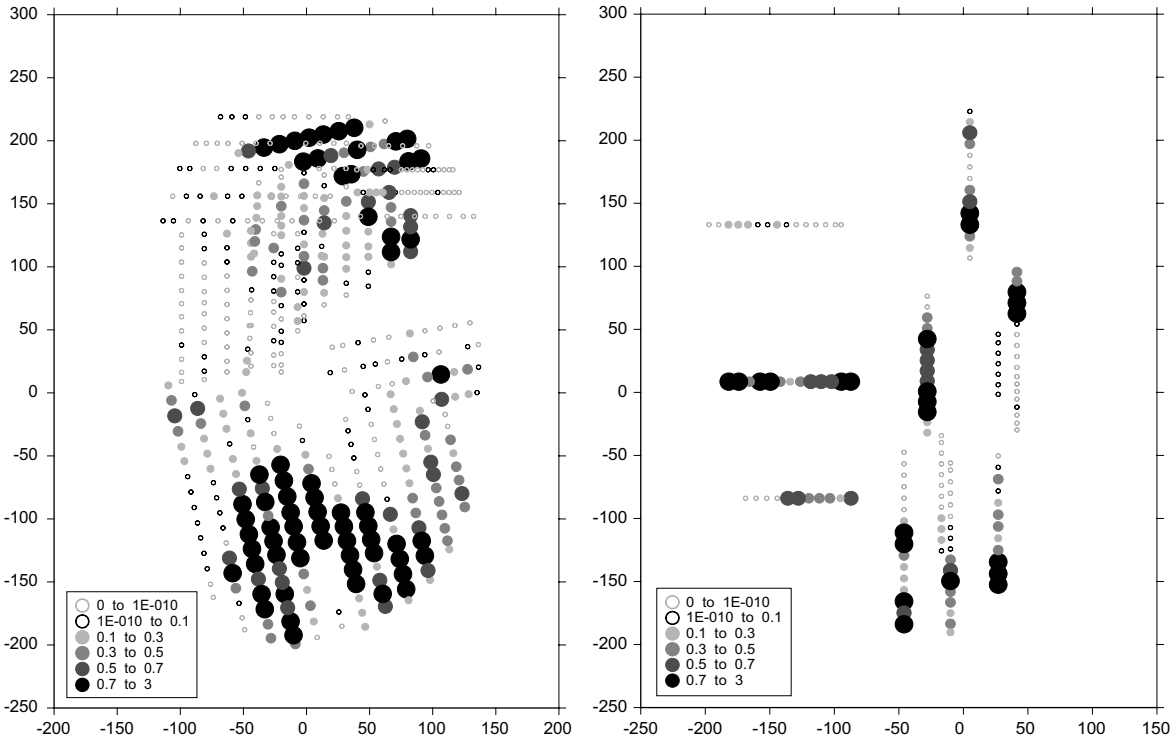

Figure 5-10. *Spatial distribution of mean cumulative aperture, b_m, for all of the photographs (both upper and lower surfaces). If an upper surface photo is positioned exactly opposite from that of the lower surface, their b_m-values are added up. Both axes and apertures in mm. a) KXTT3, Fracture 1, b) KXTT4 Feature A.*

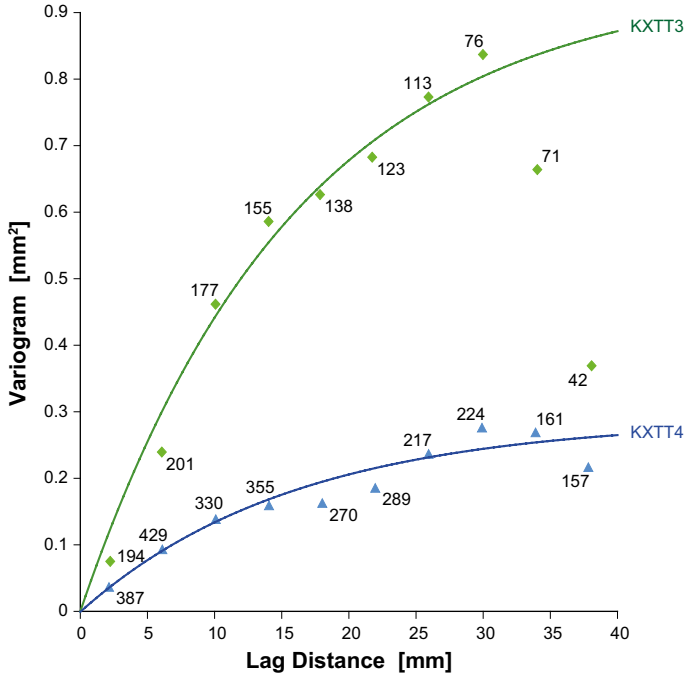

Figure 5-11. *Variograms based on aperture data from the two short profiles in KXTT3 and KXTT4 where the apertures were measured in more detail. The Y-axis shows variance of the difference between pairs of field values of b. The pairs have a certain distance (the lag distance) shown on the X-axis. The number next to the curve indicates the number of pairs supporting each point of the variogram. The curves, chosen to fit fairly well to the data, are exponential variogram model curves. Such a model increases up to a certain plateau value, called the sill value of the variance. The lag distance at which 95 % of the sill is reached is called the practical range. The larger the range the more spatial correlation between values. From the KXTT3 and KXTT4 model variogram curves it can be noted that both have a practical range of 48 mm and a sill level of 0.95 and 0.29, respectively (Hakami et al. 2014).*

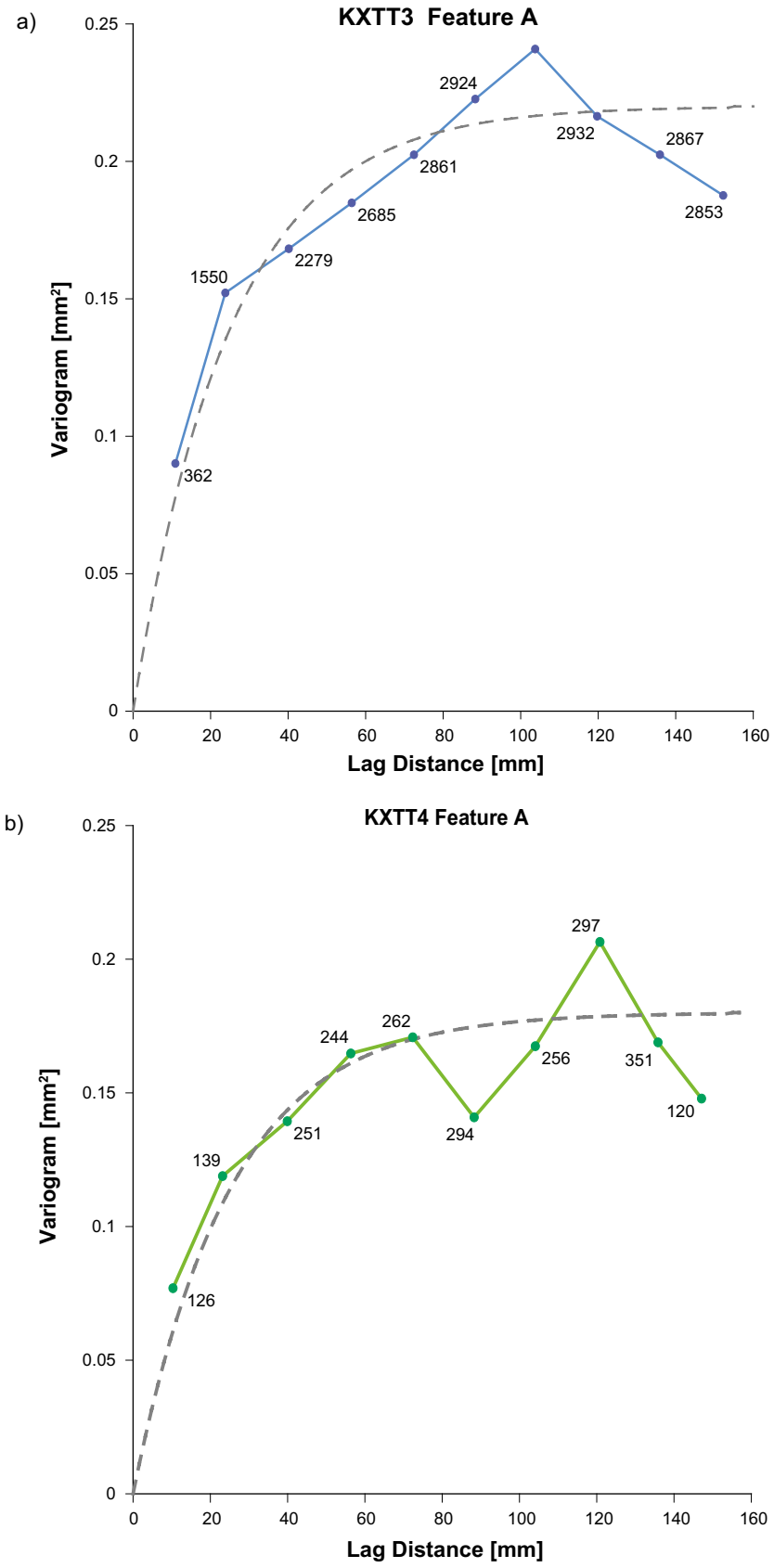

Figure 5-12. *Variograms of measured mean cumulative aperture, b_m, a) KXTT3 Feature A, and b) KXTT4 Feature A. Class F excluded. The Y-axis shows the variance of the difference between field values at a certain distance (lag) and the X-axis shows the lag. Labels are the number of pairs supporting each value. The dashed line is an exponential variogram model, having a practical range (i.e. lag when curve reaches 95 % of sill) of 75 mm (both cases) and a sill (levelling-off) level of a) 0.22 and b) 0.18, respectively (Hakami et al. 2014). See Figure 5-11 for details about the variogram construction and its characteristics.*

5.3 Mineralogical investigations

Detailed investigations have been carried out on fracture coatings from drill cores KXTT3 (Feature A) and KXTT4 (Feature A and A'), reported in Hakami et al. (2014). In earlier investigations of Feature A (and A'), clay minerals were indicated to be present based on the retention results and modelling but they were rarely identified on the fracture surfaces (Winberg et al. 2000) (indications of clay minerals from EDS analyses), mainly attributed to the double barrel drilling, in which soft or loose material is easily flushed away or otherwise lost during the drilling operation and subsequent drill core handling. Therefore it was of special importance in the Hakami et al. (2014) study, benefiting from epoxy impregnation and triple-tube drilling and large drill core diameter, to try to detect such potential clay mineral occurrences. Other objectives with the study were to characterise the history of the zone; at which events it has been reactivated, which minerals were precipitated during these events and how the flow path has varied over time. Of special importance was to characterise the outermost coatings towards the injected epoxy, both in cross-section (using thin sections) as well as the distribution and morphology of the different fracture mineral phases on the fracture surface of the main fracture, which is of special importance for retention (sorption). Wall rock alteration was also reported, and has implications for matrix diffusion, if present. One of the objectives of this study was also to evaluate if earlier suggestions that Feature A (and A') are representative for structures of this type in the Äspö area, as well as the adjacent Laxemar/Simpevarp area, are valid.

Methods used include scanning electron microscope investigation (SEM-EDS) of fracture coatings/fillings and the wall rock, both using thin sections (ten samples: four from KXTT3 and six from KXTT4) and fracture surface samples (ten samples: six from KXTT3 and four from KXTT4), as well as X-ray diffractometry (XRD, from five fracture surfaces from KXTT3) of fracture coating material. As mentioned in Hakami et al. (2014), a large part of the core from KXTT4 had to be handled inside CLAB due to radioprotection reasons, which limited the samples from this core to sections with relatively low amount of sorbed Cs, but based on the overall similar appearance of Feature A, this sample bias is considered to be insignificant. Furthermore, the KXTT4 samples were reinforced with epoxy prior to mineralogical investigations, in contrast to the investigations of KXTT3, entailing a lower number of fracture surface analyses from the KXTT4 core. The samples used are interpreted to be representative for the whole of Feature A and A', based on macroscopic observation of the entire core intercepts and on the similar features in the different boreholes, which both fit with the general characteristics and heterogeneity over relatively large distances of similar zones in the Äspö HRL and at Laxemar/Simpevarp.

5.3.1 Results and summary of mineralogical investigations of KXTT3

All of the KXTT3 samples had several generations of fracture fillings/coatings, which show that Feature A has been reactivated during several events and that it has been intermittently water-conducting since the Proterozoic, although the detailed flow path configuration has most probably varied over time. The epoxy-coated flow path occasionally cut through older fracture fillings around the main fracture plane (e.g. through mylonite and cataclasite, and in contact between mylonite and calcite), in addition to following the main fracture plane of Feature A, on top of the youngest coatings (chlorite/clay mineral dominated), see Figure 5-13.

Feature A in KXTT3 is made up of (from oldest to youngest): mylonite bands, cataclasite, a generation of brittle fractures filled with prehnite, quartz and K-feldspar, a generation of fractures filled with calcite, but also fluorite, pyrite, barite, quartz and clay minerals, and the outermost coatings (facing the main fracture planes in Feature A) dominated completely by chlorite and clay minerals, with some additional wall rock fragments, and calcite with related minerals. All fracture mineral parageneses are not present in every sample, and the amount of each fracture mineral/filling varies widely between the different samples and within the single samples, depending on the detailed flow path and the aperture of the fracture at the time of precipitation. The presently open fractures (filled with epoxy), cut through different fracture fillings in different fractures (see Figure 5-13). The fracture surfaces are mostly covered by chlorite and clay minerals (Figure 5-14), but the wall rock/mylonite may also be exposed. The clay mineral-chlorite fracture coatings are often very smooth and slickensided in places, but may be rougher when euhedral minerals, such as spherulitic corrensite, cubic fluorite and pyrite, or wall rock fragments are abundant (Figure 5-15). XRD analysis showed that the fine fraction on the fracture surface is dominated by chlorite but clay minerals are also present, mostly in a mixed-layer chlorite/smectite type (corrensite, also indicated by EDS spectra), and that wall rock fragments are included in most coatings (quartz and feldspars, see Hakami et al. 2014).

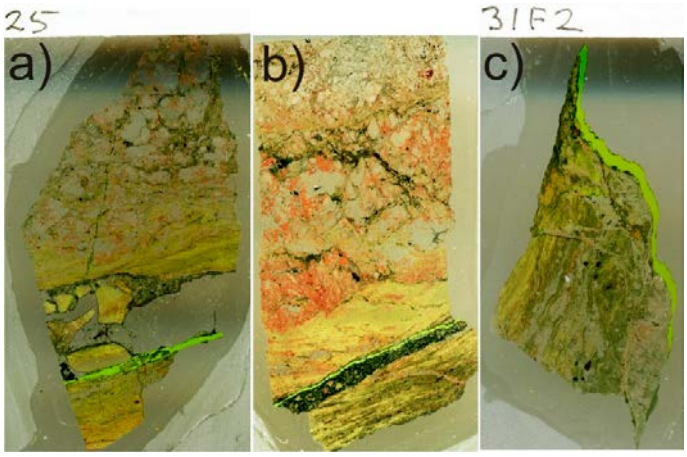

Figure 5-13. *Thin sections from KXTT3 (scanned with plane polarised light – PPL, width of view is ~2 cm each) showing cross sections of the fracture (epoxy-impregnated), fracture filling-coatings and the wall rock. a) piece 25 showing epoxy in a fracture through mylonite (in places with fragments of mylonite within the epoxy) and along the border between a calcite-filled fracture and older mylonite. b) Piece 26, showing epoxy in a fracture running on the border zone between cataclasite and older mylonite. c) Piece 31 Fracture 2, showing epoxy coating a clay mineral coated fracture which cuts older mylonite discordantly (this fracture also features cataclasite and K-feldspar-dominated fillings). From Hakami et al. (2014).*

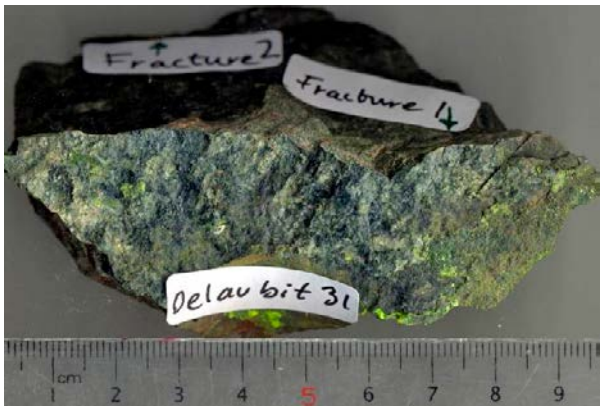

Figure 5-14. *Fracture surface of Fracture 1 from piece 31 from KXTT3, coated by chlorite and clay minerals, and in parts, epoxy (e.g. to the far right). From Hakami et al. (2014).*

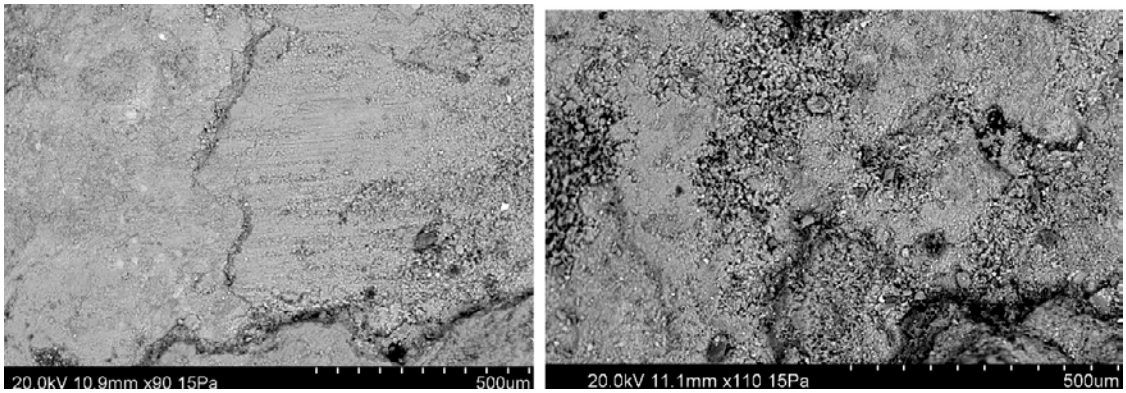

Figure 5-15. *Back-scattered SEM-images of smooth slickensided chlorite (and clay mineral) covered fracture surface (left), and by rougher part of the same fracture surface (right), where individual euhedral chlorite and clay minerals, as well as wall rock fragments are present. KXTT3, piece 31, Fracture 1. From Hakami et al. (2014).*

The rim zone, or wall rock adjacent to the fracture, is highly altered; biotite has been transformed to chlorite and plagioclase is heavily saussuritized and replaced by secondary feldspars. Quartz has often been re-crystallised. The amount of micro-fractures and the porosity is enhanced in the altered rock near the fractures, based on qualitative interpretation during thin section investigation (SEM and microscope).

5.3.2 Results and summary of mineralogical investigations of KXTT4

The KXTT4 samples show several generations of fracture fillings/coatings, indicating that both Feature A and Feature A' have been reactivated at several events and the detailed flow paths have varied, but have followed the same main planes. Feature A and A' show quite similar history but the mylonite in Feature A' seems to be somewhat thicker than the Feature A mylonite (in general 5–20 mm bands sometimes together comprising up to 5 cm all together) vs. 5–8 mm bands, respectively, Figure 5-16).

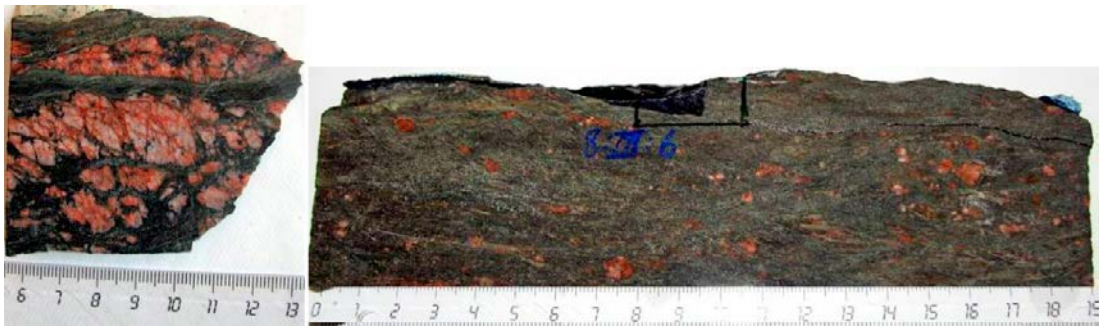

Figure 5-16. *Mylonite thickness Feature A (left, limited to two 5–8 mm subparallel mylonite bands), Feature A' (right, several thick ~20 mm mylonite bands).*

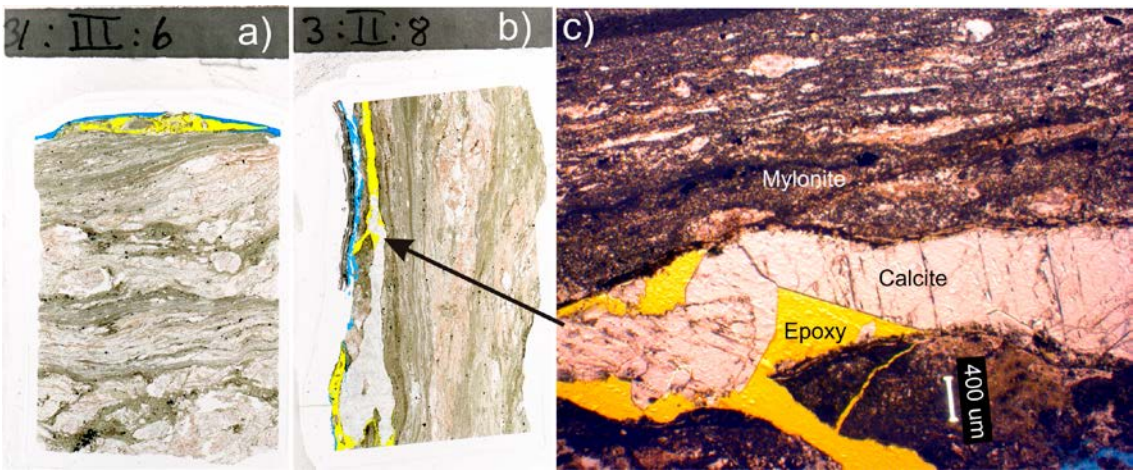

Figure 5-17(a–b). *Thin sections from KXTT4 (PPL, width of view is ~2 cm each) showing cross sections of the fracture (epoxy-injection in yellow, epoxy-reinforcement in blue), fracture filling/coatings and the wall rock. a) 1:III:6. Mylonite has been cut by a fracture filled with/coated by quartz, fluorite, barite, illite, hematite, chlorite and K-feldspar. The latter has been intruded by epoxy, which has fragments of the filling inside. The wall rock is highly altered and is made up of altered primary plagioclase and K-feldspar surrounded by fine-grained bands of mainly re-crystallised quartz and chlorite. b) 3:II:8. Almost entire thin section is made up of mylonite. Next to the main open fracture is a ~5 mm thick fracture filling of calcite (+quartz, barite, pyrite and fluorite). This fracture filling has been quite porous and the voids have been filled with epoxy. c) Microphotograph detail of epoxy-injection in the porous calcite filling of (b).*

The mylonite has been reactivated by younger cataclasite and fractures filled with calcite (with e.g. fluorite, pyrite, barite, quartz and clay minerals). The outermost coatings are often completely dominated by chlorite and clay minerals, but also calcite and K-feldspar as euhedral crystals (with sizes of clay minerals: 10–50 µm, calcite 50–100 µm, K-feldspar 50–100 µm) are present as well as additional wall rock fragments. In other places the wall rock or mylonite is exposed at the fracture surface, consistent with the conceptualisation presented in Winberg et al. (2000). The clay mineral-chlorite fracture coatings are often very smooth (Figure 5-18), sometimes showing slickensides indicating movement along the fracture plane (Figure 5-19), but may be rougher when euhedral minerals, such as corrensite, fluorite, quartz, or wall rock fragments are abundant (Figure 5-20). Cross-sections of the fracture coating show a thickness of the chlorite/clay mineral coating of typically < 100 µm (Figure 5-20 shows an example of < 50 µm). XRD analysis showed that the fine fraction on the outermost fracture coating is dominated by chlorite, with addition of mixed-layer clay of chlorite/smectite type (corrensite, also indicated by EDS spectra), and that wall rock fragments are included in most coatings. The rim zone, or wall rock adjacent to the fracture, is highly altered; biotite has been altered to chlorite and plagioclase has been heavily saussuritized and replaced by secondary feldspars, whereas quartz often has been re-crystallised. The amount of micro-fractures and the porosity is enhanced in the altered rock near the fractures.

Figure 5-18. *Photograph of the fracture surface of sample 8-III-7 (no coverage of reinforced epoxy on the left side).*

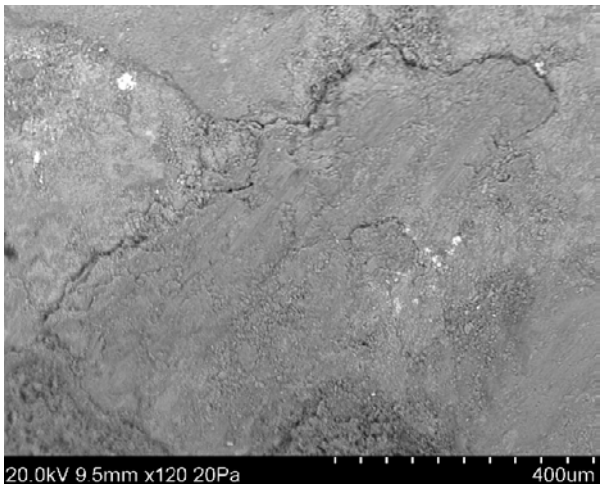

Figure 5-19. *Back-scattered SEM-image of smooth surface of slickensided chlorite/clay minerals from the fracture surface of sample 1-I-0 KXTT4. From Hakami et al. (2014).*

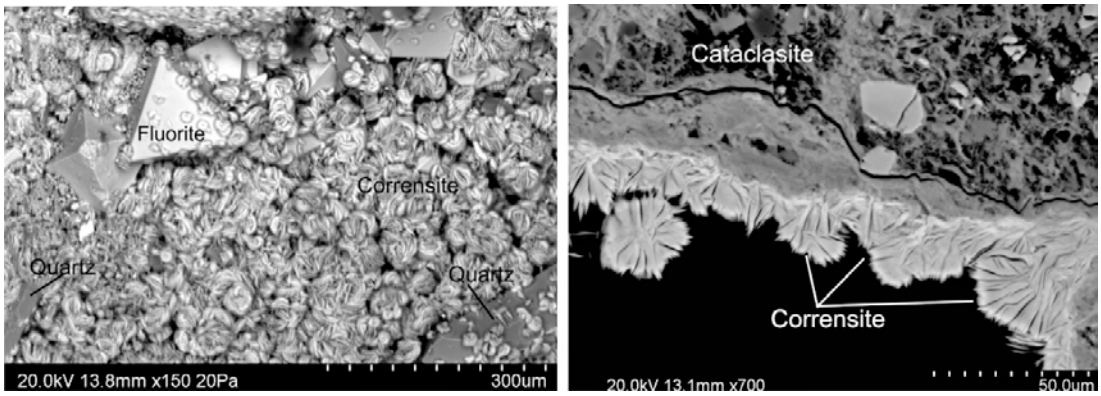

Figure 5-20. *Back-scattered SEM-image of euhedral corrensite, fluorite and quartz from the fracture surface of sample 8-III-7, KXTT4 (left). Back-scattered SEM-image of corrensite (chlorite/smectite) and chlorite as the outermost coating towards the main fracture plane of Feature A' in sample 11-III-4 (right). From Hakami et al. (2014).*

5.3.3 Summary of results from mineralogical investigations

The samples from the two drill cores of KXTT3 and KXTT4 generally show the same type of fracture mineral assemblages and deformation, although there is a variation in the proportions of each fracture mineral assemblage between the samples but also a large variation within the samples. The numerous generations of fracture fillings/coatings, show reactivation of Feature A and Feature A' during several events with variation in the detailed flow path. The fracture mineral generations in Feature A and Feature A' comprise five events;

1. Mylonite (usually epidote-dominated, shear bands of ~15 mm thickness).
2. Cataclasite.
3. Prehnite, quartz, K-feldspar, chlorite and occasionally epidote in fractures that have formed due to brittle reactivation of the mylonite.
4. Calcite, fluorite, corrensite, quartz, K-feldspar and barite in brittle fractures reactivating older fillings.
5. Chlorite and corrensite commonly constituting the outermost fracture coating on the main fracture plains (contact with epoxy). Minor minerals are calcite, pyrite, K-feldspar etc.

This sequence of events have earlier been observed and described in several studies from this area (e.g. at Laxemar and Simpevarp, summarised in Drake and Tullborg (2009)), and Feature A and Feature A' can therefore be regarded as representative structures for this area, and for Äspö. The mylonites (generation 1) and cataclasites (generation 2), have been interpreted to be more than 1.4 Ga old. Along these zones of weakness, repeated activation in the brittle regime has occurred subsequently, such as by Proterozoic prehnite-quartz-chlorite-K-feldspar (generation 3), and by Palaeozoic calcite-fluorite-quartz-barite-clay mineral-chlorite fillings/coatings (generation 4), formed at ~440–400 Ma at about 80–150 °C (Drake and Tullborg 2009). The outermost (generation 5, dominated by chlorite, but XRD and EDS analyses indicate presence of chlorite/smectite mixed-layer clay) has not been possible to date but a late Palaeozoic maximum age can be proposed and Quaternary ages are possible for at least some of the minerals, based on earlier studies in the area (Drake and Tullborg 2009). The clay mineral-chlorite fracture coatings are often very smooth and in many cases slicken sided, but may be rougher when euhedral minerals, such as corrensite, fluorite, and calcite, or wall rock fragments are abundant. The thickness of the outermost chlorite/clay mineral coatings is 10–500 µm (typically < 100 µm, outermost calcite coating is ~0.04–5 mm). The individual chlorite-clay mineral crystals are about 10 µm in smooth coatings, but individual corrensite aggregates may be up to 50 µm. The area coverage of the outermost fracture surface facing the epoxy is in the thin sections generally estimated to be:

- chlorite-clay minerals 30–51 % (mean: 42 %),
- calcite 0–20 % (14 %),
- K-feldspar 0–8 % (5 %),
- exposed altered wall rock, mylonite or cataclasite 31–58 % (39 %),

and in fracture surface samples generally not coated by epoxy:

- chlorite-clay minerals 63–90 % (mean: 81 %, of which in mean 12 % is rough euhedral crystals),
- calcite 0–9 % (4 %, comprising also pyrite, fluorite, quartz etc),
- exposed altered wall rock, mylonite or cataclasite 0–14 % (8 %),
- wall rock fragments 5–10 % (8 %).

The present identification of clay minerals is in qualitative agreement with the hypothesis presented in the conceptual modelling of Winberg et al. (2000), in which clay minerals (although not identified in the mineralogical analyses of that work) could explain the retention observed in the tracer experiments. However, the quantity of clay minerals observed in the present analyses does not seem to be sufficient to explain the entire retention effect found in earlier TRUE-1 tests. Based on the results of the present analyses, it is therefore likely that diffusion into the rock matrix plays a significant role in the retention processes. However, increased porosity in the rim zone has not been quantified, only qualitatively interpreted from thin section observations.

Note that the samples from KXTT4 had lower amount of sorbed Cs than the fracture surface in general. This may imply a bias towards samples with lower amounts of clay minerals in KXTT4. Despite this potential bias, the conclusion made above regarding diffusion into rock matrix is still considered valid.

5.4 Analysis of Cs-137 on surfaces

5.4.1 Background

In the tracer experiments performed in June 1996 (Sorbing Tracer Test 1, STT1) and in June 1997 (STT2) (Winberg et al. 2000) cocktails of radiotracers were injected, among which Cs-137 (STT1) and Cs-134 (STT2) were recovered in limited amounts; less than 38 % and 24 % (STT1 and STT2, respectively) were recovered.

Since pumping of the STT2 tracer experiment was finished (end of 1998), the borehole section has since then for the most part been closed, without any water extraction. However, several short time pumping tests have been performed from that time until now. Among them, the CEC test (cf. Section 3.3), involving injection of high chemical concentrations of stable Cs+ in the flow path, is the one that is most likely to be associated with the highest release of adsorbed radioactive Cs+ tracer. However, less than 1 % of Cs-137 not recovered in the experiments performed 10 years before was desorbed. A significant amount of radioactive tracers, especially in the injection section of borehole KXTT4, may therefore remain on the fracture surfaces of Feature A and A' of the overcored rock. For this reason, measurement of Cs-137 (the only tracer present in sufficient amounts at the time of analyse) was performed in order to possibly obtain information about the spatial distribution of the Cs+ tracer, addressing questions related to mineralogy as well as flow distribution.

5.4.2 Experimental

Three different measurement campaigns were performed for the measurement of remaining radioactivity on the overcored rock material in the surroundings of the Feature A fracture system.

Contamination monitoring

Directly after the overcoring process, the drill core was measured qualitatively using a portable contamination monitor (plastic scintillation monitor), a detector responded to Cs-137 in the range of > 500 Bq per kg. It was only for the Feature A' surface in KXTT4 that the scintillation monitor indicated presence of measurable radioactivity.

Autoradiography

The autoradiography analysis (radioactivity exposure on photographic film, method described in Hakami et al. (2014) gave no useful results, mainly because of the combination of low activity and uneven fracture surfaces that prevented close contact with the photographic film.

Gamma-spectrometry

In order to quantify the amount of radioactive tracers on the different samples, gamma-spectrometry measurements were employed. Measurements were performed using both sides of the slices (typically 10×5×1 cm size, cf. Figure 5-3) and rods (typically 1×1×2 cm) and the measurement methods are thoroughly described by Hakami et al. (2014). It should be mentioned that due to geometric irregularities of the samples, the uncertainty of the measurements was estimated to 60 % (1σ) so the method can only be used for indication of the magnitudes of the activity amounts of the samples.

The results from the gamma-spectrometry measurements are summarised in the following sections and only the Cs-137 activity is addressed hereafter, this because of the low activity (if any) of the Cs-134 tracer.

5.4.3 Results from Feature A in KXTT3

No thorough assessment of the KXTT3 samples has been made. A short measurement consisting of a large number of rod samples put in the detector simultaneously gave no indication of any activity present in these samples. This was in no way a surprise; the KXTT3 was used as the pumping borehole during the experiment and measureable activities in the range of only 1–2 Bq per litre had been found in the pumped water prior to overcoring.

5.4.4 Results from Feature A in KXTT4

The results of the measurements of Cs-137 in the Feature A are illustrated in Figure 5-21 and Figure 5-22. These figures may also be compared with the photographs in UV-light in Figure 4-3. Notably, the concentration of Cs-137 is highest in the samples closest to the borehole intercept, otherwise a comparatively homogeneous distribution is observed in the fracture sample. Presence

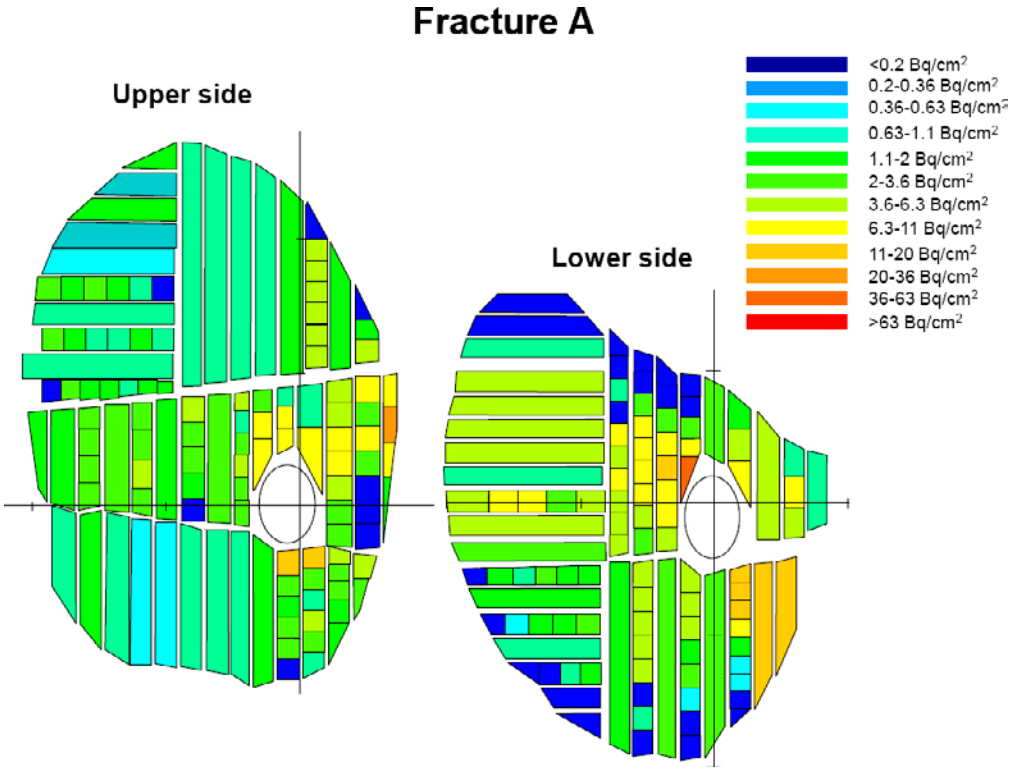

Figure 5-21*. Illustration of the Cs-137 distribution related to the upper (core piece 1 and 2) and lower (core piece 3) side of the Feature A fracture in KXTT4. The oval form of the picture is a result of the fact that a non-perpendicular cross section of the drill core and the fractures was obtained during the drilling The coordinate systems are given with the same coordinates for the two fractures; the distance between each tic mark on the scale is 10 cm. The uncertainties of the Cs-137 measurements are in the range of 60 % for the slice samples and in the range of 10 % for the rod samples (generally somewhat higher in the case of lower activity).*

of Cs-137 can thus be observed in almost all samples, however with some exceptions for samples located farthest away from the borehole intercept. The direction towards the KXTT3 borehole (the pumping borehole in the previously performed tracer experiment) is to the left of each figure and there are some indications of increased activity in samples located in a possible flow path. It is nevertheless shown that Cs-137 covers a large surface; far much more surface compared to what should be obtained from a conceptualisation of channelized flow directed towards the pumping borehole.

Given the discussion in Section 4.3 it is not possible, based on the overview photographs, to establish correlation between the observed distribution of Cs-137 and the appearance of the epoxy. However, based on the cut sections through the epoxy layer, it may be concluded that both the epoxy and the Cs-137 cover the whole sample surfaces of Feature A in KXTT4.

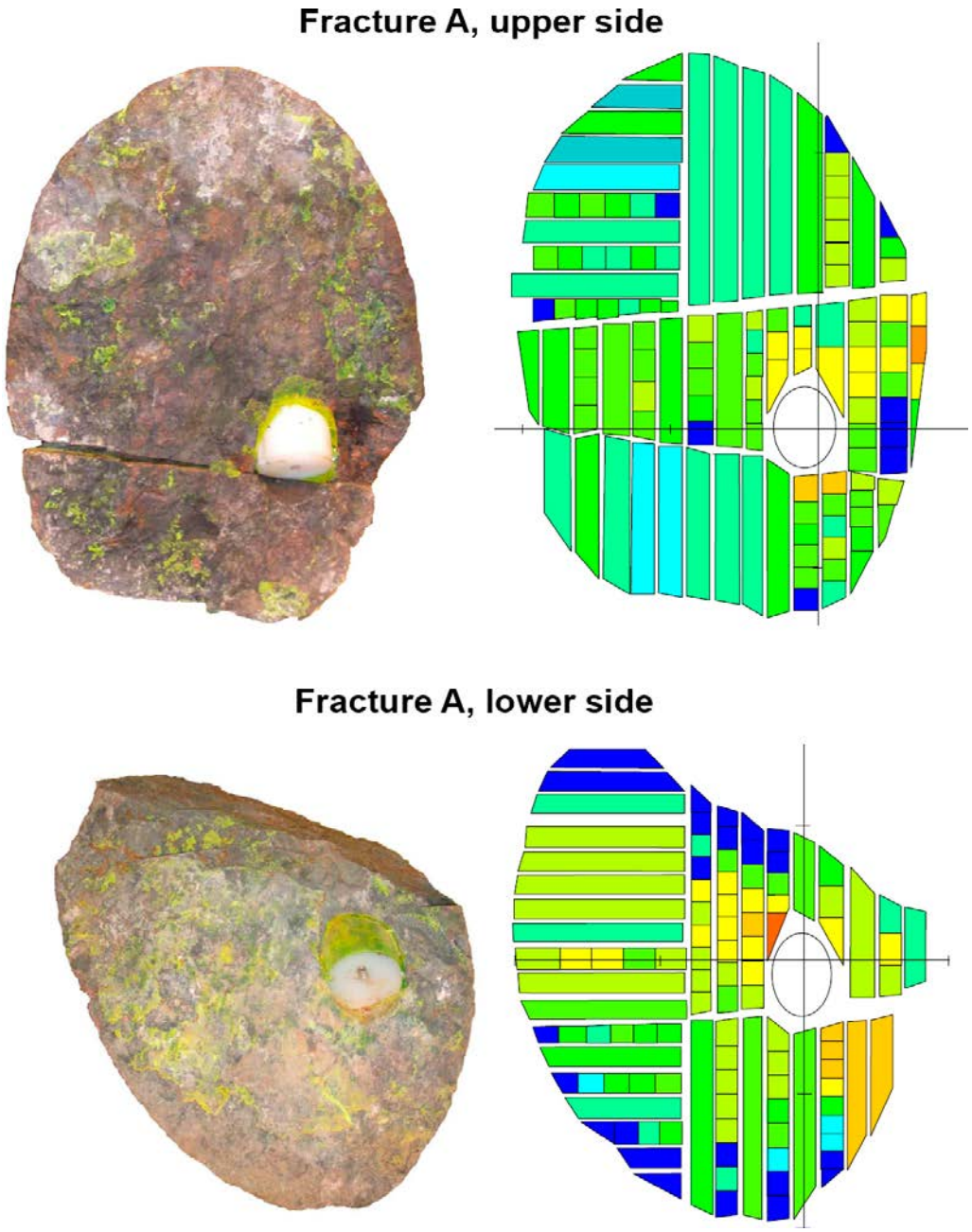

Figure 5-22. *Photography (left) and an illustration of the Cs-137 distribution (right) on the Feature A surface samples from the upper (core piece 1 and 2) and lower (core piece 3) side in KXTT4. One can observe for the lower samples that the photography was obtained in a different angle compared with the illustration of the Cs-137 distribution, which causes a slight mismatch of the figures. (See Section 4.3 concerning further details on the appearance of epoxy in the overview photographs).*

A comparison between concentration of Cs-137 and the fracture classification types (cf. Section 5.2) was also made for Feature A in KXTT4. However, no obvious correlation between fracture classification and the Cs-137 distribution was found.

5.4.5 Results from Feature A' in KXTT4

The results of the measurements of Cs-137 in the Feature A' are illustrated in Figure 5-23 and Figure 5-24. These figures may also be compared with the photographs in UV-light in Figure 4-3 and Figure 4-4. It is obvious that the concentration of Cs-137 is highest in the samples closest to the borehole intercept and that (contrary to the situation for the Feature A surface) the major part of the sample rock surface is devoid of any presence of Cs-137. The direction to the KXTT3 borehole is to the left of each figure and a flow path in this direction could be inferred.

5.4.6 Discussion of the Cs analysis

The total amount of Cs 137 found on the sample surfaces of KXTT4 (Table 7-1), is 3 kBq for Feature A and 9 kBq for Feature A'. It is notable that the amount on the mating sides of the fractures is quite similar. Further, it can be concluded that the total amount of Cs-137 measured at the two sampled surfaces at the injection borehole was only 0.29 % of the Cs-137 not recovered during the STT1 tracer experiment. This could be an indication that there could be large amounts of Cs-137 to be found in the flow path between the two boreholes. However, with a rough approximation of that a total fracture surface of 6 +6 = 12 dm^2 = 0.12 m^2 has been measured in this experiment, one would "need" a 0.12/0.0029 ≈ 40 m^2 fracture with an average surface concentration as given by the measurements closest to the injection borehole to account for the total inventory (on average). Actually, that amount of fracture would correspond to a circle with the radius of 3.6 m, which can be compared with the fact that the Euclidean distance between the boreholes is only 4.6 m. It has to be acknowledged, however, that there is a possibility that the flow in the tracer test may have taken place in several subparallel fractures, or splays to the main fracture plane, which to some extent is supported to by the mapping of the drill cores from the site (cf. Section 4.3) and the 3D fracture modelling (cf. Section 4.4).

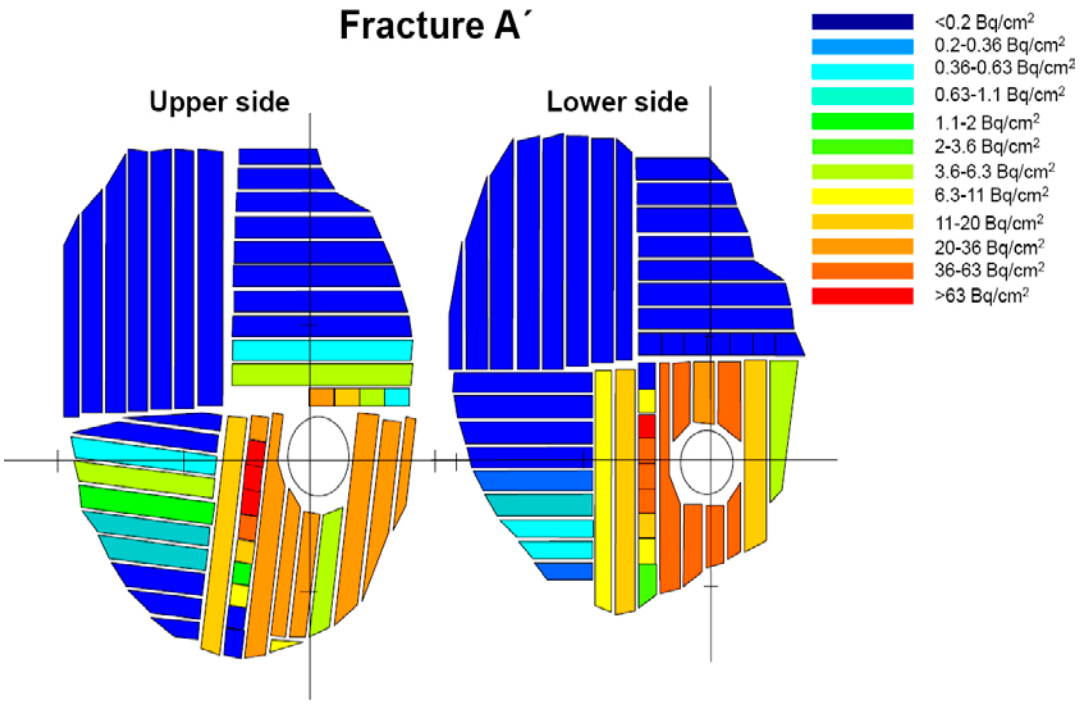

Figure 5-23. *Illustration of the Cs-137 distribution in the upper and lower side of the Feature A' fracture in KXTT4. The coordinate systems are given with the same coordinates for the two fractures; the distance between each scale unit is 10 cm. The uncertainties of the Cs-137 measurements are in the range of 60 % for the slice samples and in the range of 10 % for the rod samples (generally somewhat higher in case of lower activity).*

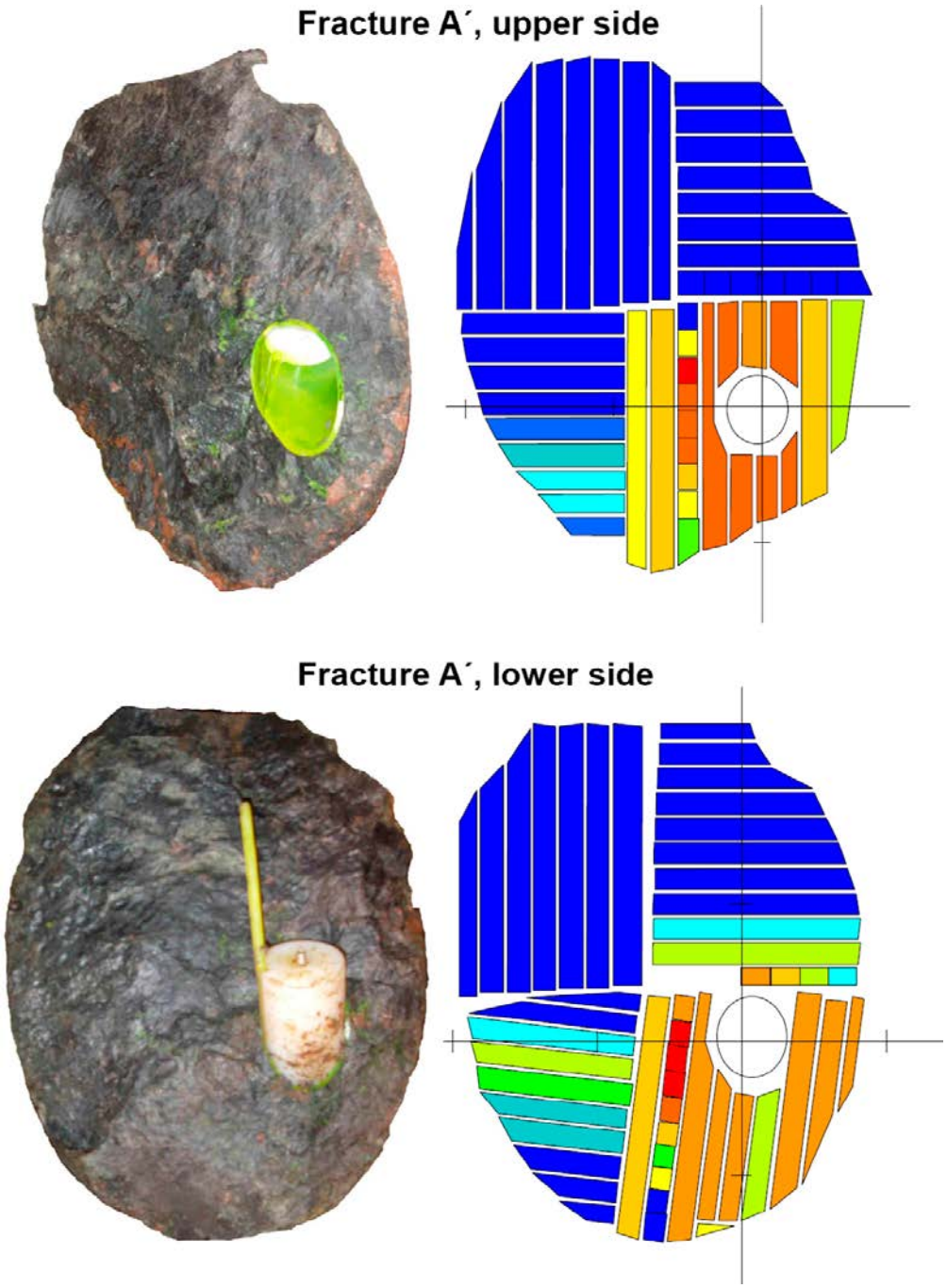

Figure 5-24. *Photography (left) and an illustration of the Cs-137 distribution (right) on the Feature A surface samples in KXTT4.*

When making these comparisons, the fact that that the cylindrical surface of the original 56 mm injection borehole was not fully measured for its Cs+ content should be addressed; only the borehole surfaces located in the vicinity of the Feature A and Feature A' intercepts have been measured. It is therefore possible that a significant amount of the tracer was sorbed on the wall of the packed off section containing Feature A and Feature A', which could influence the calculated material balance. However, based on contamination measurements, it is not likely that all the non-recovered Cs-137 is present on the borehole wall of the injection section.

One possible explanation to the location of the non-recovered part of the Cs-137 tracer is that there is a higher amount of strongly sorbing material (e.g. fault gouge material) in the undisturbed fracture, i.e. that the drilling and the overcoring caused flushing and removal of non-consolidated

fracture material in the vicinity of the borehole intercepts. This may have caused depletion of non-consolidated fracture material (and therefore also of Cs-137) in the measured surface samples and one should according to this explanation expect higher sorption capacity some dm further in to the fracture compared with the overcored surfaces. This explanation is in line with the results of the cation exchange capacity (CEC) experiment performed at the same site (Nordqvist et al. 2014) where adsorbed amount of Cs+ was found to exceed the amount expected from the results of the laboratory experiment measuring the sorption capacity of the mylonite from the Feature A (Byegård and Tullborg 2012). This indicates an interaction with a rock material having far more sorption capacity than what has been found on the mylonite surfaces, tentatively fault gouge material. However, the rock and mineralogy analyses of this work does not provide quantitative support for the existence of fault gouge material in sufficient amounts to explain the non recovered Cs in the different tracer experiments of the TRUE detailed scale experiments.

In summary, it can be concluded that neither of the proposed explanations above (separately or in combination) is enough to account for the Cs not being recovered in conjunction with the Cs tracer experiments.

The most striking observation is, however, the agreement between the epoxy injection characteristics and the distribution of the Cs-137 tracer. The Feature A fracture seems to have been sufficiently conductive to allow a significant inflow of epoxy resin which can be interpreted to be in agreement with the relatively homogeneous distribution of Cs-137 tracer. Feature A' is less conductive to inflow of epoxy resin which is in agreement with the low amount of surface that, according to the results of the Cs-137 measurements, seem to have been in contact with the flowing water. These observations provide a general support for the dual pathway transport indicated by the STT2 experiment (Andersson et al. 1999).

Table 5-1. Total amounts of Cs-137 found on the different surface samples from the KXTT4 fracture surfaces. The amounts presented are also compared to the total amount of tracer injected in the STT1 experiment and a comparison is also made with the part of the Cs-137 tracer that was not recovered during the pumping phase of the experiment.

Total amount Cs-137 injected in the STT1 experiment: 6 400 kBq

Non-recovered amount in the STT1 experiment: 4 200 kBq

Borehole	Fracture	Side	[Cs-137] kBq	Part of total injected	Part of non-recovered
KXTT4	Feature A	Upper surface	1.5 ± 0.1	0.02 %	0.04 %
		Lower surface	1.6 ± 0.2	0.02 %	0.04 %
		Sum, Feature A	3.1 ± 0.2	0.05 %	0.07 %
	Feature A'	Upper surface	4.4 ± 0.7	0.07 %	0.11 %
		Lower surface	4.5 ± 0.7	0.07 %	0.11 %
		Sum, Feature A' A'	8.9 ± 1.0	0.14 %	0.21 %
		Sum, KXTT4	12.0 ± 1.1	0.19 %	0.29 %

6 Updating of conceptual models of Feature A

Conceptual models describing various aspects of Feature A have earlier been presented by Winberg et al. (2000). Additional and complementary analyses, assessments, investigations and conclusions regarding Feature A have been reported e.g. by Cvetkovic and Cheng (2008), Widestrand et al. (2007), Cvetkovic et al. (2007), Mazurek et al. (2003), Jacob et al. (2003), Andersson et al. (2002c), Neretnieks (2002), Neretnieks and Moreno (2003), Bossart et al. (2001) and Cvetkovic et al. (2000).

6.1 Hydrostructural model

In the fundamental hydrostructural model, as presented by Winberg et al. (2000), Feature A is considered to be one of several major structures in the TRUE-1 block. In this model, Feature A is interpreted as well separated from other major hydraulic features within the borehole array, i.e. the flow between the borehole intercepts of Feature A is assumed being essentially two dimensional.

An alternative model of the TRUE-1 block as a system influenced by a network of interconnected fractures has been proposed by Neretnieks and Moreno (2003) which implies that the flow in the fracture system under converging flow conditions essentially is three dimensional.

Results in Andersson et al. (2002c) support the interpretation made in Winberg et al. (2000) of Feature A as being well separated from other major hydraulic features within the borehole array. This conclusion is also supported by the review of tracer tests made by Löfgren et al. (2007). These results were not available when the majority of the work presented in Neretnieks and Moreno (2003) was carried out.

It is not within the objectives of the TRUE-1 Completion to make investigations and decide which of these two alternative models is the most plausible one. However, some remarks about the conflicting conceptualizations can be made from findings made within the TRUE-1 Completion project and previous investigations:

- Hydraulic tests earlier performed in Feature A revealed a flow dimension larger than two (Winberg et al. 2000), which may be interpreted as a system influenced by a network of interconnected fractures at the site. However, the derived flow dimensions may also reflect conditions beyond the intercepts with Feature A (i.e. boundary condition effects) and/or an increasing transmissivity with distance within Feature A as illustrated in Figure 3-6.
- Small amounts of epoxy were found in some fractures not considered being part of Feature A, showing that fractures separated from Feature A also are conductive. However, the amounts of epoxy found in these fractures indicate that they have a significantly lower transmissivity than Feature A. It is therefore likely that the flow in these fractures is considerably lower compared with that in Feature A. The findings of epoxy in these minute low-transissive fractures are therefore not considered as a support of a model dominated by three-dimensional flow.
- The results presented in Table 4-9 in Nordqvist et al. (2014) show that the flow was unevenly distributed in Feature A during the COM tests (c.f. Section 3.2). If a significant part of the flow within the borehole array took place in other structures than Feature A, a flow rate ratio well below 1 (on average) for each row in Table 4-9 in Nordqvist et al. (2014) was to be expected. This is not the case, thereby lending additional support to the interpretation that the flow between borehole sections involved in the performed tracer tests is dominated by flow in Feature A.

In summary, results from the TRUE-1 Completion investigations do not indicate that the flow in Feature A to a high degree is influenced by a network of interconnected fractures as suggested by Neretnieks and Moreno (2003). Instead, the results from TRUE-1 Completion, together with the findings presented by Andersson et al. (2002c), support the original hydrostructural model presented by the TRUE team where Feature A is interpreted as being well separated from other major hydraulic features within the borehole array and the flow between the borehole sections intersecting Feature A being essentially two dimensional.

The crosshole interference tests (COM tests) show that Feature A is heterogeneous in terms of hydraulic transmissivity, with a higher transmissivity at the KXTT3 intercept (in the order of 10^{-7} m^2s^{-1}) and a lower transmissivity at KXTT2 (in the order of 10^{-9} m^2s^{-1}), respectively, than the other borehole sections (in the order of 10^{-8} m^2s^{-1}). This is in agreement with earlier investigations reported by Winberg et al. (2000). The COM tests also indicate a higher transmissivity and/or connectivity in the area around KXTT3 and KXTT5, while an area of lower transmissivity and/or connectivity is found between KXTT1, KXTT2, KXTT4 and KA3005A. These observations are in agreement with the results from the SWIW tests, where the transport from KXTT4 was found to be faster to KXTT3 and KXTT5 than to KXTT1 and KXTT2. A two-dimensional interpretation of the transmissivity and/or connectivity in the plane of Feature A was made based on the results from the COM tests (Figure 3-6). It should be noted that this interpretation is qualitative and alternative interpretations are possible. The combination of pressure and flow responses, as used in the COM tests, should be very suitable for further evaluation using hydraulic tomography as e.g. Illman et al. (2009) have used for modelling of hydraulic tests in fractured granite. This could be a suitable method for testing, confirming and further refining the hydraulic conceptual model of Feature A.

Analyses of position, strike and dip of the fractures earlier interpreted as Feature A support the interpretation of Feature A as a continuous, undulating fracture. A detailed study of the open (epoxy filled) fractures from the over-coring of KXTT3 and KXTT4 (as shown in Figure 4-1) may support an interpretation of a stepwise character of Feature A between KXTT3 and KXTT4. Hence, Feature A is considered to have an undulating and/or stepwise character, as illustrated in Figure 6-1, with possible splays (Feature A').

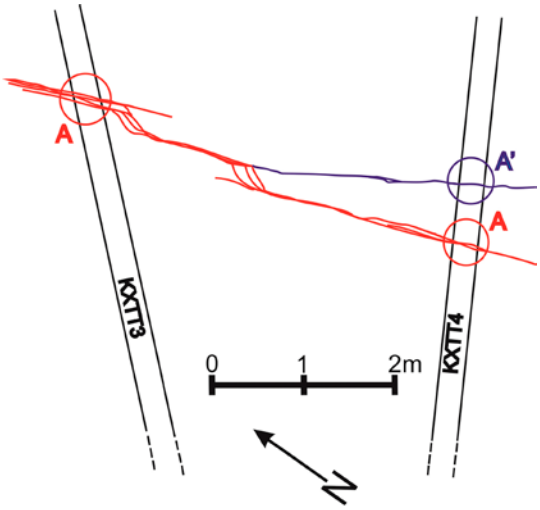

Figure 6-1. *Interpretation of Feature A (red) with an undulating and/or stepwise character and the splay Feature A' (purple).*

6.2 Microstructural model

Detailed investigations carried out on fracture coatings from drill cores KXTT3 (Feature A) and KXTT4 (Feature A and A'), reveal the presence of several generations of fracture fillings/coatings, which shows that both parts of the structure have been reactivated at several geological events and have been intermittently water-conducting for a very long time, although the detailed flow path configuration has most probably varied over time. This is in line with the previous model (cf. Winberg et al. 2000), that has now been developed further, refined and verified. One particularly important improvement is related to the occurrence of clay minerals on the outermost surface along the flow paths (constituting the currently interactive layer in respect to sorption). Although indicated already in Winberg et al. (2000) this has now been verified through XRD and SEM (see BSE-SEM-images below).

As shown in the schematic microstructural model in Figure 6-2, Feature A in KXTT3 and KXTT4 is made up of (from oldest to youngest): mylonite bands, cataclasite, one generation of brittle fractures filled with dominantly K-feldspar followed by a generation of fractures filled with dominantly calcite, and the youngest outermost coatings (phasing the main fracture planes in Feature A and A') dominated completely by chlorite and clay minerals, together with some wall rock fragments, and calcite with related accessory minerals (e.g. fluorite, quartz, pyrite). This sequence of events has earlier been observed and described in several studies from this area (e.g. at Laxemar and Simpevarp, summarised in Drake and Tullborg (2009)), and Feature A (and Feature A') can therefore be regarded as being a representative structure for this area. Although there is a variable proportion of each fracture mineral assemblage between the samples and also a large variation within the samples, Feature A shows similar appearance (fracture mineral assemblages and deformation) in both KXTT3 and KXTT4 and is therefore presented in a joint fashion in the microstructural model (Figure 6-2). The observed variation in amounts of each fracture mineral/filling between the different samples and within single samples depends on the detailed flow path and the aperture of the fracture at the time of precipitation. Both Feature A and A' show quite similar historic records but the mylonite in Feature A' seems to be slightly thicker than the Feature A mylonite (in general 5–20 mm bands, together sometimes comprising up to 5 cm thickness in all) vs. 5–8 mm bands, respectively, Figure 6-2). The presently open fractures (those filled with epoxy) cut through different fracture fillings in different fractures, showing that they have re-activated several fracture planes (see Figure 5-13, Figure 5-17 and Figure 6-3).

The fracture surfaces are mostly covered by chlorite and clay minerals (see microphotograph and SEM-images in Figure 6-3), but the wall rock/mylonite may also be exposed. The clay mineral-chlorite fracture coatings are often very smooth (occasionally manifested by slickensides), but rougher varieties exist where euhedral minerals, such as spherulitic corrensite, cubic fluorite and pyrite, or wall rock fragments are abundant (Figure 6-3). Chlorite is dominant in the outermost coatings but is always accompanied by clay minerals, mostly of mixed-layer chlorite/smectite type (corrensite), and quartz and feldspar fragments from the wall rock are included in most coatings. The thickness of the outermost chlorite/clay mineral coatings is 10–500 µm (typically < 100 µm, the outermost calcite coating is ~0.04–5 mm), which gives an indication about the virgin original aperture. The mean area coverage of the outermost chlorite/clay mineral coatings on the studied fracture surfaces is ~80 %, of which ~10 % is euhedral crystals resulting in a rough fracture surface. The wall rock shows, on the average, a ~10 % exposure. In the thin sections, the mean coverage of chlorite and clay minerals is smaller (~40 %) and exposed wall rock larger (~40 %). Other minerals have a maximum coverage of ~20 %.

The rim zone (wall rock adjacent to the fracture) is highly altered and features chloritization of biotite, saussuritization of plagioclase, re-crystallisation of quartz, preferred orientation of crystals, increased micro-fracturing and porosity near the fractures.

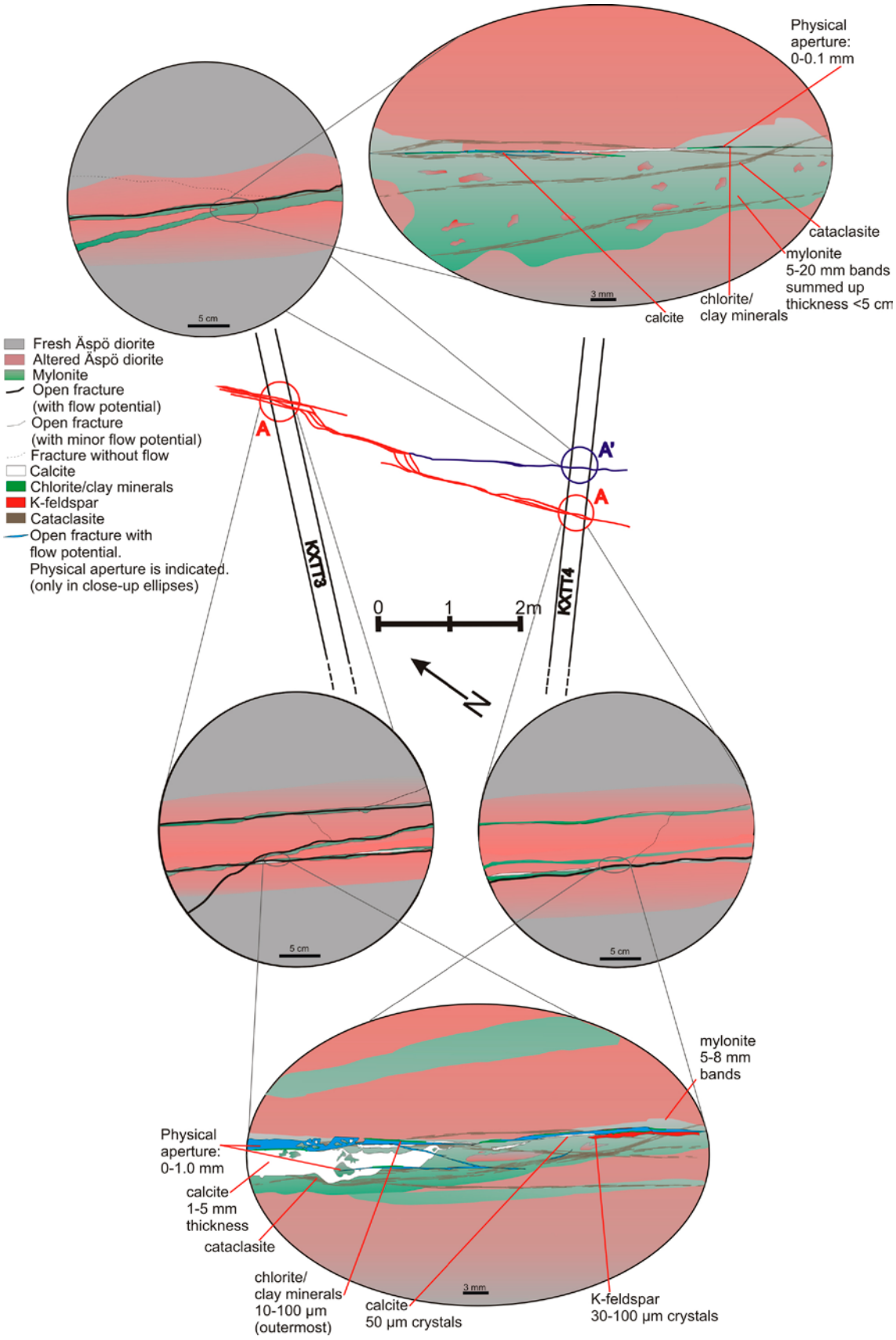

Figure 6-2. *Schematic conceptual microstructural model (1), showing representative characteristics of Feature A' (in KXTT4 – top) and Feature A (in KXTT3 and KXTT4 – bottom). In the detailed image (bottom), the characteristics of Feature A are presented jointly for the KXTT3 and KXTT4 intercepts.*

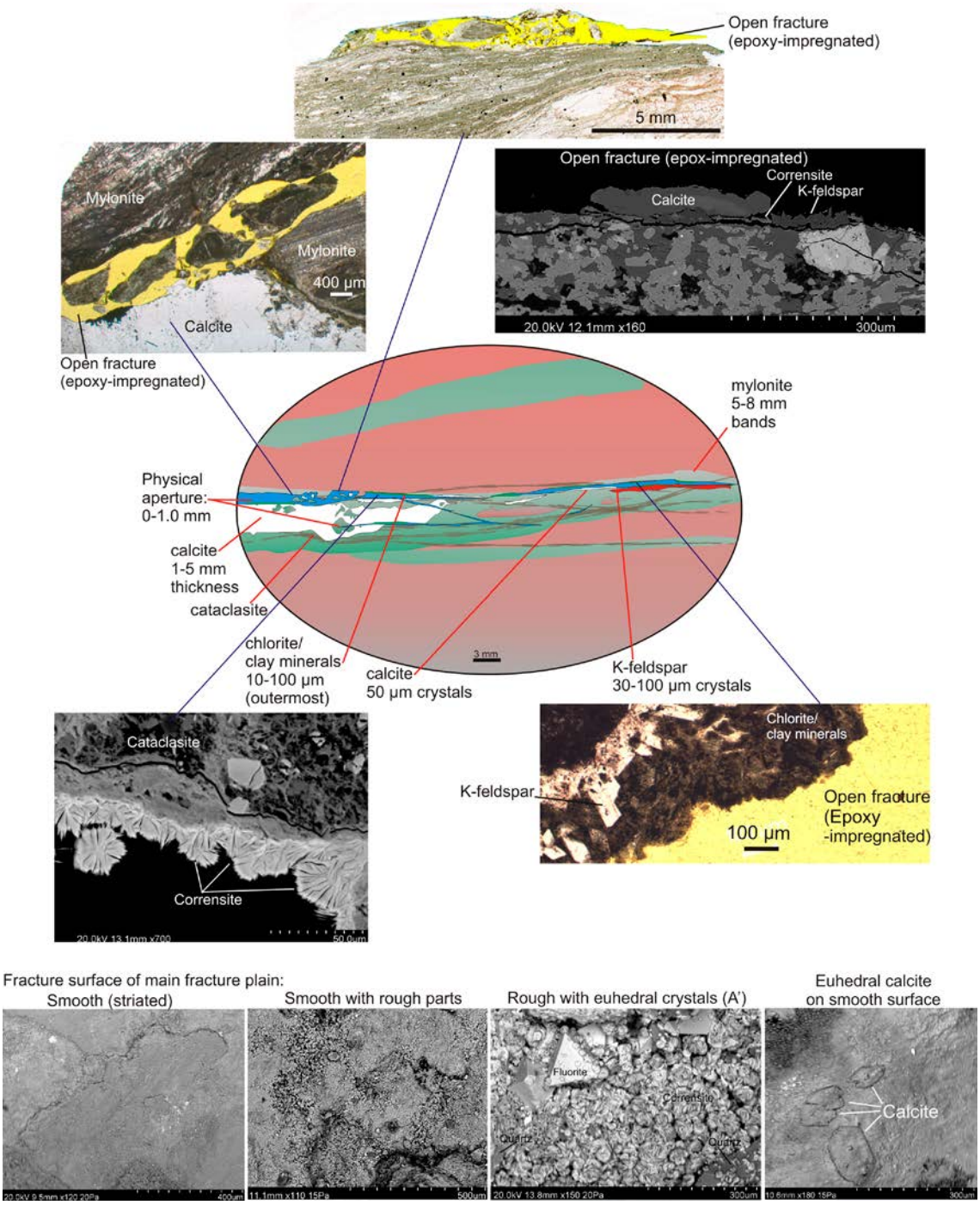

Figure 6-3. *Schematic conceptual microstructural model (2), showing representative details of Feature A (in KXTT3 and KXTT4), from thin sections (microphotographs and back-scattered SEM-images – five images around the conceptual sketch) and from fracture surface samples (back-scattered SEM-images at the bottom).*

6.2.1 Aperture

The physical aperture of the main fracture plane of Feature A has also been measured through photographs of sections cutting through the drill core samples, as described in Chapter 5. The results showed that the pore space pattern varied over the surface of Feature A, from a single plane to more complex patterns. About one third is complex, having several subparallel fracture planes and smaller rock particles embedded in epoxy along the fracture plane. One third of the fracture plane is expected to be slightly complex and one third is consisting of one single open fracture plane alone.

No quantification of the fracture complexity was performed in previous TRUE-1 modelling, but the (physical) aperture was expected to be variable and in the order of 1–3 mm, based only on what was seen at the borehole intercepts (Winberg et al. 2000). The average physical aperture (average of the mean cumulative aperture, b_m) presented in this report for analysed fractures of Feature A, is 0.45 mm with a variation in the span 0–1 mm (Figure 6-3). Note that this estimate is for Fracture 1 and 2 separately in KXTT3 and that the nearby Fractures 3–5 (cf. Figure 4-2) also contain epoxy which means that the total aperture for all fractures at Feature A in KXTT3 is larger.

The current study of Feature A resulted in an estimation of the spatial correlation distance (practical range) for the aperture of about 75 mm. This is in agreement with the results from previous studies concerning aperture distributions (Hakami 1995), in which the spatial correlation distance is seen to be correlated to the aperture and in particular to the coefficient of variation (Figure 6-4).

The average physical aperture of Feature A' is uncertain, but is estimated to be about 0.04 mm, based on a few measurements on sections through the small area where epoxy has penetrated Feature A'. The aperture is thus much smaller in Feature A' compared with Feature A.

The mass balance aperture evaluated from cross hole tracer tests in Feature A from KXTT4 to KXTT3 is in the range of 1–2 mm (Winberg et al. 2000). This is rather similar to the range of physical aperture reported in the present report, especially if Fracture 3–5 in KXTT3 also contributes significantly to the total physical aperture of Feature A in KXTT3. A larger total physical aperture of Feature A in KXTT3 than in KXTT4 is also in agreement with higher estimates of transmissivity in KXTT3 (order of 10^{-7} m^2/s) than in KXTT4 (order of 10^{-8} m^2/s) (Winberg et al. 2000, Nordqvist et al. 2014).

Modelling of the STT-1 and STT-2 tests by Cvetkovic et al. (2007), using a plausible rim zone porosity in the range 1 %–2 %, constrained the effective retention aperture to the range 0.2–0.7 mm. Earlier modeling of the same tests by Cvetkovic et al. (2000) indicated a transport aperture of 0.9 mm.

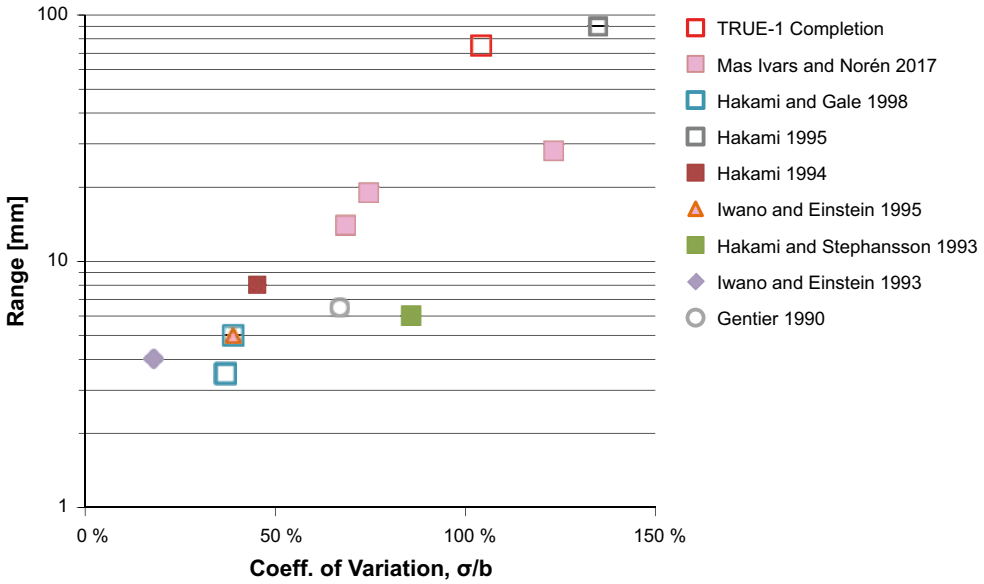

Figure 6-4. *Compilation of some previous data on fracture aperture spatial distribution. The y-axis shows the practical range of model variograms fitted to the data and the x-axis shows the coefficient of variation (standard deviation of physical fracture aperture σ / mean value of the physical fracture aperture b). All square symbols correspond to fractures (or faults) at Äspö HRL. Note that for TRUE-1 Feature A the coefficient of variation is estimated using the mean values from images, i.e. this would give an underestimation of the point wise aperture variation. It may be concluded that the results for Feature A is in agreement with previous findings on spatial aperture distribution, i.e. following the general trend of increasing range with increasing coefficient of variation.*

Mass balance aperture is normally evaluated from the pumping flow rate and the mean residence time under the assumption of homogeneous two-dimensional flow. The experimental setup of the CEC test makes it possible to use the flow rate through the tracer injection section instead of the pumping flow rate in the evaluation. In this case no assumption of homogeneous two-dimensional flow is required, instead the flow could just as well be three dimensional. Using the data provided in Nordqvist et al. (2014) from the CEC test (a mean residence time of 1–3 h and a flow rate 36–45 ml/h) and an assumption of converging flow lines, the mass balance aperture is calculated at 0.3–0.9 mm. If a convergence factor of 2 is applied for the injection borehole, the mass balance aperture would be 0.15–0.45 mm. This range of estimated mass balance aperture is very close to the physical aperture reported above but smaller than the mass balance apertures reported in Winberg et al. (2000).

A general discussion on the different apertures is given in Tsang (1992) and in Section 3.3 of Hjerne et al. (2010), whereas the different apertures originally inferred for the TRUE-1 tests are summarized in Cvetkovic et al. (2000, Table 5.4).

6.3 Sorption model

Concerning the sorption part of this work, the present work has (in addition to the earlier attempts to formulate a sorption model (Winberg et al. 2000, Andersson et al. 2002a) also included:

- Use of higher chemical concentration of Cs in an in situ tracer experiment (CEC-experiment) in order to investigate the cation exchange capacity of the transport path used in the earlier experiments.
- Overcoring of the injection and withdrawal boreholes in order to obtain information of the spatial distribution of the adsorbed Cs in the rock.

The main result of the CEC experiment is that neither of the experimental concentrations used were high enough to obtain a saturation of the cation exchange sites along the transport path. According to the scoping calculation based on earlier results obtained in laboratory and field experiments, saturation should have been established. This can be regarded as an indication of more sorption capacity (in terms of the number of cation exchange sites) in the fracture than what can be predicted from laboratory experiments.

On the other hand, the preliminary modelling performed from the CEC experiment results indicated that the selectivity coefficient (i.e. a parameter corresponding to the sorption distribution coefficient, K_d, in the case of linear sorption) is considerably lower in this case with tracer concentrations in the range of 1–10 mM compared with what has been estimated from the radiotracer experiments (typically < 0.1 μM) within the TRUE-1 program. Based on these findings, one may formulate a sorption model in which interaction with Cs in low concentration occurs with a relatively small number of sorption sites with high selectivity for Cs binding. When the concentration is increased, interaction will mainly occur with a comparatively large number of sorption sites that are not so selective in binding to Cs. This observation indicates a need of a heterogeneous sorption model (in this case demonstrated for Cs) with different sorption sites with varying sorption strength; i.e. a contradiction to a linear sorption model.

It is observed that Cs concentration increase in the CEC experiment does not cause any significant desorption of the Cs radiotracer used in the earlier in situ tracer experiment. Of the 4 200 kBq Cs-137 that was not recovered during the in situ radiotracer experiment, only ~ 1 % was recovered during the CEC experiment. This can be compared with the results of the CEC experiment where it was found that ~70 % of the Cs then injected into the transport path of the fracture was recovered. By applying the reasonable assumption that the flow in the CEC experiment occurred in the same path as the earlier radiotracer experiment, one can thus establish a different transport behaviour of the earlier injected radiotracer Cs compared with the high concentration Cs injected during the CEC experiment. A sorption model featuring fully reversible cation exchange interaction at the surface of the single transport path would imply that the 4 200 kBq Cs-137 radiotracer remaining in the flow path would behave analogously to the non-radioactive Cs tracer injected in the experiment, e.g. showing the same recovery. Unless the flow paths of the two experiments have significantly different

spatial geometrical arrangement, one must regard the combined result as an indication of a sorption mechanism of Cs that deviates from an ordinary cation exchange model; e.g. involving influences of kinetical restrictions of the desorption of the tracer. Indications of non- or (within the time frames of the experiments) slowly reversible processes of Cs sorption were found in laboratory experiments within the TRUE program (e.g. Byegård et al. 1998) and also in studies of Cs sorption in different clay material (e.g. Comans et al. 1991, Comans and Hockley 1992). The present work gives some further indications that non- or slowly reversible sorption of Cs can also be demonstrated not only for sampled rock material but also for rock fracture material in an in situ situation, a topic also dealt with by Bradbury and Baeyens (1992).

Concerning the attempt to study the location of the adsorbed Cs in the sampled natural fracture samples, one cannot clearly observe any dependence of the pore space geometry character classification and the amount of adsorbed Cs. The amount of Cs on mating sides of the fractures is quite similar which supports a standard diffusion-sorption model where retention is symmetric with respect to the two fracture surfaces. From the available samples, one cannot find any support of an increased sorption capacity in Feature A that could be caused by presence of clay rich material, e.g. fault gouge material. On the other hand, the CEC experiment indicates that the amount of interacting sorption sites found is difficult to explain only from the results of laboratory experiments on the site specific mylonites and cataclasites, even if a matrix diffusion mechanism is addressed. To explain the CEC results using only laboratory experiments on the CEC for mylonite and cataclasites, one would have to address the transport in a network of fractures, i.e. a concept involving far more available surface area than a concept of e.g. a single fracture. Since the studies of the overcored rock samples lend very little support for a significant part of the flow taking place in a complex fracture network, an explanation for the large sorption capacity of the fracture could be that the area of the fracture samples has been influenced by the flushing during the drilling of the original boreholes. Such flushing could have decreased the presence of clay rich material in the studied samples compared with the undisturbed parts of the fracture further away from the borehole. Notable in this context is that both boreholes involved in the earlier experimentation, KXTT3 and KXTT4, were drilled with double tube core barrel.

The overall conclusion of the TRUE experiments concerning retardation is therefore that it has been shown that sorbing tracer transport is mainly governed by a reversible sorption mechanism. The late arrival (pulse retardation) of e.g. Rb, Ba, Cs and Co compared with non-sorbing tracers proves that at least a part of the tracer interaction with the rock material can be attributed to reversible sorption/desorption reactions that causes a delay (retardation) of the tracers. However, it is indicated (particularly for Cs) that low mass recovery can only be explained by tracer interactions with the rock material that is a subject to non- or (within the time frames of the experiments) slowly reversible sorption. It is therefore obvious that a simple cation exchange model is not sufficient for satsifactory explaining and understanding of the behaviour of the presently used tracers and that this calls for application of models addressing heterogeneity; both with respect to matrix rock heterogeneity, transport path heterogeneity and heterogeneity in sorption mechanisms.

7 Main findings and principal conclusions

7.1 Main findings

Feature A and Feature A' are well characterized from earlier investigations at the TRUE-1 site (Andersson et al. 2002c, Winberg et al. 2000). The results obtained in the present project, as presented in this report, do not contradict earlier results and conclusions established in the TRUE-1 project. Instead, the results strengthen and complement earlier findings. The main findings of Feature A in the TRUE-1 Completion project may be summarised by the following statements:

- Both the COM tests and the SWIW tests clearly demonstrate that the flow is heterogeneously distributed in Feature A during pumping or injection. An area with higher transmissivity and/or connectivity is indicated around KXTT3 and KXTT5, while an area of lower transmissivity and/or connectivity is found between KXTT1, KXTT2, KXTT4 and KA3005A. The transport from KXTT4 was found to be faster to KXTT3 and KXTT5 than to KXTT1 and KXTT2.
- The main result of the CEC experiment is that neither of the concentrations used were high enough to obtain saturation of the cation exchange sites of the transport path, even though this was to be expected based on scoping calculations made prior to the test.
- Epoxy was found in the fractures earlier reported as open in the target sections of KXTT3 and KXTT4. Feature A in KXTT4 is dominated by one epoxy filled fracture while the area around Feature A in KXTT3 consists of five epoxy filled fractures.
- The amount of epoxy found in Feature A' in KXTT4 is small and limited to the area close to the borehole intercept.
- It was possible to fit a single plane with a strike and dip of 341/79 to the intercepts of Feature A in boreholes KXTT1 through KXTT5 and KA3005A with a maximum deviation of 10 cm from the plane to any of the borehole intercepts.
- The analysis showed that the pore space pattern of Feature A varied over the surface with an equal distribution between the surfaces of a single open fracture plane, a slightly complex fracture and a complex fracture with several subparallel fracture planes and embedded particles. The analysis of the studied fractures of Feature A showed a mean cumulative aperture of 0.45 mm, with a variation in aperture in the span 0–1 mm and a spatial correlation distance (practical range) for the aperture of about 75 mm.
- The analysis of the pore space pattern provides a detailed characterization of aperture distribution. This gives, in combination with the results from the COM tests and SWIW tests, a good basis for detailed simulations to study local flow paths and channelling effects.
- The occurrence of clay minerals on the outermost surface along the flow paths has been verified through analysis using XRD and SEM. However, the quantities of clay minerals found do not seem to be large enough to explain the entire retention found in earlier TRUE-1 tests. In addition, it is likely that diffusion into the rock matrix also plays a part in the retention processes, but the significance is uncertain because no quantitative porosity investigations were carried out.
- The wall rock is highly altered with several generations of fracture coatings showing that Feature A has been reactivated at several events and that it has been intermittently water-conducting for a very long time.
- Feature A shows similar appearance in terms of fracture mineral assemblages, deformation and pore space geometry in both KXTT3 and KXTT4. Similar fracture mineral assemblages and multiple fault re-activation have also been observed in water-conducting deformation zones at Laxemar (and Simpevarp) (Drake and Tullborg 2009), and at Forsmark (Sandström et al. 2008).
- The physical aperture of Feature A' is very small, approximately 0.04 mm.
- The presence of radioactive Cs, remaining from earlier tracer tests involving KXTT4, is larger in the sample of Feature A' compared to the sample of Feature A. But the presence of radioactive Cs is similar to the presence of epoxy in the sense that there is a rather even distribution of Cs over the surface of Feature A while there is radioactivity only close to the injection borehole in Feature A'.

7.2 Principal conclusions in relation to other TRUE-1 projects

As for the main findings presented above, the principal conclusions made in the project support conclusions made in earlier TRUE project studies. The principal conclusions made in the TRUE-1 Completion project are:

- Feature A is heterogeneous in terms of transmissivity and/or connectivity within the borehole array and has an undulating and/or stepwise character. The average physical aperture is 0.45 mm, varying in the span 0–1 mm; this value is consistent with the range 0.2–0.7 mm hypothesised in the interpretation of the TRUE-1 tracer test outcomes (point 4 of Conclusions in Cvetkovic et al. (2007)).
- The overall similarities of the characteristics of Feature A in KXTT3 and KXTT4 support the interpretation of Feature A as a continuous fracture. The key elements of the micro-structural model of Feature A is repeated fracturing and related wall rock alteration, i.e. several generations of fracture coatings with a dominant coverage of the main fracture surfaces of chlorite and clay minerals together with some wall rock fragments, and calcite with related accessory minerals on the fracture walls as well as highly altered rock adjacent to these fractures. This confirms the main hypothesis of the TRUE-1 tracer test interpretation, namely, the presence of a rim zone due to alterations (Winberg et al. 2000), with properties different from the intact (unaltered) rock matrix (point 2 of Conclusions in Cvetkovic et al. 2007). Note that alteration of the rim zone has also been an important hypothesis for the interpretation of retention in the entire TRUE program (Winberg et al. 2000, Cvetkovic 2010a, b, Cvetkovic et al. 2010).
- Interpretation of the TRUE-1 tracer tests has been based on the assumption that retardation of sorbing tracers is governed by a reversible sorption mechanism in the rock matrix of the rim zone (Winberg et al. 2000, Cvetkovic et al. 2007). The results of the CEC tests indicate that at least for the relatively strongly sorbing tracer Cs, interactions with the rock material may to some extent be irreversible, or slowly reversible on the scale of the TRUE-1 tracer tests; this reaffirms the suggestion in point 6 of Conclusions in Cvetkovic et al. (2007), that the discrepancy between modelled and measured breakthrough e.g. for Cs (clearly visible in Fig 5 (Cvetkovic et al. 2007)), may be due to sorption kinetics.

Table 7-1 provides an overview of the conclusions made in TRUE-1 Completion in relation to conclusions made in other parts of TRUE-1.

Table 7-1. Overview of conclusions in TRUE-1 Completion in comparison with conclusions from other TRUE-1 projects.

Issue	TRUE-1	TRUE-1 Completion
Conceptual geometrical model of Feature A	Feature A is interpreted as well separated from other major hydraulic features within the borehole array (Winberg et al. 2000). Supported by results in Andersson et al. (2002c). Alternative model of the TRUE-1 block as a system influenced by a network of inter-connected fractures proposed by Neretnieks and Moreno (2003).	Indirectly supported by results from crosshole interference tests and epoxy findings. The alternative model is not supported by results.
Overall heterogeneity	Figure 10-2 in Winberg et al. (2007), Figure 5.2 in Cvetkovic et al. (2000).	Comparable level of heterogeneity confirmed.
Matrix structure	Altered rim zone.	Confirmed and generalized.
Aperture	Mass balance aperture 1–2 mm (Winberg et al. 2000). Transport aperture 0.9 mm according to modelling by Cvetkovic et al. (2000). Most probable estimated range is 0.2–0.7 mm (point 4 of Conclusions in Cvetkovic et al. (2007).	Range of 0.2–0.7 mm confirmed by measurement of physical aperture and mass balance aperture estimated from the flow rate through the tracer injection section and mean residence time during the CEC test.
Matrix porosity	Most likely range estimated as 1–2 % (point 4 of Conclusions in Cvetkovic et al. (2007).	Not available.
Sorption	Estimated in-situ K_d values are generally higher than generic values obtained on unaltered rock samples using through diffusion tests (point 5 of Conclusions in Cvetkovic et al. 2007).	Supplemented: A Cs sorption capacity of at least 0.05 moles is measured for the ~5 m (Euclidian distance) fracture flow path, which is higher than what was estimated from the TRUE-1 laboratory results. However, it is indicated from the CEC experiment that a large portion of these increased number of sorption sites do not have as high selectivity for Cs sorption as was indicated by the TRUE-1 laboratory experiments.
Retention processes	Linear equilibrium sorption and diffusion in matrix as the “standard model retention” was shown to be sufficient for interpreting observed breaktrough curves (BTCs) (Cvetkovic et al. 2007).	Not contradicted.
Other	Deviation in BTC modelling for Cs in STT-1 (Cvetkovic et al. 2000, Fig 6.1): The measured BTC is lower than modelled after ca 200h; this has not been explained and may be due to irreversible (slowly reversible) sorption.	Indications of irreversible (or slowly reversible) sorption for Cs confirmed.

References

SKB's (Svensk Kärnbränslehantering AB) publications can be found at www.skb.com/publications.

Andersson P, Byegård J, Cvetkovic V, Johansson H, Nordqvist R, Selroos J-O, Winberg A, 1997. Äspö Hard Rock Laboratory. TRUE 1st stage tracer test programme. Experimental plan for tests with sorbing tracers at the TRUE-1 site. Experimental description and preliminary evaluation. SKB HRL Progress Report HRL-97-07, Svensk Kärnbränslehantering AB.

Andersson P, Wass, E, Johansson H, Skarnemark G, Skålberg M, 1999a. Äspö Hard Rock Laboratory. TRUE 1st stage tracer test programme. Tracer tests with sorbing tracers, STT-1b. Experimantal descriptrion and preliminary evaluation. SKB IPR-99-12, Svensk Kärnbränslehantering AB.

Andersson P, Wass E, Byegård J, Johansson H, Skarnemark G, 1999b. Äspö Hard Rock Laboratory. TRUE 1st stage tracer test programme. Tracer tests with sorbing tracers, STT-2. Experimental description and preliminary evaluation. SKB IPR-99-15, Svensk Kärnbränslehantering AB.

Andersson P, Byegård J, Dershowitz B, Doe T, Hermanson J, Meier P, Tullborg E-L, Winberg A (ed), 2002a. Final report of the TRUE Block Scale project. 1. Characterisation and model development. SKB TR-02-13, Svensk Kärnbränslehantering AB.

Andersson P, Byegård J, Winberg A, 2002b. Final report of the TRUE Block Scale project. 2. Tracer test in the block scale. SKB TR-02-14, Svensk Kärnbränslehantering AB.

Andersson P, Wass E, Gröhn S, Holmqvist M, 2002c. Äspö Hard Rock Laboratory. TRUE-1 Continuation project. Complementary investigations at the TRUE-1 site – Crosshole interference, dilution and tracer tests, CX-1–CX-5. SKB IPR-02-47, Svensk Kärnbränslehantering AB.

Andersson P, Gröhn S, Nordqvist R, Wass E, 2004. Äspö Hard Rock Laboratory. TRUE Block Scale continuation project. BS2B pretests. Crosshole interference, dilution and tracer tests, CPT-1 – CPT-4. SKB IPR-04-25, Svensk Kärnbränslehantering AB.

Andersson P, Byegård J, Billaux D, Cvetkovic V, Dershowitz W, Doe T, Hermanson J, Poteri A, Tullborg E-L, Winberg A (ed), 2007. TRUE Block Scale Continuation project. Final report. SKB TR-06-42, Svensk Kärnbränslehantering AB.

Becker M W, Shapiro A M, 2003. Interpreting tracer breakthrough tailing from different forced-gradient tracer experiment configurations in fractured bedrock. Water Resources Research 39. doi:10.1029/2001WR001190

Birgersson L, Gale J, Hakami E, 2000a. Äspö Hard Rock Laboratory. First True Stage. Pilot resin experiment. Summary report. SKB IPR-00-04, Svensk Kärnbränslehantering AB.

Birgersson L, Gale J, Hakami E, 2000b. Äspö Hard Rock Laboratory. First True Stage. Pilot resin experiment. Background information. SKB IPR-00-05, Svensk Kärnbränslehantering AB.

Bossart P, Hermanson J, Mazurek M, 2001. Äspö Hard Rock Laboratory. Analysis of fracture networks based on the integration of structural and hydrogeological observations on different scales. SKB TR-01-21, Svensk Kärnbränslehantering AB.

Bradbury M H, Baeyens B, 1992. Modelling the sorption of Cs: application to the Grimsel Migration Experiment. In Dury T V (ed). PSI Annual Report 1992, Paul Scherrer Institute, Switzerland, Annex IV, 59–64.

Byegård J, Tullborg E-L, 2012. Äspö Hard Rock Laboratory. Sorption experiments and leaching studies using fault gouge material and rim zone material from the Äspö Hard Rock Laboratory. TRUE-1 Continuation project. SKB P-11-20, Svensk Kärnbränslehantering AB.

Byegård J, Johansson H, Skålberg M, Tullborg E-L, 1998. The interaction of sorbing and non-sorbing tracers with different Äspö rock types. Sorption and diffusion experiments in the laboratory scale. SKB TR-98-18, Svensk Kärnbränslehantering AB.

Byegård J, Selnert E, Tullborg E-L, 2008. Bedrock transport properties. Data evaluation and retardation model. Site descriptive modelling, SDM-Site Forsmark. SKB R-08-98, Svensk Kärnbränslehantering AB.

Comans R N J, Hockley D E, 1992. Kinetics of cesium sorption on illite. Geochimica et Cosmochimica Acta 56, 1157–1164.

Comans R N J, Haler M, De Preter P, 1991. Sorption of cesium on illite: nonequilibrium behaviour and reversibility. Geochimica et Cosmochimica Acta 55, 433–440.

Cornell R M, 1993. Adsorption of cesium on minerals: a review. Journal of Radioanalytical and Nuclear Chemistry 171, 483–500.

Crawford J (ed), 2008. Bedrock transport properties Forsmark. Site descriptive modelling, SDM-Site Forsmark. SKB R-08-48, Svensk Kärnbränslehantering AB.

Cvetkovic V, 2010a. Diffusion-controlled tracer retention in crystalline rock on the field scale. Geophysical Research Letters 37, L13401. doi:10.1029/2010GL0434

Cvetkovic V, 2010b. Significance of fracture rim zone heterogeneity for tracer transport in crystalline rock. Water Resources Research 46. doi: 10.1029/2009WR007755

Cvetkovic V, Cheng H, 2008. Sorbing tracer experiments in a crystalline rock fracture at Äspö (Sweden): 3. Effect of micro-scale heterogeneity. Water Resources Research 44, W12447. doi: 10.1029/2007WR006797

Cvetkovic V, Cheng H, Selroos J-O, 2000. First TRUE Stage. Evaluation of tracer retention understanding experiments (first stage) at Äspö. SKB ICR-00-01, Svensk Kärnbränslehantering AB.

Cvetkovic V, Frampton A, 2010. Transport and retention from single to multiple fractures in crystalline rock at Äspö (Sweden): 2. Fracture network simulations and generic retention model. Water Resources Research 46, W05506. doi: 10.1029/2009WR008030

Cvetkovic V, Cheng H, Widestrand H, Byegård J, Winberg A, Andersson P, 2007. Sorbing tracer experiments in a crystalline rock fracture at Äspö (Sweden): 2. Transport model and effective parameter estimation. Water Resources Research 43, W11421. doi:10.1029/2006WR005278

Cvetkovic V, Cheng H, Byegård J, Winberg A, Tullborg E-L, Widestrand H, 2010. Transport and retention from single to multiple fractures in crystalline rock at Äspö (Sweden): 1. Evaluation of tracer test results and sensitivity analysis. Water Resources Research 46, W055505. doi: 10.1029/2009WR008013

Dershowitz W, Winberg A, Hermanson J, Byegård J, Tullborg E-L, Andersson P, Mazurek M, 2003. Äspö Hard Rock Laboratory. Äspö Task Force on modelling of groundwater flow and transport of solutes. Task 6C. A semi-synthetic model of block scale conductivite structures at the Äspö HRL. SKB IPR-03-13, Svensk Kärnbränslehantering AB.

Drake H, Tullborg E-L, 2009. Fracture mineralogy Laxemar. Site descriptive modelling, SDM-Site Laxemar. SKB R-08-99, Svensk Kärnbränslehantering AB.

Elert M, 1999. Evaluation of modelling of the TRUE-1 radially converging and dipole tests with conservative tracers The Äspö Task Force on Modelling of Groundwater Flow and Transport of Solutes Tasks 4C and 4D. SKB TR-99-04, Svensk Kärnbränslehantering AB.

Elert M, Svensson H, 2001. Evaluation of modelling of the TRUE-1 radially converging tests with sorbing tracers. The Äspö Task Force on Modelling of Groundwater Flow and Transport of Solutes. Tasks 4E and 4F. SKB TR-01-12, Svensk Kärnbränslehantering AB.

Gelhar L W, Welty C, Rehfeldt K R, 1992. A critical review of data on field-scale dispersion in aquifers. Water Resources Research 28, 1955–1974.

Gentier S, 1990. Morphological Analysis of a natural fracture. In Simpson E S, Sharp J M (eds). Selected papers on hydrogeology from the 28th International Geological Congress, Washington, DC, July 1986. International Association of Hydrologists, Vol 1, 315–326.

Hakami E, 1994. Pore volume characterization. Aperture distribution of a highly conductive single fracture. SKB HRL Progress Report 25-94-30, Svensk Kärnbränslehantering AB.

Hakami E, 1995. Aperture distribution of rock fractures. PhD thesis. Division of Engineering Geology, Department of Civil and Environmental Engineering, Royal Institute of Technology (KTH), Sweden.

Hakami E, Gale J, 1998. Äspö Hard Rock Laboratory. First TRUE Stage pilot resin experiment. Pore space analysis. SKB IPR-99-14, Svensk Kärnbränslehantering AB.

Hakami E, Wang W, 2005. Äspö Hard Rock Laboratory. TRUE-1 Continuation project. Fault rock zones characterisation. Characterisation and quantification of resin-impregnated fault rock pore space using image analysis. SKB IPR-05-40, Svensk Kärnbränslehantering AB.

Hakami E, Johansson M, Byegård J, Drake H, Tullborg E-L, 2014. Analysis of core material from the TRUE-1 site. Fracture mineralogy, fracture pore volume geometry and Cs sorption. SKB P-11-28, Svensk Kärnbränslehantering AB.

Hjerne C, Nordqvist R, Harrström J, 2010. Compilation and analyses of results from cross-hole tracer tests with conservative tracers. SKB R-09-28, Svensk Kärnbränslehantering AB.

Illman W A, Liu X, Takeuchi S, Yeh T-C J, Ando K, Saegusa H, 2009. Hydraulic tomography in fractured granite: Mizunami Underground Research site, Japan. Water Resources Research 45. doi:10.1029/2007WR006715

Iwano N, Einstein H H, 1993. Stochastic analysis of surface roughness, aperture and flow in single fracture. In Sousa L R E, Grossmann N F (eds). Safety and environmental issues in rock engineering: proceedings of ISRM International Symposium EUROCK '93, Lisbon, 21–24 June 1993. Rotterdam: Balkema, 135–141.

Jakob A, Mazurek M, Heer W, 2003. Solute transport in crystalline rocks at Äspö – II: Blind predictions, inverse modelling and lessons learnt from test STT1. Journal of Contaminant Hydrology 61, 175–190.

Löfgren M, Crawford J, Elert M, 2007. Tracer tests – possibilities and limitations. Experience from SKB fieldwork: 1977–2007. SKB R-07-39, Svensk Kärnbränslehantering AB.

Marschall P, Elert M, 2003. Overall evaluation of the modelling of the TRUE-1 tracer tests – Task 4. The Äspö Task Force on Modelling of Groundwater Flow and Transport of Solutes. SKB TR-03-12, Svensk Kärnbränslehantering AB.

Mas Ivars D, Norén K, 2017. Äspö Pillar Stability Experiment. Coupled stress-flow tests on large fracture samples from the APSE site. SKB R-13-29, Svensk Kärnbränslehantering AB.

Mazurek M, Bossart P, Eliassion T, 1996. Classification and characterization of water-conduction featrus at Äspö: Results of investigations on the outcrop scale. SKB ICR-97-01, Svensk Kärnbränslehantering AB.

Mazurek M, Jakob A, Bossart P, 2003. Solute transport in crystalline rocks at Äspö – I: Geological basis and model calibration. Journal of Contaminant Hydrology 61, 157–174.

Mærsk Hansen L, Staub I, 2004. Äspö Hard Rock Laboratory. TRUE-1 Continuation project. Fault rock zones characterisation. Overcoring (300 mm) of impregnated fault rock zones at chainages 2/430, 2/545, 2/163 and 1/600 m. SKB IPR-04-10, Svensk Kärnbränslehantering AB.

Neretnieks I, 2002. A stochastic multi-channel model for solute transport—analysis of tracer tests in fractured rock. Journal of Contaminant Hydrology 55, 175–211.

Neretnieks I, Moreno L, 2003. Prediction of some in situ tracer tests with sorbing tracers using independent data. Journal of Contaminant Hydrology 61, 351–360.

Nordqvist R, 2008. Evaluation and modelling of SWIW tests performed within the SKB site characterisation programme. SKB R-08-104, Svensk Kärnbränslehantering AB.

Nordqvist R, Byegård J, Hjerne C, 2014. Complementary tracer tests – SWIW, CEC and multi-hole reciprocal cross flow tests at the TRUE-1 site. TRUE-1 Continuation project. TRUE-1 Completion. SKB P-11-27, Svensk Kärnbränslehantering AB.

Poteri A, Billaux D, Dershowitz W, Gómez-Hernández J, Cvetkovic V, Hautojärvi A, Holton D, Medina A, Winberg A (ed), 2002. Final report of the TRUE Block Scale project. 3. Modelling of flow and transport. SKB TR-02-15, Svensk Kärnbränslehantering AB.

Sandström B, Tullborg E-L, Smellie J, MacKenzie A B, Suksi J, 2008. Fracture mineralogy of the Forsmark site. SDM-Site Forsmark. SKB R-08-102, Svensk Kärnbränslehantering AB.

Sigurdsson O, Hjerne C, 2014. Overcoring of resin-impregnated boreholes KXTT3 and KXTT4 at the TRUE-1 site. TRUE-1 Completion. SKB P-11-21, Svensk Kärnbränslehantering AB.

SKB, 2011. Long-term safety for the final repository for spent nuclear fuel at Forsmark. Main report of the SR-Site project. SKB TR-11-01, Svensk Kärnbränslehantering AB.

Tsang Y W, 1992. Usage of "equivalent apertures" for rock fractures as derived from hydraulic and tracer tests. Water Resources Research 28, 1451–1455.

Widestrand H, Byegård J, Cvetkovic V, Tullborg E-L, Winberg A, Andersson P, Siitari-Kauppi M, 2007. Sorbing tracer experiments in a crystalline rock fracture at Äspö (Sweden): 1. Experimental setup and microscale characterization of retention properties. Water Resources Research 43, W10413. doi:10.1029/2006WR005277

Winberg A (ed), 1996. First TRUE Stage – Tracer retention understanding experiments. Descriptive structural-hydraulic models on block and detailed scales of the TRUE-1 site. SKB ICR-96-04, Svensk Kärnbränslehantering AB.

Winberg A, 1997. Tracer Retention Understanding Experiments (TRUE). Test plan for the TRUE Block Scale Experiment. Swedish SKB ICR-97-02, Svensk Kärnbränslehantering AB.

Winberg A (ed), 2010. Fault rock zones characterisation – Final report. TRUE-1 Continuation Project. SKB TR-10-36, Svensk Kärnbränslehantering AB.

Winberg A, Andersson P, Hermanson J, Byegård J, Cvetkovic V, Birgersson L, 2000. Äspö Hard Rock Laboratory. Final report of the first stage of the tracer retention understanding experiments. SKB TR-00-07, Svensk Kärnbränslehantering AB.

Winberg A, Andersson P, Byegård J, Poteri A, Cvetkovic V, Dershowitz W, Doe T, Hermanson J, Gómez-Hernández J J, Hautojärvi A, Billaux D, Tullborg E-L, Holton D, Meier P, Medina A, 2003. Final report of the TRUE Block Scale project. 4. Synthesis of flow, transport and retention in the block scale. SKB TR-02-16, Svensk Kärnbränslehantering AB.